

# Understanding London Dispersion Forces in Solution

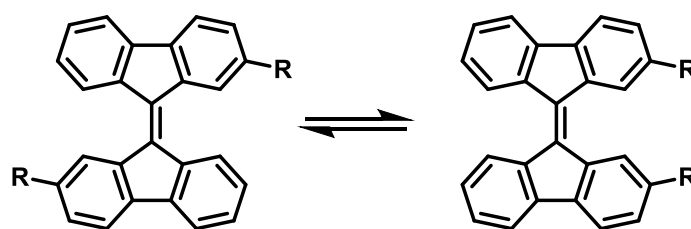
– Quantification of Noncovalent Interactions with a Bifluorenylidene Molecular Balance –

---

Inauguraldissertation zur Erlangung des Doktorgrades der naturwissenschaftlichen  
Fachbereiche

im Fachgebiet Organische Chemie (Fachbereich 08)

der Justus-Liebig-Universität Gießen



vorgelegt von

**Finn Wilming**

aus Gießen

angefertigt im Zeitraum von Juli 2019 bis September 2022

am Institut für Organische Chemie

der Justus-Liebig-Universität Gießen

**Betreuer: Prof. Dr. Peter R. Schreiner, PhD**



## **Eidesstattliche Erklärung**

Ich erkläre: Ich habe die vorgelegte Dissertation selbstständig und ohne unerlaubte fremde Hilfe und nur mit den Hilfen angefertigt, die ich in der Dissertation angegeben habe. Alle Textstellen, die wörtlich oder sinngemäß aus veröffentlichten Schriften entnommen sind, und alle Angaben, die auf mündlichen Auskünften beruhen, sind als solche kenntlich gemacht. Ich stimme einer evtl. Überprüfung meiner Dissertation durch eine Antiplagiat-Software zu. Bei den von mir durchgeführten und in der Dissertation erwähnten Untersuchungen habe ich die Grundsätze guter wissenschaftlicher Praxis, wie sie in der „Satzung der Justus-Liebig-Universität Gießen zur Sicherung guter wissenschaftlicher Praxis“ niedergelegt sind, eingehalten.

---

Ort, Datum

---

Unterschrift

Dekan: Prof. Dr. Thomas Wilke

Prodekan: Prof. Dr. Klaus Müller-Buschbaum

Studiendekan: Prof. Dr. Reinhard Dammann

Erstgutachter: Prof. Dr. Peter R. Schreiner, PhD

Zweitgutachter: Prof. Dr. Derck Schlettwein



## Zusammenfassung

London'schen Dispersionswechselwirkungen wurde in den ersten Jahrzehnten nach ihrer Entdeckung nur wenig Aufmerksamkeit geschenkt, da die Fehlannahme existierte, sie seien generell schwach und können dementsprechend nur vernachlässigbaren Einfluss auf chemische Prozesse haben. Heute wissen wir, dass die durch London Dispersion hervorgerufene Stabilisation zwischen zwei einzelnen Atomen zwar tatsächlich eher schwach ist, sich diese kleinen stabilisierenden Beiträge jedoch in größeren Systemen schnell zu einer signifikanten Kraft kumulieren können. Es wurde klar: London'sche Dispersionswechselwirkungen können die Struktur und Stabilität von Molekülen und die Selektivität chemischer Reaktionen signifikant beeinflussen. Im Rahmen dieser Arbeit wurde mit Hilfe einer molekularen Waage, einem Messgerät für nonkovalente Wechselwirkungen auf molekularer Ebene, ein besseres Verständnis für London'sche Dispersionswechselwirkungen in Lösung erlangt. Dies ist von besonderer Bedeutung, da über die letzten Jahre diskutiert wurde, zu welchem Anteil London Dispersion in Lösung, durch kompetitive Wechselwirkungen mit dem Lösungsmittel abgeschwächt wird.

In der ersten Veröffentlichung stellen wir die Synthese und verschiedene lösungsmittelabhängige NMR-Experimente einer molekularen Waage auf Basis des 9,9'-Bifluorenylidene-Grundgerüsts vor. Da die *E/Z* Isomerisierung des hier verwendeten Systems hauptsächlich durch solvophobe Effekte beeinflusst wird kann so der Einfluss des Lösungsmittels auf die Stärke ebendieser untersucht werden. Ein genaues Verständnis von Solvophobizität ist für Untersuchungen an London Dispersion in Lösung essentiell, da dort beide Effekte häufig gemeinsam auftreten.

In der zweiten Publikation haben wir insgesamt 14 verschiedene, sich durch die verwendeten Substituenten unterscheidende, molekulare Waagen, auf Basis des gleichen unpolaren Grundgerüsts synthetisiert und ebenfalls das Gleichgewicht zwischen *E*- und *Z*-Isomer mittels NMR in sieben verschiedenen organischen Lösungsmitteln untersucht. Dabei wurde das durch London Dispersion stabilisierte *Z*-Isomer in nahezu allen Experimenten als bevorzugt vorkommendes Isomer identifiziert. Mittels computerchemischer Berechnungen wurde nachgewiesen, dass die höhere Stabilität des *Z*-Isomers durch London'sche Dispersionswechselwirkungen zwischen den benachbarten Substituenten hervorgerufen wird. Dadurch konnten wir unterstreichen, dass London'sche Dispersionswechselwirkungen in Lösung nicht vollständig durch kompetitive Wechselwirkungen mit dem Lösungsmittel aufgehoben werden.



## Abstract

London dispersion interactions received little attention in the first decades after their discovery because of the misconception that they are generally weak and, could accordingly only have negligible influence on chemical processes. Today it is known that, although the stabilization between two individual atoms caused by London dispersion is indeed rather weak, these small stabilizing contributions can quickly accumulate to a significant force in larger systems. London dispersion interactions can therefore strongly influence the structure and stability of molecules and the selectivity of chemical reactions.

In this work, a better understanding of London dispersion interactions in solution was obtained using a molecular balance. These are small molecular devices that can be used to measure noncovalent interactions at the microscopic scale. This is of particular importance because over the past several years there has been a debate about the extent to which stabilization caused by London dispersion in solution is attenuated by competitive interactions with the solvent.

In the first publication, we present the synthesis and various solvent dependent NMR measurements of a hydrocarbon molecular balance based on the 9,9'-bifluorenylidene backbone. Since the different *E/Z*-ratios of this molecular balance in a group of 15 organic solvents are mainly induced by the solvophobic effect, it allows us to understand the influence that the choice of solvent can have on the strength of solvophobic effects. These effects are particularly important to fully understand opportunities and limits of the strategic use of London dispersion interactions in solution, where both forces oftentimes occur simultaneously.

In the second publication, we synthesized a total of 14 differently substituted molecular balances based on the same nonpolar backbone. We studied their *E/Z*-equilibrium by NMR in seven different organic solvents. The *Z*-isomer was favored in almost all experiments. We used computations to show that the *Z*-isomers higher stability is caused by London dispersion interactions between the neighboring substituents and therefore underlined that London dispersion interactions in solution are not fully compensated by competing interactions with the solvent.



## Table of Contents

Eidesstattliche Erklärung.....	III
Zusammenfassung .....	V
Abstract .....	VII
<b>1. Introduction.....</b>	<b>1</b>
1.1 Motivation.....	1
1.2 London Dispersion Interactions .....	2
1.4 London Dispersion Interactions in Solution .....	7
1.4 London Dispersion Interactions in Quantum Mechanical Computations .....	10
1.5 Molecular Balances .....	13
1.5.1 The General Concept of a Molecular Balance .....	13
1.5.2 Different Classes of Molecular Balances.....	15
1.5.2.1 Molecular Torsion Balances.....	15
1.5.2.2 Dimerization Balances .....	17
1.5.2.3 Molecular Balances Based on Double Bond Isomerization.....	18
1.6 Conclusions and Outlook.....	19
1.7 Bibliography .....	21
<b>2. Publications .....</b>	<b>32</b>
2.1 Quantifying Solvophobic Effects in Organic Solvents Using a Hydrocarbon Molecular Balance .....	32
2.2 Probing the Size-Limit of Dispersion Energy Donors with a Bifluorenylidene Balance: Magic Cyclohexyl.....	38
<b>3. Acknowledgement – Danksagung.....</b>	<b>51</b>



## 1. Introduction

### 1.1 Motivation

London dispersion (LD) interactions are attractive noncovalent forces which arise from the spontaneous polarization of an atom or molecule, which then induces a dipole in neighbouring atoms or molecules.<sup>1</sup> Fritz London predicted the existence of this quantum mechanical electron correlation effect in 1930 to explain the condensation of noble gases at cryogenic temperatures.<sup>2,3</sup> The first 50 years after their discovery were mainly shaped by the common misconception that the influence of LD on chemical systems is generally negligible due to their relative weakness in comparison to other noncovalent forces when considering pairwise interactions between single atoms. Contrarily, more recent studies were able to experimentally and theoretically highlight structures or reactions that are significantly influenced by LD, particularly in systems with an increasing number of atoms and pairwise interactions.<sup>4</sup> Since LD interactions are ubiquitous forces, their recent “renaissance” had implications on almost all areas of chemistry. For example, the structures of large biomolecules like proteins or DNA were found to be heavily influenced by LD interactions<sup>5</sup> and catalysts of the future could be designed to strategically use LD interactions between substrate and catalyst to generate selectivity.<sup>6</sup> This process is driven by modern computational chemistry methods which are able to accurately predict the strength of LD interactions further opening the door to the deliberate use of LD in the design of reactions, catalysts or in other fields of use.

In this work, we focus on the effects that the presence of solvent can have on LD interactions. This is still a field of discussion because it remains unclear to which degree solute-solute LD stabilization could be attenuated due to competing solute-solvent LD interactions.<sup>7-9</sup> Our work is based on the use of small molecular switches called “molecular balances”, consisting only of carbon and hydrogen. These molecular devices allow us to measure noncovalent interactions at the microscopic level without the interference of local dipoles generated by the presence of heteroatoms like oxygen or nitrogen. In addition, they provide experimental insights into how size, shape, and flexibility of different substituents impact the amount of LD stabilization present in different solvents and how we can identify the presence of solvophobic effects which are linked to LD in solution. The obtained experimental results will be compared to state-of-the-art computational chemistry methods to assess the accuracy of present methods and generate experimental benchmark datasets which could be used by theoretical chemists and physicists.

## 1.2 London Dispersion Interactions

London dispersion interactions, named after Fritz London, represent the attractive part of the van der Waals potential.<sup>1-3</sup> They can be described as the result of quantum mechanical fluctuations of the electron density around an atom or a molecule which create an instantaneous electric field that induces an inverse dipole in neighbouring atoms or molecules. The approximated dispersion attraction between two atoms or molecules is described by equation (1).<sup>4</sup>

$$E_{disp} = - \sum_{AB}^{atom\ pairs} \frac{C_6^{AB}}{r_{AB}^6} \quad (1)$$

Here, every diatomic interaction energy is calculated by dividing the dispersion coefficient  $C_6^{AB}$ , which includes the specific polarizability of the considered structures, by the sixth power of the interatomic distance. For systems with more than two atoms, all pairwise interaction energies are summed up to obtain an approximation of the overall dispersion attraction, still more sophisticated methods of calculating LD interactions in larger systems have to go beyond pairwise additivity.<sup>10</sup> This implies that LD interactions increase for systems with increasing size and polarizability. It also becomes clear that atoms or molecules need to be in close proximity to each other to significantly attract each other due to the  $r^{-6}$  dependence. The rather small interaction energies calculated for the pairwise interactions of single atoms led to the common misconception that LD could be neglected even in larger systems. However, over the last decades, it was repeatedly shown that structure and stability of systems with an increasing number of atoms is often severely influenced by LD, since all small pairwise interactions add up to a significant attractive force.<sup>4</sup> One of the most prominent examples to show the importance of LD in large systems is the successful, LD driven, synthesis of derivatives of the elusive hexaphenylethane (**1**) (Figure 1).<sup>11</sup>

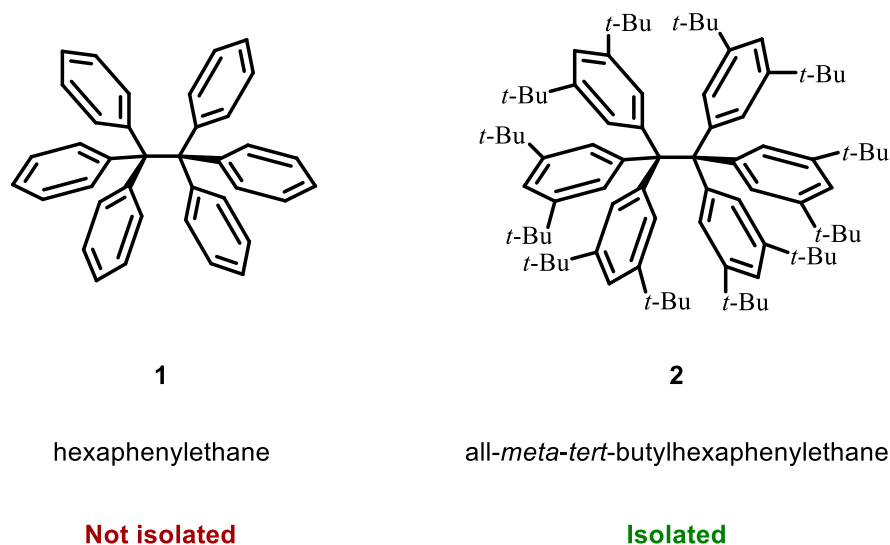


**Figure 1:** The unstable hexaphenylethane **1** can be stabilized through the addition of 12 *tert*-butyl groups in all *meta*-positions.

Starting with the pioneering work of Moses Gomberg,<sup>12</sup> the synthesis of unsubstituted hexaphenylethane **1** has been the topic of scientific discussions for decades.<sup>13</sup> (Figure 1) To date, all experimental and computational evidence points towards its instability at standard conditions due to steric repulsion between the phenyl groups.<sup>14</sup> Strikingly, the addition of 12 *tert*-butyl groups, which, from a classical perspective, would have been considered to add even more steric bulk to the system, instead stabilized the strained hexaphenylethane core. This unexpected stability is also predicted by quantum chemical computations in which the LD stabilization present between the two trityl moieties of all-*meta-tert*-butylhexaphenylethane **2** amounts to over 60 kcal mol<sup>-1</sup>.<sup>15</sup> A major part of this stabilization can be attributed to the LD interactions between the added *tert*-butyl groups. Figuratively speaking, the LD interactions in the *tert*-butyl-shell of the molecule act as a noncovalent glue to stabilize a generally unstable structure in the core of the molecule. With a very similar system, the shortest intermolecular H···H contact in a hydrocarbon structure was achieved.<sup>16</sup> The very unfavorable H···H distance of only 1.566(5) Å was compensated by over 50 kcal mol<sup>-1</sup> of LD stabilization present between the *tert*-butyl groups. Other examples for extraordinary hydrocarbon structures stabilized by LD are diamandoid-diamandoid dimers like **3** with exceptionally long C–C bonds,<sup>17</sup> Tetra-*tert*-butyltetrahedrane **5**, a structure with unusual bond angles held together by the corset effect,<sup>18,19</sup> or the “hairpin”-foldamers of chained alkanes with 18 or more carbon atoms (**4**) which are computationally predicted to be the energetic minimum structure despite bearing two unfavorable gauche-contacts.<sup>20</sup> (Figure 2).

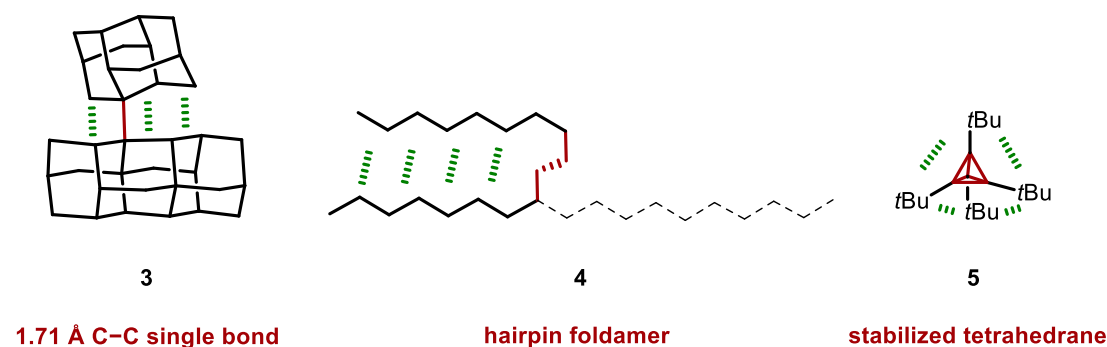


**Figure 2:** Different examples of unusual hydrocarbon structures enabled *via* LD. Areas of key LD stabilizations are highlighted in green.

LD also significantly influences the structure and stability of many molecules outside of the realm of hydrocarbons. For example, hexa-*tert*-butylcyclotrisilane<sup>21</sup> and hexa-*tert*-butyldisilane<sup>22</sup> are part of a group of several silanes with exceptionally long Si-Si bonds that are stabilized *via* LD. Additionally, the germanium-analogue of the latter features the longest reported Ge-Ge (2.563(1) Å) and Ge-C (2056(3) Å) single bond.<sup>23</sup> LD is also significantly stabilizing a large amount of different transition or lanthanide metal complexes.<sup>24,25</sup>

Another field in which LD was found to be influential is the structure and stability of biomolecules like proteins, enzymes or DNA. Grimsley *et al.* measured the stability of several different proteins with varying side chains and found that hydrophobic interactions, to which LD interactions contribute, are the major driving force towards the generation of protein tertiary and quaternary structure.<sup>26,27</sup> Additionally, computational studies focussed on noncovalent interactions in biomolecules emphasized the importance of LD to these systems.<sup>5,28</sup>

Alongside the multitude of examples presented in which LD influences the structure and stability of molecules, the (2 + 2) cyclodimerization of substituted benzyne (**6**) reported by Akai *et al.* represents an important example of a chemical reaction in which LD acts as a driving force towards a certain reactivity.<sup>29</sup> (Figure 3)

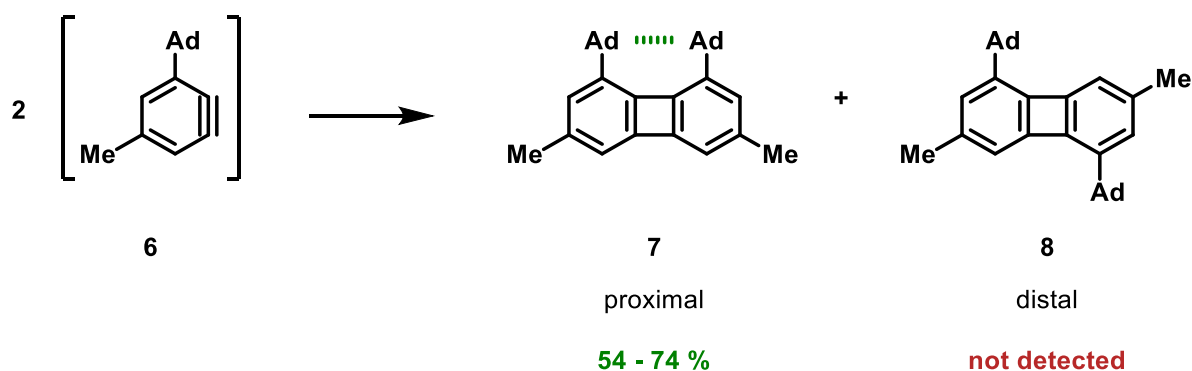


**Figure 3:** LD interactions between the two adamantyl groups is decisive for the regioselectivity of the (2 + 2) cyclodimerization of the benzynes **6**.

Here, the proximal regioisomer **7** with both adamantyl moieties on the same side of the molecule is the major product of this reaction. The distal isomer **8**, in which the adamantyl substituents point away from each other and consequently do not interact noncovalently, is not formed at all. Therefore, the classical idea that bulky groups like the adamantyl moieties have to repel each other if in close contact is proven to be not generally applicable. Instead, the reaction is directed towards the product with maximized LD stabilization in the transition state. A comparable reactivity was shown in the synthesis of 1,8-di(1-adamantyl)naphthalenes in which the favoured regioisomer also is the one with two adamantyl-groups positioned on the same side of the molecule.<sup>30</sup>

Not only the structure of starting materials in a chemical reaction can influence its outcome through LD interactions. In catalysis, selectivities or yields of reactions can be influenced by the strategic use of DEDs as well.<sup>31,32</sup> For example, Schreiner *et al.* studied the famous organocatalytic Corey-Bakshi-Shibata (CBS) reduction which was originally claimed to be directed to high enantioselectivities only due to repulsive interactions between catalyst and substrate. A series of experiments with a variety of substrates was able to falsify this claim by showing, that “*the success of the CBS reduction is due to an excellent balance of attractive and repulsive steric interactions, with LD interactions being key to rationalizing the experimental findings.*”<sup>33</sup> They were able to increase the yield and enantioselectivity of the reaction by adding large, bulky, and highly polarizable groups to the substrate and the backbone of the oxazaborolidine catalyst. Bistoni *et al.* also studied “*the delicate balance of steric and dispersion interactions in organocatalysis using high-level computational methods*”.<sup>34</sup> They found that LD could be an important design feature of future generations of organic catalysts, emphasizing the class of imidodiphosphorimidates (IDPi) as especially promising due to their clear recognition site with which the activated substrate can interact.<sup>35</sup>

In transition-metal-catalysis, we find another example for catalytic reactions which are significantly influenced by LD interactions. In the copper(I) hydride catalyzed hydroamination of unactivated olefins, the catalyst shows a significant increase in reactivity when substituted with bulky phosphine ligands.<sup>36</sup> (Figure 4)

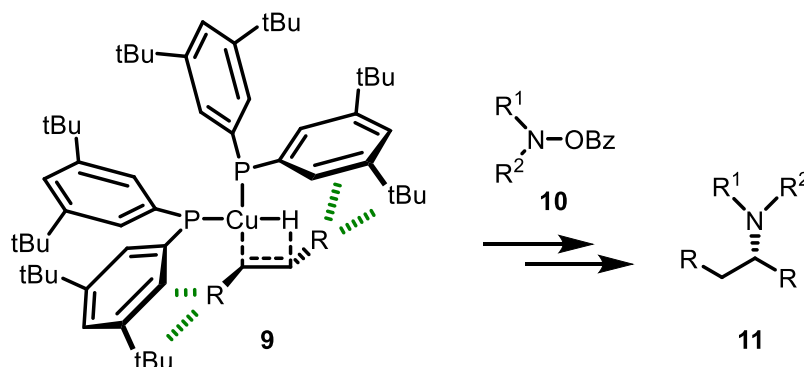


**Figure 4:** The reaction rate of the copper(I) hydride catalyzed hydroamination of unactivated olefins increases with increasing ligand size.

The authors anticipate “*that the dispersion-enabled reactivity revealed in the present study has broad implications in the design and development of more effective ligands for transition metal catalysis.*” This idea has been referred to in a variety of reviews discussing the possibility to systematically use LD interactions in the field of catalyst design.<sup>6,37</sup> Although today, easily accessible approaches towards truly rational catalyst design have not yet been developed, recent advances in computational chemistry represent a big step towards this goal.

## 1.4 London Dispersion Interactions in Solution

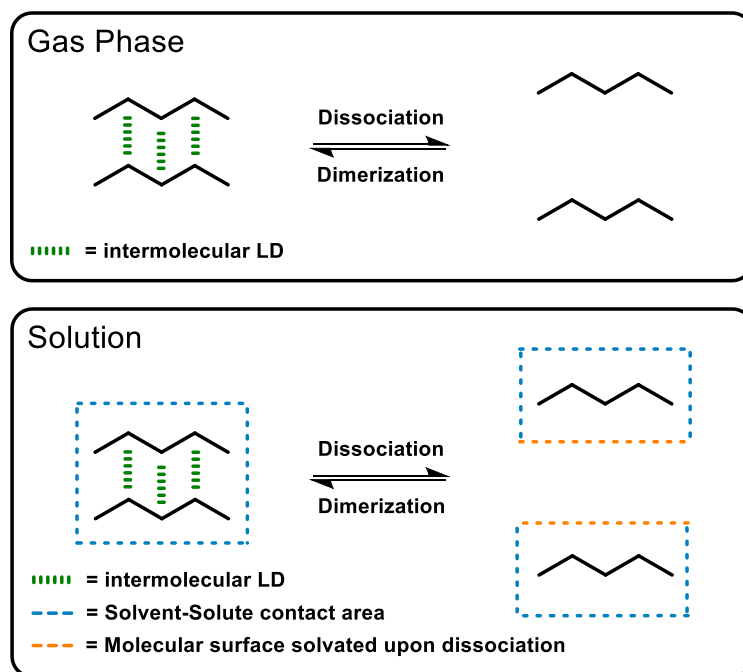


**Figure 5:** Schematic representation of the solvation effects that have to be taken into account to understand LD-bound dimers in solution.

Figure 5 uses the simplified monomer-dimer-equilibrium of pentane in both the gas phase and in solution as an example to explain the important difference between the quantification of LD in the gas phase and in solution. In the gas phase, the measurement of the equilibrated monomer/dimer ratio is sufficient, because the only energetic difference between associated and dissociated form is the LD stabilization present in the dimer. In solution, whilst the dimer is stabilized by LD interactions, the previously unsolvated molecular surface between the two pentane molecules in the monomer state is, upon dissociation, additionally solvated. This changes the net energy difference between the associated and dissociated form compared to the gas phase and ultimately leads to the compensation of a part of the LD stabilization in the dimer. Solute-solute and solute-solvent LD interactions are therefore competing with each other.<sup>38</sup> This phenomenon was studied extensively over the last decade with various different experimental approaches which are described in the following.

In 2013, Cockroft *et al.* raised the question: “*How much do van der Waals dispersion forces contribute to molecular recognition in solution?*”<sup>7</sup> The experimental setup used to answer this question is based on the renowned Wilcox molecular balance **12**. (Figure 6)

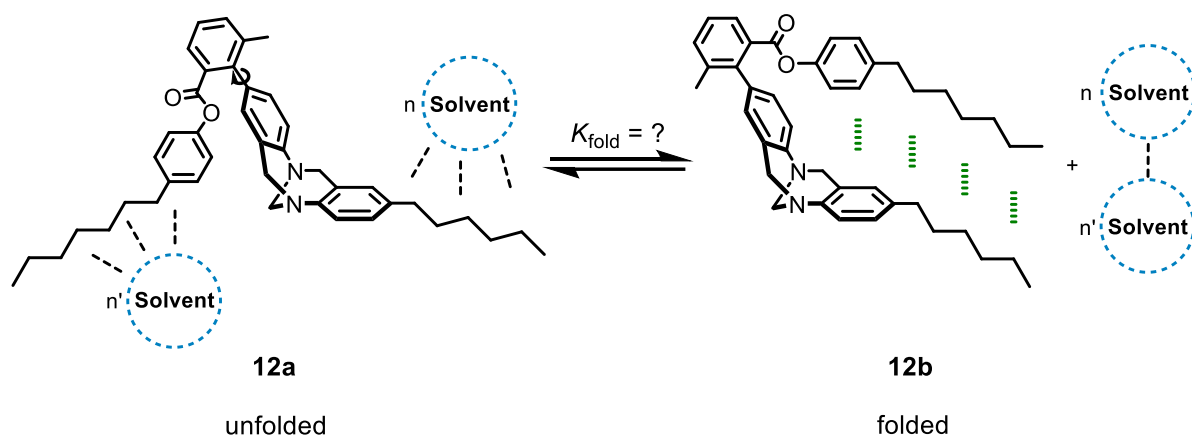


**Figure 6:** Wilcox type molecular torsion balance used for the quantification of LD in solution.

The experimentally obtained LD-stabilization between the alkyl chains was found to be one order of magnitude smaller than predicted by quantum chemical computations. “*The most likely explanation [...] is that dispersion forces are effectively cancelled by competitive dispersion interactions with the solvent*”, they state. Furthermore, the authors mention that this discrepancy could also be caused by computations which did not consider the entropic penalty required for alkyl chain association. Since the alkyl chains in **12** are flexible, there could be a variety of conformers in which the two alkyl moieties are not, or only partly, in close proximity to each other.

To circumvent the use of gas-phase computations as a comparison to solution phase experiments, Chen *et al.* studied “*the contribution of LD to the bond dissociation of proton bound dimers, both in the gas phase and in dichloromethane solution*”.<sup>8</sup> (Figure 7)

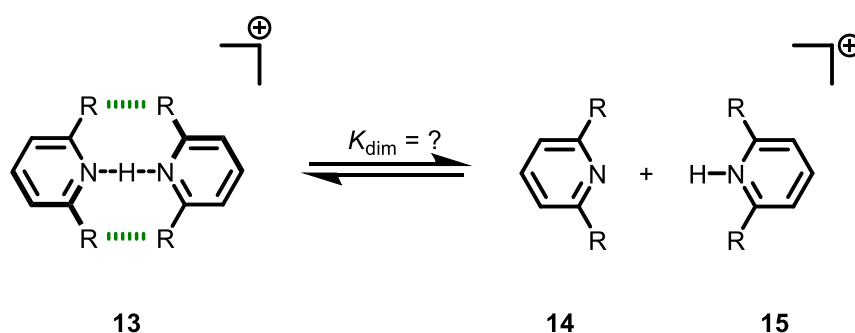


**Figure 7:** The equilibrium of proton-bound dimers with their respective monomers was studied both in the gas phase and in solution.

The comparison of gas- and solution-phase measurements for the same system allows for a more precise quantification of the compensation of LD in solution compared to the previous example. For dichloromethane as the solvent, this compensation was estimated to be around

70%, which is still large, but smaller than the order of magnitude proposed earlier. To study the solvent and temperature dependence of this compensation, comparable experiments were repeated in a group of solvents covering a wide range of refractive indices and bulk polarizabilities.<sup>39</sup> It was shown that the compensation of LD in solution throughout all solvents and at a broad range of temperatures is ranging between 60% and 80%. This indicates that the amount of LD-compensation in solution is largely solvent independent.

To exclude the influence of local dipoles introduced to the molecular balance system by the presence of different heteroatoms, Schreiner *et al.* studied the solvent and temperature dependency of the equilibrium between 1,4- and 1,6-di-*tert*-butyl-1,3,5,7-cyclooctatetraene **16** (COT).<sup>9</sup> (Figure 8)

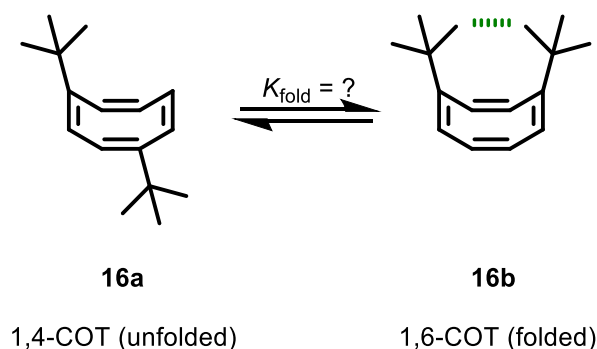
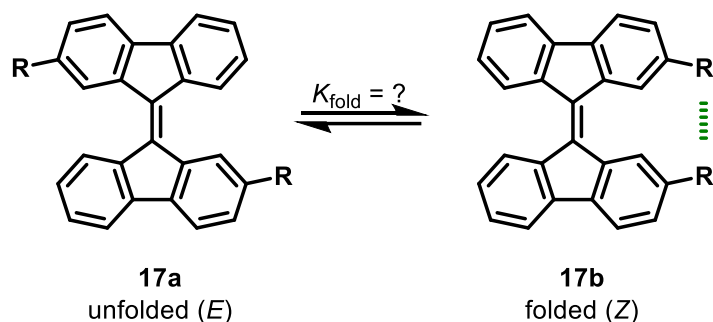


**Figure 8:** The “folded” 1,6-COT is favored throughout 16 common organic solvents.

It was found that the LD-stabilized 1,6-COT **16b** is favored in all solvents, underlining that LD is not fully compensated in solution. The same molecular balance equipped with diamantoid-substituents was used to explore the “limits of London dispersion stabilization” in alkane solvents.<sup>40</sup>

In our study, which is based on the 9,9'-bifluorenylidene molecular balance system **17**, a multitude of different substituents were attached to understand the influence of size and flexibility of the interacting groups on the overall interaction energy present in solution. (Figure 9)



R = Methyl, Ethyl, *n*-Propyl, *n*-Butyl, *n*-Pentyl, *n*-Nonyl, *iso*-Propyl, Cyclohexyl, *tert*-Butyl, Adamantyl, Diamantyl, Phenyl, Pentafluorophenyl, Trityl.

**Figure 9:** Various 2,2'-substituted-9,9'-bifluorenylidene were used as molecular balances to study the influence of DED-size and flexibility on the overall interaction energy in solution

### 1.4 London Dispersion Interactions in Quantum Mechanical Computations

Today, the use of computational chemistry methods that take LD into account is considered best practice.<sup>41</sup> This was significantly driven by several examples, where traditional computational methods, which did not adequately account for LD interactions, conflicted with experimental results.<sup>42,43</sup> To begin, we will briefly explain the different tools that were developed for the quantification of LD in computational chemistry.

The first main method for the computational quantification of noncovalent interactions is based on symmetry-adapted perturbation theory (SAPT).<sup>44,45</sup> It assesses the interaction energy of molecular fragments *via* the perturbation of the molecular complex and allows qualitative comparison of the different types of interactions which constitute the overall interaction energy. This makes it a useful tool to understand how strongly LD influences a certain system. Also, the distance-dependency of these different noncovalent interactions can be probed using SAPT. (Figure 10)

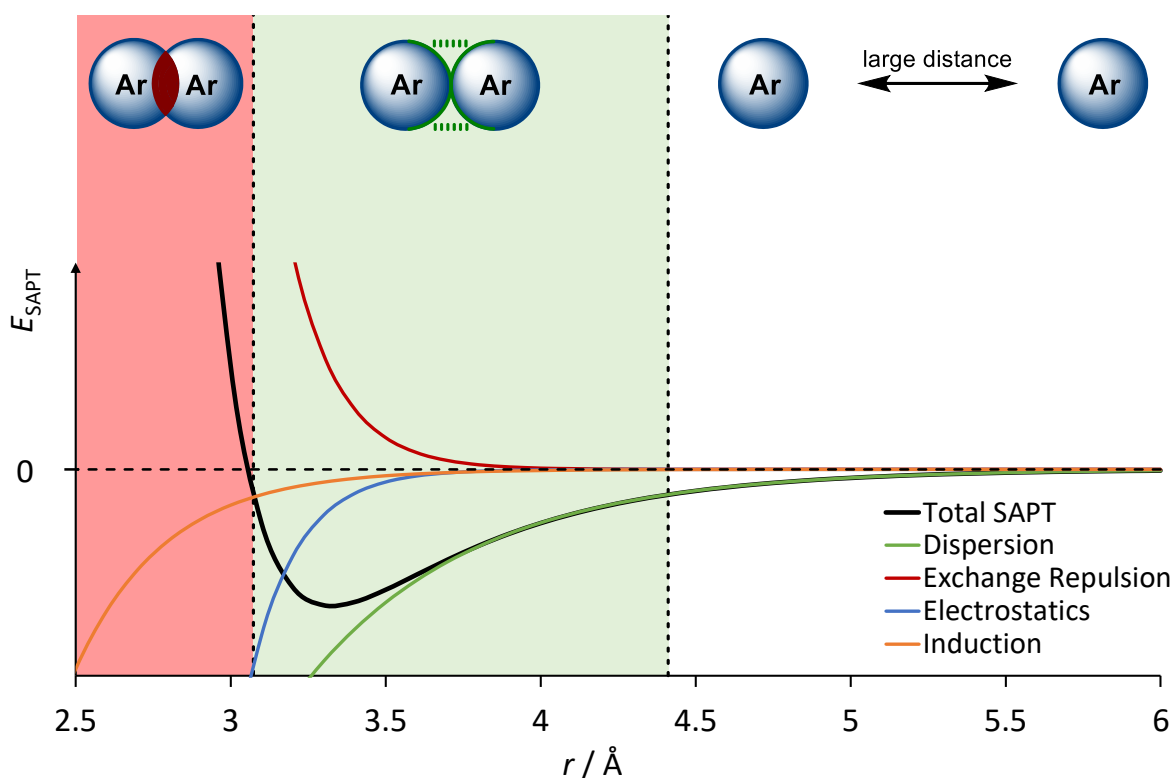


**Figure 10:** Exemplary SAPT results for the argon dimer as a model system. In dependence of the interatomic distance, the interaction can either be repulsive, attractive, or nonexistent.

Secondly, one can simply compute the energy of a LD-bound complex and subtract the computed monomer energies to obtain estimates for the overall interaction energy present in the dimer. (Figure 11)

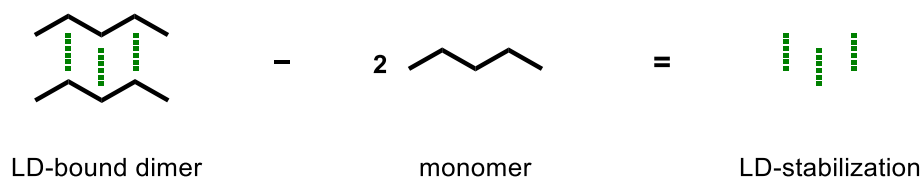


**Figure 11:** Isolation of the LD-stabilization present in a dimer by subtracting the computed monomer energies.

A similar approach is used for the quantification of LD-stabilization in intramolecular interactions. By computing the same system twice, once while employing a LD-correction and once without, one can subtract the obtained energies and therefore estimate the overall LD-stabilization present in the system.<sup>46</sup> Additionally, energy decomposition analysis (EDA) can be used to quantify the LD-contribution to the overall interaction energy in a system.<sup>47</sup>

Since LD is an electron correlation effect, the computational quantification of LD requires an accurate description of electron correlation. Thus, within the family of wave function theory (WFT), post-HF methods are suitable for the quantification of LD. Coupled cluster methods such as CCSD(T) are considered to be the gold standard in this area of theory.<sup>48-50</sup> Due to high computational costs, the DLPNO variants of these methods are frequently used instead of their canonical counterparts.<sup>51</sup>

While local DFT is intrinsically unable to cover LD effects, there are modern DFT methods that are explicitly designed to treat electron correlation more precisely and to account for LD.<sup>52-55</sup> In recent years, empirical double hybrid DFT methods combined the chemical accuracy of WFT with the shorter computation times of DFT.<sup>56</sup>

For molecules with a large conformational flexibility it is apparent that the comparison of just two single point energies will not lead to accurate results for overall LD-stabilization which is strongly distance-dependent. The conformer-rotamer ensemble sampling tool (CREST) can be used to address this issue.<sup>57</sup> It employs fast, semiempirical tight-binding based methods like GFN2-xTB<sup>58</sup> to efficiently generate conformer ensembles even for very large systems.<sup>59</sup> These can be employed in the command-line energetic sorting (CENSO) algorithm which gives a Boltzmann-averaged free energy value representing the full ensemble.<sup>60</sup>

The most important computational tool for the visualization of noncovalent interactions is NCIPLOT.<sup>61,62</sup> It is based on the reduced density gradient which was conceived as a correction factor for semi-local density approximations in DFT.<sup>63</sup> As an example, Figure 12 shows the NCIPLOT of *Z*-2,2'-Dicyclohexyl-9,9'-bifluorenylidene, one of our molecular balances.

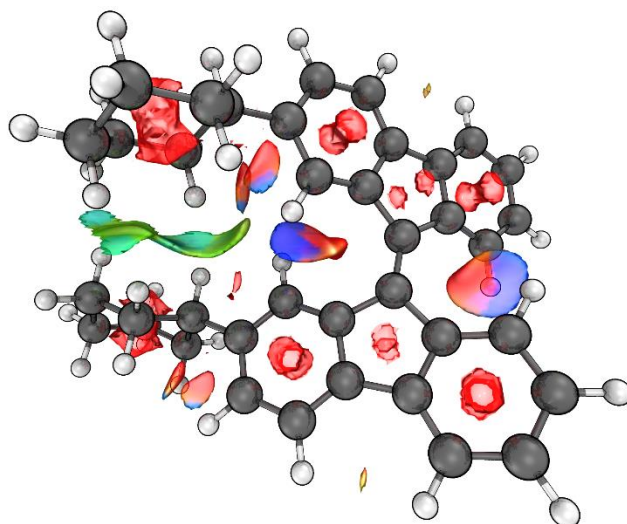


**Figure 12:** NCIPLOT of Z-2,2'-dicyclohexyl-9,9'-bifluorenylidene. Green symbolizes areas in which attractive noncovalent interactions are present, while red shows areas in which Pauli repulsion is present.

The increased accuracy of today's computational chemistry methods allows us to decently describe effects with chemical accuracy. One way to continuously improve today's computational accuracy is to compare very accurate experimental benchmark measurements with the results of state-of-the-art computations.<sup>64</sup> One of the most important classes of organic experimental benchmark systems for computational chemistry are molecular balances.

## 1.5 Molecular Balances

### 1.5.1 The General Concept of a Molecular Balance

In contrast to a macroscopic scale that is used to determine the mass of an object in everyday life, a molecular balance is a microscopic system used to quantify noncovalent interactions on the molecular level. The term “*molecular torsion balance*” was first introduced in 1994,<sup>65</sup> although, organic molecules were used to quantify noncovalent interactions as early as 1974.<sup>66</sup> Until today, molecular balances were used to study  $\pi$ - $\pi$ ,<sup>67,68</sup> functional group- $\pi$ ,<sup>67,69</sup> LD,<sup>70</sup> and solvophobic interactions.<sup>71</sup>

To introduce this topic, we will focus on molecular torsion balances which are the most commonly used systems in this field. A molecular torsion balance is generally based on the equilibrium between two spectroscopically distinguishable rotamers often called “*folded*” and “*unfolded*”. In the folded state, the two functional groups of interest are brought into

close proximity to each other and therefore interact noncovalently. In the unfolded state, these noncovalent interactions are “switched off” due to a larger distance between the groups. (Figure 13)

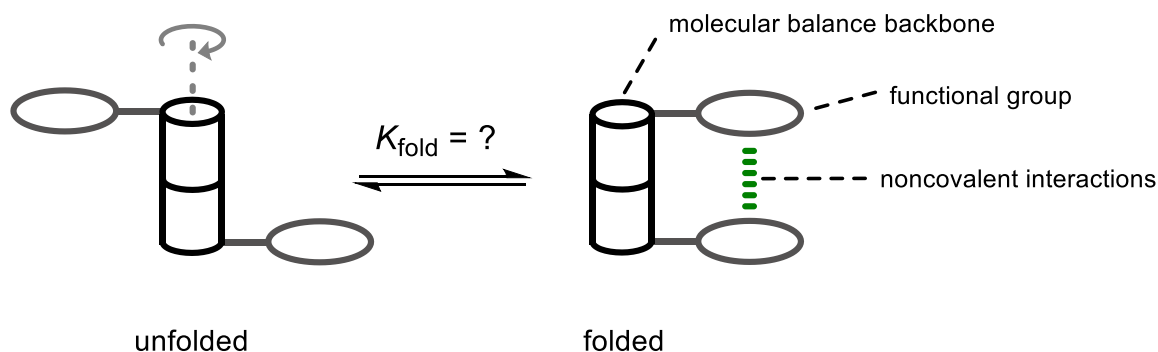


**Figure 13:** Schematic representation of a molecular torsion balance.

In these systems, equilibration between these two states takes place *via* slow rotation of a single bond. The ratio between the folded and the unfolded state of the molecular torsion balance can be introduced into the law of mass action (2) to receive the equilibrium constant of the folding reaction.

$$K_{\text{fold}} \cong \frac{\text{folded}}{\text{unfolded}} \quad (2)$$

For an ideal molecular balance investigated in the gas phase (Figure 13),  $K_{\text{fold}}$  is exclusively influenced by stabilizing or destabilizing noncovalent interactions between the functional groups in the folded state. When  $K_{\text{fold}}$  is now inserted into (3), where  $T$  is the absolute temperature and  $R$  the gas constant, the obtained folding free energy  $\Delta G_{\text{fold}}$  gives direct thermodynamic information about the nature and dimension of the interaction between both functional groups.

$$\Delta G_{\text{fold}} = -RT \ln (K_{\text{fold}}) \quad (3)$$

Since the molecular balances that have been experimentally employed for the quantification of noncovalent interactions are not ideal systems, their folded/unfolded equilibrium is not only influenced by the noncovalent interactions between the substituents, but also by other effects. Most importantly, since  $K_{\text{fold}}$  is mainly measured in solution using nuclear magnetic resonance spectroscopy (NMR), solvophobic effects must be taken into account when interpreting the experimental results.<sup>7,8,72–74</sup>

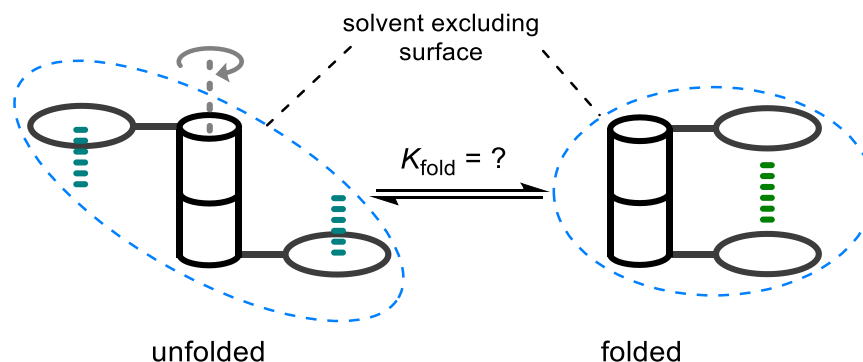


**Figure 14:** The solvophobic effect influences the folded/unfolded equilibrium of molecular balances in solution, as folded and unfolded isomers possess different solvent excluding surfaces.

This is due to the fact that the unfolded isomer generally has a larger solvent excluding surface (SES) compared to the folded isomer because of its lack of intramolecular contact area between the functional groups (Figure 14). A larger solute-solvent contact area in the unfolded state also leads to a larger solvation free energy  $\Delta G_{\text{solv}}$  compared to the folded state which influences the folded/unfolded equilibrium towards the unfolded state. For LD, the attenuation by solvophobic effects was measured to be between 60% and 80%.<sup>8,39</sup> Other secondary factors that could distort the experimental results are “*background steric, solvent and secondary intramolecular interactions*”.<sup>67</sup> To account for these effects, control balances were synthesized and used in thermodynamic double-mutant cycles.<sup>75</sup> Also, molecular balances were designed to possess a high degree of symmetry which lead to a decrease in experimental distortion due to secondary effects.<sup>9,74,76,77</sup>

## 1.5.2 Different Classes of Molecular Balances

### 1.5.2.1 Molecular Torsion Balances

Pioneering work in the field of molecular torsion balances was performed by Ōki *et al.* by using 1,9-disubstituted triptycene derivatives<sup>78</sup> like **18** to study  $\sigma$ - $\sigma$ <sup>79–83</sup> and  $\sigma$ - $\pi$ <sup>84,85</sup> interactions (Figure 15).

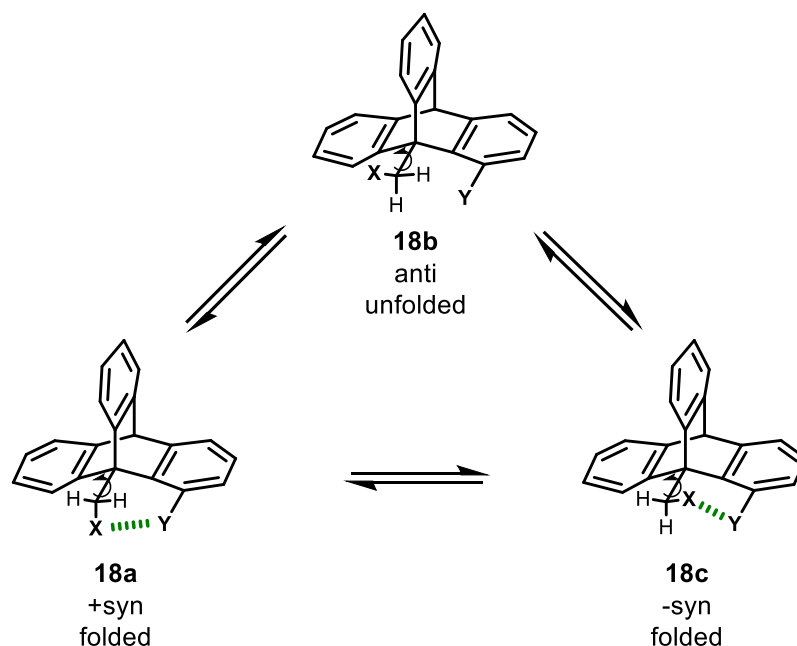


**Figure 15:** Slow rotation around the single bond in the 1-position of 1,9-disubstituted triptycenes allows for quantification of the differently stabilized rotamers via NMR.

More recently, Gung *et al.* used similar balances to study  $\pi$ - $\pi$  interactions.<sup>86-90</sup> The bond rotation of the substituent in the 1-position of triptycene based balances is slow enough to allow for NMR peak separation of the three different rotamers. Deviations from the statistical 2:1 folded/unfolded ratio can be interpreted with regard to noncovalent interactions between the substituents X and Y or solvent effects.

Another very important and widely employed class of molecular torsion balances was developed by Wilcox *et al.* in 1994.<sup>65</sup> (Figure 16) Its structure based on Tröger's base with a biphenyl-rotor allows switching between a folded (**19b**) and an unfolded (**19a**) state.

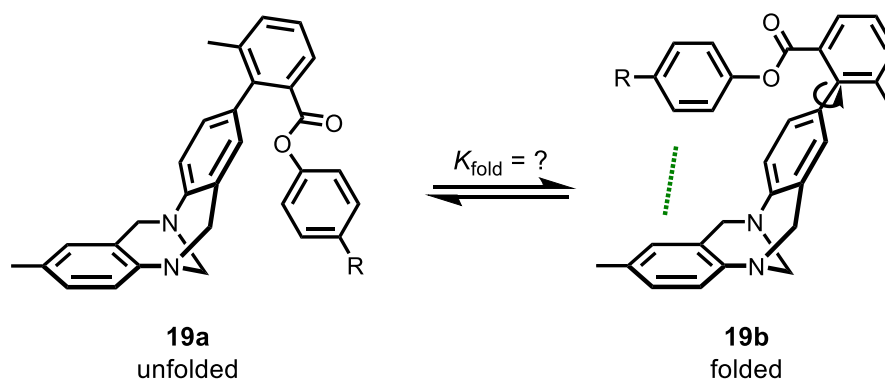


**Figure 16:** The Wilcox molecular torsion balance was intensively used to study aromatic edge-to-face interactions.

Slow bond rotation due to double-*ortho* substitution of the biphenyl rotor allows for quantification of folded/unfolded ratios *via* NMR. Wilcox-balances were used to study aromatic edge-to-face interactions,<sup>65,91–93</sup> CH- $\pi$  interactions,<sup>91,94</sup> functional group interactions,<sup>95–97</sup> LD,<sup>7</sup> and solvent effects.<sup>72,73,94,98,99</sup> In contrast to **19** which aligns the two aromatic moieties for interaction in an edge-to-face fashion, the molecular balance **20** developed by Shimizu *et al.* was designed to study aromatic face-to-face interactions (Figure 17).<sup>69,100–103</sup>

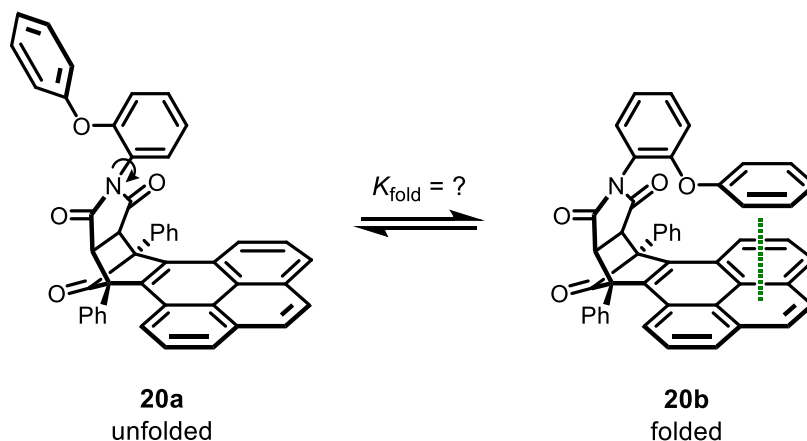


**Figure 17:** Molecular torsion balance developed by Shimizu *et al.* for the quantification of noncovalent interactions between various functional groups with an aromatic surface.

Additionally, systems that are based on the same *N*-arylamide backbone were used to study CH/D- $\pi$ <sup>104–107</sup> and heteroatom- $\pi$ <sup>108–112</sup> interactions as well as the distance dependence of the interplay of London dispersion and Pauli repulsion.<sup>113</sup>

### 1.5.2.2 Dimerization Balances

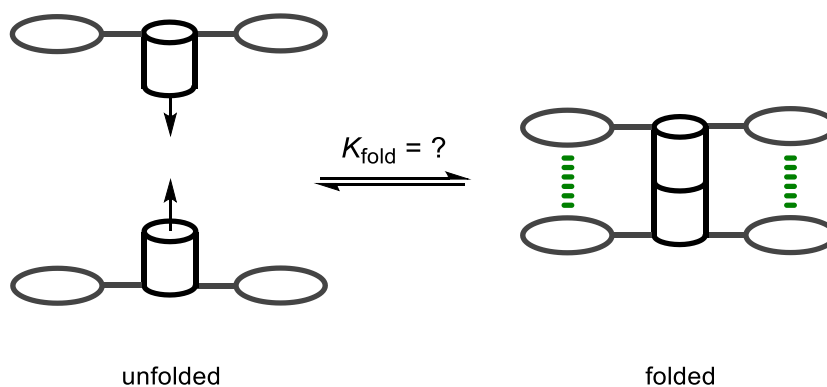


**Figure 18:** Schematic representation of a molecular balance based on a monomer-dimer equilibrium.

Compared to the aforementioned unimolecular balances, monomer-dimer balances are based on the quantifiable equilibrium between free monomers and their dimeric form which is stabilized via noncovalent interactions (Figure 18). For example, Chen *et al.* measured the dissociation energy of various differently substituted proton-bound *N*-heterocyclic dimers (Figure 7) in solution as well as in the gas phase.<sup>8,39</sup> The comparison of both measurements lead to the conclusion that in dichloromethane LD is attenuated by about 70% compared to the gas phase due to competitive interactions with the solvent. Albrecht *et al.* used hierarchically assembled dinuclear titanium(IV) helicates as a molecular balance based on a monomer-dimer equilibrium to quantify LD between linear, branched, and cyclic alkyl substituents in deuterated DMSO.<sup>114</sup> In addition, the dimerization of all-*meta* substituted trityl radicals to the respective hexaphenylethanes has been studied extensively to understand the stabilizing influence dispersion energy donors can have on strained systems.<sup>115,116</sup>

### 1.5.2.3 Molecular Balances Based on Double Bond Isomerization

The group of Wegner established the use of substituted azobenzene switches as molecular balances for the quantification of LD.<sup>117</sup> (Figure 19) For this, a solution of the thermodynamically favoured *E*-isomer **21a** is irradiated with UV-light to generate the strained *Z*-isomer **21b** which is then slowly reacting back to the *E*-isomer. The reaction kinetics of this process were measured with UV-Vis spectroscopy in dependence of the substituents attached to the azobenzene core.

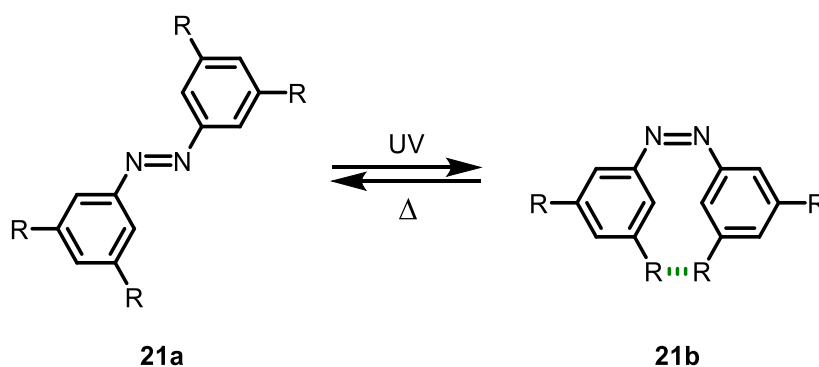


**Figure 19:** The influence of DEDs on the relaxation kinetics of the photochemically generated *Z*-azobenzenes is measured.

They demonstrated that the introduction of bulky and highly polarizable substituents in the *meta*-positions of the azobenzene increases the *Z*-isomers half-life from 3 h (unsubstituted) to over 50 h (adamantyl-substituted) due to LD interactions. The same system was employed to measure the influence of increasing length of alkyl-chains on the equilibration kinetics in

different solvents.<sup>118,119</sup> These measurements showed that an increase in chain length only led to a significant increase in the *Z*-isomers half-life until *n*-butyl-substitution. For longer chains, the obtained half-lives plateaued at a comparable level, indicating an increasing influence of entropic penalties for chain association. The half-life also increased with increasing solvent polarity, suggesting that solvophobicity is a major driver for chain association in linear alkyl chains.

Another example of this subclass of molecular balances is the equilibrium between 1,4- and 1,6-di-substituted cycloocta-1,3,5,7-tetraenes which has been used to study the solvent dependency of LD for different bulky hydrocarbons.<sup>9,40</sup> (Figure 8) Equilibration already takes place at room temperature through a double bond valence shift in combination with a ring inversion. Additionally, this system was used to study LD between silyl protecting groups<sup>76</sup> and to experimentally assess the strength of hydrogen bonding interactions in the cyclic water dimer.<sup>77</sup>

In our work, we employed various 2,2'-disubstituted-9,9'-bifluorenylidenes as synthetically more accessible molecular balances based on double bond isomerization. (Figure 9) Pioneering work with this class of molecular balances was performed by Minabe *et al.* by studying the influence of difference in chain length of acyl-substituents on the *E/Z*-ratios *via* base-catalyzed isomerization.<sup>120,121</sup> To exclude the influence of the base on the obtained ratios, we studied the kinetics of the thermal *E/Z*-equilibration at elevated temperatures. At 333 K, we found the equilibration to be fast enough to be completed over night whilst the temperature was still low enough to allow us the use of most of the important organic solvents. We used this class of molecular balance to study the interplay of solvophobic effects, LD, and Pauli repulsion in solution.<sup>74,122</sup>

## 1.6 Conclusions and Outlook

In this work we synthesized and spectroscopically investigated a variety of differently substituted molecular balances based on the 9,9'-bifluorenylidene backbone in several different organic solvents.

In the first publication, we used the hydrocarbon molecular balance 2,2'-diethynyl-9,9'-bifluorenylidene to emphasize that the cohesive energy density (ced) of the solvent is a decent quantitative descriptor of solvophobic effects in organic solvents. We measured the *E/Z*-equilibrium of the molecular balances in 15 deuterated organic solvents *via* <sup>1</sup>H-NMR and found a good correlation between the ced of the solvent and the *E/Z* ratio obtained experimentally.

In the second publication we synthesized a group of 14 differently substituted molecular balances also based on the 9,9'-bifluorenylidene backbone. We measured the *E/Z*-equilibrium of all molecular balance in 7 deuterated organic solvents *via* <sup>1</sup>H-NMR and found that LD generally shifts the *E/Z* equilibrium towards the *Z*-isomer. Only for very small substituents (no interaction) or very large substituents (repulsive interactions), some examples were found in which the *Z*-isomer was not favoured or even disfavoured. This clearly demonstrated that in dependence of the structural surroundings, the size, shape, and degree of flexibility of a DED are decisive for the maximization of LD-stabilization in a certain system. In our work, the substitution of the molecular balance with two cyclohexyl-groups led to the largest *Z*-preference. We attribute this to the large size and polarizability of the cyclohexyl moiety combined with enough flexibility to perfectly position each other right on the energy-minimum of the delicate balance between LD and Pauli repulsion. Along with other studies, this work contradicts the recent suggestion that LD interactions could be completely cancelled out in solution due to competing interactions with the solvent.<sup>8,9,39</sup>

Furthermore, our experimental measurements could be used as a dataset of very accurate solution phase data on LD-influenced systems which could be employed by the computational chemistry community as a benchmark set to test the accuracy of computational solvent models, which to date still lack accuracy. The improved computational tools of tomorrow could give future chemists the ability to strategically use LD as a design principle in molecular solution phase chemistry.

## 1.7 Bibliography

- (1) London, F. The General Theory of Molecular Forces. *T. Faraday Soc.* **1937**, *33* (0), 8b–26. <https://doi.org/10.1039/TF937330008B>.
- (2) London, F. Zur Theorie Und Systematik Der Molekularkräfte. *Z. Phys.* **1930**, *63* (3), 245–279. <https://doi.org/10.1007/BF01421741>.
- (3) Eisenschitz, R.; London, F. Über Das Verhältnis Der van Der Waalsschen Kräfte Zu Den Homöopolaren Bindungskräften. *Z. Phys.* **1930**, *60* (7–8), 491–527. <https://doi.org/10.1007/BF01341258>.
- (4) Wagner, J. P.; Schreiner, P. R. London Dispersion in Molecular Chemistry—Reconsidering Steric Effects. *Angew. Chem. Int. Ed.* **2015**, *54* (42), 12274–12296. <https://doi.org/10.1002/ANIE.201503476>.
- (5) Černý, J.; Hobza, P. Non-Covalent Interactions in Biomacromolecules. *Phys. Chem. Chem. Phys.* **2007**, *9* (39), 5291–5303. <https://doi.org/10.1039/B704781A>.
- (6) Neel, A. J.; Hilton, M. J.; Sigman, M. S.; Toste, F. D. Exploiting Non-Covalent  $\pi$  Interactions for Catalyst Design. *Nature* **2017**, *543* (7647), 637–646. <https://doi.org/10.1038/nature21701>.
- (7) Yang, L.; Adam, C.; Nichol, G. S.; Cockroft, S. L. How Much Do van Der Waals Dispersion Forces Contribute to Molecular Recognition in Solution? *Nat. Chem.* **2013**, *5* (12), 1006–1010. <https://doi.org/10.1038/nchem.1779>.
- (8) Pollice, R.; Bot, M.; Kobylanskii, I. J.; Shenderovich, I.; Chen, P. Attenuation of London Dispersion in Dichloromethane Solutions. *J. Am. Chem. Soc.* **2017**, *139* (37), 13126–13140. <https://doi.org/10.1021/JACS.7B06997>.
- (9) Schümann, J. M.; Wagner, J. P.; Eckhardt, A. K.; Quanz, H.; Schreiner, P. R. Intramolecular London Dispersion Interactions Do Not Cancel in Solution. *J. Am. Chem. Soc.* **2021**, *143* (1), 41–45. <https://doi.org/10.1021/JACS.0C09597>.
- (10) Dobson, J. F. Beyond Pairwise Additivity in London Dispersion Interactions. *Int. J. Quantum Chem.* **2014**, *114* (18), 1157–1161. <https://doi.org/10.1002/qua.24635>.
- (11) Kahr, B.; Engen, D. Van; Mislow, K. Length of the Ethane Bond in Hexaphenylethane and Its Derivatives. *J. Am. Chem. Soc.* **1986**, *108* (26), 8305–8307. <https://doi.org/10.1021/JA00286A053>.
- (12) Gomberg, M. An Instance of Trivalent Carbon: Triphenylmethyl. *J. Am. Chem. Soc.* **1900**, *22* (11), 757–771. <https://doi.org/10.1021/JA02049A006>.
- (13) McBride, J. M. The Hexaphenylethane Riddle. *Tetrahedron* **1974**, *30* (14), 2009–2022. [https://doi.org/10.1016/S0040-4020\(01\)97332-6](https://doi.org/10.1016/S0040-4020(01)97332-6).
- (14) Rösel, S.; Schreiner, P. R. Computational Chemistry as a Conceptual Game Changer: Understanding the Role of London Dispersion in Hexaphenylethane Derivatives (Gomberg Systems). *Isr. J. Chem.* **2022**, *62* (1–2), e202200002. <https://doi.org/10.1002/IJCH.202200002>.

- (15) Grimme, S.; Schreiner, P. R. Steric Crowding Can Stabilize a Labile Molecule: Solving the Hexaphenylethane Riddle. *Angew. Chem. Int. Ed.* **2011**, *50* (52), 12639–12642. <https://doi.org/10.1002/ANIE.201103615>.
- (16) Rösel, S.; Quanz, H.; Logemann, C.; Becker, J.; Mossou, E.; Cañadillas-Delgado, L.; Caldeweyher, E.; Grimme, S.; Schreiner, P. R. London Dispersion Enables the Shortest Intermolecular Hydrocarbon H···H Contact. *J. Am. Chem. Soc.* **2017**, *139* (22), 7428–7431. <https://doi.org/10.1021/jacs.7b01879>.
- (17) Fokin, A. A.; Chernish, L. V.; Gunchenko, P. A.; Tikhonchuk, E. Yu.; Hausmann, H.; Serafin, M.; Dahl, J. E. P.; Carlson, R. M. K.; Schreiner, P. R. Stable Alkanes Containing Very Long Carbon–Carbon Bonds. *J. Am. Chem. Soc.* **2012**, *134* (33), 13641–13650. <https://doi.org/10.1021/ja302258q>.
- (18) Maier, G.; Pfriem, S.; Schäfer, U.; Matusch, R. Tetra-Tert-Butyltetrahedrane. *Angew. Chem. Int. Ed.* **1978**, *17* (7), 520–521. <https://doi.org/10.1002/ANIE.197805201>.
- (19) Monteiro, N. K. V.; De Oliveira, J. F.; Firme, C. L. Stability and Electronic Structures of Substituted Tetrahedranes, Silicon and Germanium Parents – a DFT, ADMP, QTAIM and GVB Study. *New J. Chem.* **2014**, *38* (12), 5892–5904. <https://doi.org/10.1039/C4NJ01271B>.
- (20) Lüttschwager, N. O. B.; Wassermann, T. N.; Mata, R. A.; Suhm, M. A. The Last Globally Stable Extended Alkane. *Angew. Chem. Int. Ed.* **2013**, *52* (1), 463–466. <https://doi.org/10.1002/ANIE.201202894>.
- (21) Schäfer, A.; Weidenbruch, M.; Peters, K.; von Schnering, H.-G. Hexa-Tert-Butylcyclotrisilane, a Strained Molecule with Unusually Long Si–Si and Si–C Bonds. *Angew. Chem. Int. Ed.* **1984**, *23* (4), 302–303. <https://doi.org/10.1002/anie.198403021>.
- (22) Wiberg, N.; Schuster, H.; Simon, A.; Peters, K. Hexa-Tert-Butyldisilane—the Molecule with the Longest Si–Si Bond. *Angew. Chem. Int. Ed.* **1986**, *25* (1), 79–80. <https://doi.org/10.1002/anie.198600791>.
- (23) Weidenbruch, M.; Grimm, F.-T.; Herrndorf, M.; Schäfer, A.; Peters, K.; von Schnering, H. G. Hexa-t-Butyldigerman Und Hexa-t-Butylcyclotrigerman: Moleküle Mit Den Derzeit Längsten Ge–Ge- Und Ge–C-Bindungen. *J. Organomet. Chem.* **1988**, *341* (1), 335–343. [https://doi.org/10.1016/0022-328X\(88\)89087-9](https://doi.org/10.1016/0022-328X(88)89087-9).
- (24) Liptrot, D. J.; Power, P. P. London Dispersion Forces in Sterically Crowded Inorganic and Organometallic Molecules. *Nat. Rev. Chem.* **2017**, *1* (1), 1–12. <https://doi.org/10.1038/s41570-016-0004>.
- (25) Mears, K. L.; Power, P. P. Beyond Steric Crowding: Dispersion Energy Donor Effects in Large Hydrocarbon Ligands. *Accounts Chem. Res.* **2022**, *55* (9), 1337–1348. <https://doi.org/10.1021/ACS.ACCOUNTS.2C00116>.
- (26) Pace, C. N.; Fu, H.; Fryar, K. L.; Landua, J.; Trevino, S. R.; Shirley, B. A.; Hendricks, M. M.; Imura, S.; Gajiwala, K.; Scholtz, J. M.; Grimsley, G. R. Contribution of Hydrophobic Interactions to Protein Stability. *J. Mol. Biol.* **2011**, *408* (3), 514–528. <https://doi.org/10.1016/j.jmb.2011.02.053>.

- (27) Nick Pace, C.; Martin Scholtz, J.; Grimsley, G. R. Forces Stabilizing Proteins. *FEBS Lett.* **2014**, *588* (14), 2177–2184. <https://doi.org/10.1016/J.FEBSLET.2014.05.006>.
- (28) Kolář, M.; Kubař, T.; Hobza, P. On the Role of London Dispersion Forces in Biomolecular Structure Determination. *J. Phys. Chem. B* **2011**, *115* (24), 8038–8046. <https://doi.org/10.1021/jp202878d>.
- (29) Ikawa, T.; Yamamoto, Y.; Heguri, A.; Fukumoto, Y.; Murakami, T.; Takagi, A.; Masuda, Y.; Yahata, K.; Aoyama, H.; Shigeta, Y.; Tokiwa, H.; Akai, S. Could London Dispersion Force Control Regioselective (2 + 2) Cyclodimerizations of Benzynes? YES: Application to the Synthesis of Helical Biphenylenes. *J. Am. Chem. Soc.* **2021**, *143* (29), 10853–10859. <https://doi.org/10.1021/jacs.1c05434>.
- (30) Aikawa, H.; Takahira, Y.; Yamaguchi, M. Synthesis of 1,8-Di(1-Adamantyl)Naphthalenes as Single Enantiomers Stable at Ambient Temperatures. *Chem. Commun.* **2011**, *47* (5), 1479–1481. <https://doi.org/10.1039/C0CC03025B>.
- (31) Wende, R. C.; Seitz, A.; Niedek, D.; Schuler, S. M. M.; Hofmann, C.; Becker, J.; Schreiner, P. R. The Enantioselective Dakin–West Reaction. *Angew. Chem. Int. Ed.* **2016**, *55* (8), 2719–2723. <https://doi.org/10.1002/ANIE.201509863>.
- (32) Procházková, E.; Kolmer, A.; Ilgen, J.; Schwab, M.; Kaltschnee, L.; Fredersdorf, M.; Schmidts, V.; Wende, R. C.; Schreiner, P. R.; Thiele, C. M. Uncovering Key Structural Features of an Enantioselective Peptide-Catalyzed Acylation Utilizing Advanced NMR Techniques. *Angew. Chem. Int. Ed.* **2016**, *55* (51), 15754–15759. <https://doi.org/10.1002/ANIE.201608559>.
- (33) Eschmann, C.; Song, L.; Schreiner, P. R. London Dispersion Interactions Rather than Steric Hindrance Determine the Enantioselectivity of the Corey–Bakshi–Shibata Reduction. *Angew. Chem. Int. Ed.* **2021**, *60* (9), 4823–4832. <https://doi.org/10.1002/ANIE.202012760>.
- (34) Yepes, D.; Neese, F.; List, B.; Bistoni, G. Unveiling the Delicate Balance of Steric and Dispersion Interactions in Organocatalysis Using High-Level Computational Methods. *J. Am. Chem. Soc.* **2020**, *142* (7), 3613–3625. <https://doi.org/10.1021/jacs.9b13725>.
- (35) Schreyer, L.; Properzi, R.; List, B. IDPi Catalysis. *Angew. Chem. Int. Ed.* **2019**, *58* (37), 12761–12777. <https://doi.org/10.1002/anie.201900932>.
- (36) Lu, G.; Liu, R. Y.; Yang, Y.; Fang, C.; Lambrecht, D. S.; Buchwald, S. L.; Liu, P. Ligand-Substrate Dispersion Facilitates the Copper-Catalyzed Hydroamination of Unactivated Olefins. *J. Am. Chem. Soc.* **2017**, *139* (46), 16548–16555. <https://doi.org/10.1021/JACS.7B07373>.
- (37) Wheeler, S. E.; Seguin, T. J.; Guan, Y.; Doney, A. C. Noncovalent Interactions in Organocatalysis and the Prospect of Computational Catalyst Design. *Accounts Chem. Res.* **2016**, *49* (5), 1061–1069. <https://doi.org/10.1021/acs.accounts.6b00096>.
- (38) Shimizu, K. D. A Solution to Dispersion Interactions. *Nat. Chem.* **2013**, *5* (12), 989–990. <https://doi.org/10.1038/nchem.1808>.

- (39) Pollice, R.; Fleckenstein, F.; Shenderovich, I.; Chen, P. Compensation of London Dispersion in the Gas Phase and in Aprotic Solvents. *Angew. Chem. Int. Ed.* **2019**, *58* (40), 14281–14288. <https://doi.org/10.1002/ANIE.201905436>.
- (40) Schümann, J. M.; Ochmann, L.; Becker, J.; Altun, A.; Harden, I.; Bistoni, G.; Schreiner, P. R. Exploring the Limits of Intramolecular London Dispersion Stabilization with Bulky Dispersion Energy Donors in Alkane Solution. *J. Am. Chem. Soc.* **2023**. <https://doi.org/10.1021/JACS.2C13301>.
- (41) Grimme, S. Density Functional Theory with London Dispersion Corrections. *WIREs Comput. Mol. Sci.* **2011**, *1* (2), 211–228. <https://doi.org/10.1002/WCMS.30>.
- (42) Grimme, S. Seemingly Simple Stereoelectronic Effects in Alkane Isomers and the Implications for Kohn–Sham Density Functional Theory. *Angew. Chem. Int. Ed.* **2006**, *45* (27), 4460–4464. <https://doi.org/10.1002/ANIE.200600448>.
- (43) Schreiner, P. R. Relative Energy Computations with Approximate Density Functional Theory—A Caveat! *Angew. Chem. Int. Ed.* **2007**, *46* (23), 4217–4219. <https://doi.org/10.1002/ANIE.200700386>.
- (44) Szalewicz, K. Symmetry-Adapted Perturbation Theory of Intermolecular Forces. *WIREs Comput. Mol. Sci.* **2012**, *2* (2), 254–272. <https://doi.org/10.1002/WCMS.86>.
- (45) Jansen, G. Symmetry-Adapted Perturbation Theory Based on Density Functional Theory for Noncovalent Interactions. *WIREs Comput. Mol. Sci.* **2014**, *4* (2), 127–144. <https://doi.org/10.1002/WCMS.1164>.
- (46) Schreiner, P. R.; Chernish, L. V.; Gunchenko, P. A.; Tikhonchuk, E. Y.; Hausmann, H.; Serafin, M.; Schlecht, S.; Dahl, J. E. P.; Carlson, R. M. K.; Fokin, A. A. Overcoming Lability of Extremely Long Alkane Carbon–Carbon Bonds through Dispersion Forces. *Nature* **2011**, *477* (7364), 308–311. <https://doi.org/10.1038/nature10367>.
- (47) Kitaura, K.; Morokuma, K. A New Energy Decomposition Scheme for Molecular Interactions within the Hartree-Fock Approximation. *Int. J. Quantum Chem.* **1976**, *10* (2), 325–340. <https://doi.org/10.1002/QUA.560100211>.
- (48) Raghavachari, K.; Trucks, G. W.; Pople, J. A.; Head-Gordon, M. A Fifth-Order Perturbation Comparison of Electron Correlation Theories. *Chem. Phys. Lett.* **1989**, *157* (6), 479–483. [https://doi.org/10.1016/S0009-2614\(89\)87395-6](https://doi.org/10.1016/S0009-2614(89)87395-6).
- (49) Hopkins, B. W.; Tschumper, G. S. Ab Initio Studies of  $\Pi \cdots \pi$  Interactions: The Effects of Quadruple Excitations. *J. Phys. Chem. A* **2004**, *108* (15), 2941–2948. <https://doi.org/10.1021/JP0369084>.
- (50) Hohenstein, E. G.; Sherrill, C. D. Wavefunction Methods for Noncovalent Interactions. *WIREs Comput. Mol. Sci.* **2012**, *2* (2), 304–326. <https://doi.org/10.1002/WCMS.84>.
- (51) Riplinger, C.; Neese, F. An Efficient and near Linear Scaling Pair Natural Orbital Based Local Coupled Cluster Method. *J. Chem. Phys.* **2013**, *138* (3), 034106. <https://doi.org/10.1063/1.4773581>.

- (52) Becke, A. D.; Johnson, E. R. A Density-Functional Model of the Dispersion Interaction. *J. Chem. Phys.* **2005**, *123* (15), 154101. <https://doi.org/10.1063/1.2065267>.
- (53) Becke, A. D.; Johnson, E. R. Exchange-Hole Dipole Moment and the Dispersion Interaction Revisited. *J. Chem. Phys.* **2007**, *127* (15), 154108. <https://doi.org/10.1063/1.2795701>.
- (54) Grimme, S.; Antony, J.; Ehrlich, S.; Krieg, H. A Consistent and Accurate Ab Initio Parametrization of Density Functional Dispersion Correction (DFT-D) for the 94 Elements H-Pu. *J. Chem. Phys.* **2010**, *132* (15), 154104. <https://doi.org/10.1063/1.3382344>.
- (55) Caldeweyher, E.; Bannwarth, C.; Grimme, S. Extension of the D3 Dispersion Coefficient Model. *J. Chem. Phys.* **2017**, *147* (3), 034112. <https://doi.org/10.1063/1.4993215>.
- (56) Martin, J. M. L.; Santra, G. Empirical Double-Hybrid Density Functional Theory: A ‘Third Way’ in Between WFT and DFT. *Isr. J. Chem* **2020**, *60* (8–9), 787–804. <https://doi.org/10.1002/IJCH.201900114>.
- (57) Pracht, P.; Bohle, F.; Grimme, S. Automated Exploration of the Low-Energy Chemical Space with Fast Quantum Chemical Methods. *Phys. Chem. Chem. Phys.* **2020**, *22* (14), 7169–7192. <https://doi.org/10.1039/C9CP06869D>.
- (58) Bannwarth, C.; Ehlert, S.; Grimme, S. GFN2-XTB—An Accurate and Broadly Parametrized Self-Consistent Tight-Binding Quantum Chemical Method with Multipole Electrostatics and Density-Dependent Dispersion Contributions. *J. Chem. Theory Comput.* **2019**, *15* (3), 1652–1671. <https://doi.org/10.1021/acs.jctc.8b01176>.
- (59) Grimme, S. Exploration of Chemical Compound, Conformer, and Reaction Space with Meta-Dynamics Simulations Based on Tight-Binding Quantum Chemical Calculations. *J. Chem. Theory Comput.* **2019**, *15* (5), 2847–2862. <https://doi.org/10.1021/ACS.JCTC.9B00143>.
- (60) Grimme, S.; Bohle, F.; Hansen, A.; Pracht, P.; Spicher, S.; Stahn, M. Efficient Quantum Chemical Calculation of Structure Ensembles and Free Energies for Nonrigid Molecules. *J. Phys. Chem. A* **2021**, *125* (19), 4039–4054. <https://doi.org/10.1021/ACS.JPCA.1C00971>.
- (61) Johnson, E. R.; Keinan, S.; Mori-Sánchez, P.; Contreras-García, J.; Cohen, A. J.; Yang, W. Revealing Noncovalent Interactions. *J. Am. Chem. Soc.* **2010**, *132* (18), 6498–6506. <https://doi.org/10.1021/ja100936w>.
- (62) Laplaza, R.; Peccati, F.; A. Boto, R.; Quan, C.; Carbone, A.; Piquemal, J.-P.; Maday, Y.; Contreras-García, J. NCIPLOT and the Analysis of Noncovalent Interactions Using the Reduced Density Gradient. *WIREs Comput. Mol. Sci.* **2021**, *11* (2), e1497. <https://doi.org/10.1002/wcms.1497>.
- (63) Perdew, J. P.; Burke, K.; Ernzerhof, M. Generalized Gradient Approximation Made Simple. *Phys. Rev. Lett.* **1996**, *77* (18), 3865–3868. <https://doi.org/10.1103/PhysRevLett.77.3865>.

- (64) Mata, R. A.; Suhm, M. A. Benchmarking Quantum Chemical Methods: Are We Heading in the Right Direction? *Angew. Chem. Int. Ed.* **2017**, *56* (37), 11011–11018. <https://doi.org/10.1002/anie.201611308>.
- (65) Paliwal, S.; Geib, S.; Wilcox, C. S. Molecular Torsion Balance for Weak Molecular Recognition Forces. Effects of “Tilted-T” Edge-to-Face Aromatic Interactions on Conformational Selection and Solid-State Structure. *J. Am. Chem. Soc.* **1994**, *116* (10), 4497–4498. <https://doi.org/10.1021/JA00089A057>.
- (66) Nakamura, M.; Oki, M.; Nakanishi, H.; Yamamoto, O. Restricted Rotation Involving the Tetrahedral Carbon. X. Barriers to Rotation of Methyl Groups in 9-Methyltritycene Derivatives. *B. Chem. Soc. Jpn.* **1974**, *47* (10), 2415–2419. <https://doi.org/10.1246/bcsj.47.2415>.
- (67) Mati, I. K.; Cockroft, S. L. Molecular Balances for Quantifying Non-Covalent Interactions. *Chem. Soc. Rev.* **2010**, *39* (11), 4195–4205. <https://doi.org/10.1039/B822665M>.
- (68) Aliev, A. E.; Motherwell, W. B. Some Recent Advances in the Design and Use of Molecular Balances for the Experimental Quantification of Intramolecular Noncovalent Interactions of  $\pi$  Systems. *Chem. Eur. J.* **2019**, *25* (45), 10516–10530. <https://doi.org/10.1002/CHEM.201900854>.
- (69) Li, P.; Vik, E. C.; Shimizu, K. D. N-Arylimide Molecular Balances: A Comprehensive Platform for Studying Aromatic Interactions in Solution. *Accounts Chem. Res.* **2020**, *53* (11), 2705–2714. <https://doi.org/10.1021/ACS.ACCOUNTS.0C00519>.
- (70) Strauss, M. A.; Wegner, H. A. Molecular Systems for the Quantification of London Dispersion Interactions. *Eur. J. Org. Chem.* **2019**, *2019* (2–3), 295–302. <https://doi.org/10.1002/EJOC.201800970>.
- (71) Elmi, A.; Cockroft, S. L. Quantifying Interactions and Solvent Effects Using Molecular Balances and Model Complexes. *Accounts Chem. Res.* **2021**, *54* (1), 92–103. <https://doi.org/10.1021/ACS.ACCOUNTS.0C00545>.
- (72) Yang, L.; Adam, C.; Cockroft, S. L. Quantifying Solvophobic Effects in Nonpolar Cohesive Interactions. *J. Am. Chem. Soc.* **2015**, *137* (32), 10084–10087. <https://doi.org/10.1021/JACS.5B05736>.
- (73) Adam, C.; Yang, L.; Cockroft, S. L. Partitioning Solvophobic and Dispersion Forces in Alkyl and Perfluoroalkyl Cohesion. *Angew. Chem. Int. Ed.* **2015**, *54* (4), 1164–1167. <https://doi.org/10.1002/ANIE.201408982>.
- (74) Wilming, F. M.; Becker, J.; Schreiner, P. R. Quantifying Solvophobic Effects in Organic Solvents Using a Hydrocarbon Molecular Balance. *J. Org. Chem.* **2022**, *87* (3), 1874–1878. <https://doi.org/10.1021/ACS.JOC.1C01813>.
- (75) Cockroft, S. L.; Hunter, C. A. Chemical Double-Mutant Cycles: Dissecting Non-Covalent Interactions. *Chem. Soc. Rev.* **2007**, *36* (2), 172–188. <https://doi.org/10.1039/B603842P>.

- (76) König, H. F.; Rummel, L.; Hausmann, H.; Becker, J.; Schümann, J. M.; Schreiner, P. R. Gauging the Steric Effects of Silyl Groups with a Molecular Balance. *J. Org. Chem.* **2022**, *87* (7), 4670–4679. <https://doi.org/10.1021/ACS.JOC.1C03103>.
- (77) König, H. F.; Hausmann, H.; Schreiner, P. R. Assessing the Experimental Hydrogen Bonding Energy of the Cyclic Water Dimer Transition State with a Cyclooctatetraene-Based Molecular Balance. *J. Am. Chem. Soc.* **2022**, *144* (37), 16965–16973. <https://doi.org/10.1021/JACS.2C06141>.
- (78) Oki, M. 1,9-Disubstituted Triptycenes: An Excellent Probe for Weak Molecular Interactions. *Accounts Chem. Res.* **1990**, *23* (11), 351–356. <https://doi.org/10.1021/AR00179A001>.
- (79) Oki, M.; Izumi, G.; Yamamoto, G.; Nakamura, N. Intramolecular Interactions Between Carbonyl Moieties and Chloro or Methoxyl Groups in Triptycene Systems. *Chem. Lett.* **1980**, *9* (2), 213–216. <https://doi.org/10.1246/cl.1980.213>.
- (80) Izumi, G.; Yamamoto, G.; Oki, M. Intramolecular Interaction Between Methoxyl and Acyloxymethyl Groups in Triptycene Systems. *Chem. Lett.* **1980**, *9* (8), 969–972. <https://doi.org/10.1246/cl.1980.969>.
- (81) Oki, M.; Izumi, G.; Yamamoto, G.; Nakamura, N. Attractive Interactions between Carbonyls and Groups Bearing Lone-Pair Electrons in Triptycene Systems. *B. Chem. Soc. Jpn.* **1982**, *55* (1), 159–166. <https://doi.org/10.1246/bcsj.55.159>.
- (82) Tamura, Y.; Yamamoto, G.; Oki, M. Substituent Effects on the Populations of Rotational Isomers in 9-(Aryloxymethyl)-1,4-Dimethyltriptycenes. Implications for the Presence of CH<sub>3</sub>···O Hydrogen Bond. *Chem. Lett.* **1986**, *15* (9), 1619–1622. <https://doi.org/10.1246/cl.1986.1619>.
- (83) Tamura, Y.; Yamamoto, G.; Oki, M. Effects of CH<sub>3</sub>···O Hydrogen Bond on the Rotamer Populations in 9-(Alkoxymethyl)-1,4-Dimethyltriptycenes. *B. Chem. Soc. Jpn.* **1987**, *60* (10), 3789–3790. <https://doi.org/10.1246/bcsj.60.3789>.
- (84) Suzuki, F.; Oki, M. Restricted Rotation Involving the Tetrahedral Carbon. : XII. Anomalous Conformer Distribution in 9-Benzyltriptycenes Carrying Substituent at Peri-Position. *Tetrahedron Lett.* **1974**, *15* (33), 2845–2848. [https://doi.org/10.1016/S0040-4039\(01\)91759-9](https://doi.org/10.1016/S0040-4039(01)91759-9).
- (85) Suzuki, F.; Oki, M. Restricted Rotation Involving the Tetrahedral Carbon. XIV. Conformational Equilibria and Attractive Interactions in Substituted 9-Benzyltriptycenes. *B. Chem. Soc. Jpn.* **1975**, *48* (2), 596–604. <https://doi.org/10.1246/bcsj.48.596>.
- (86) Gung, B. W.; Patel, M.; Xue, X. A Threshold for Charge Transfer in Aromatic Interactions? A Quantitative Study of  $\pi$ -Stacking Interactions. *J. Org. Chem.* **2005**, *70* (25), 10532–10537. <https://doi.org/10.1021/JO051808A>.
- (87) Gung, B. W.; Xue, X.; Reich, H. J. Off-Center Oxygen–Arene Interactions in Solution: A Quantitative Study. *J. Org. Chem.* **2005**, *70* (18), 7232–7237. <https://doi.org/10.1021/jo050874+>.

- (88) Gung, B. W.; Xue, X.; Zou, Y. Enthalpy ( $\Delta H$ ) and Entropy ( $\Delta S$ ) for  $\pi$ -Stacking Interactions in near-Sandwich Configurations: Relative Importance of Electrostatic, Dispersive, and Charge-Transfer Effects. *J. Org. Chem.* **2007**, *72* (7), 2469–2475. <https://doi.org/10.1021/JO062526T>.
- (89) Gung, B. W.; Wekesa, F.; Barnes, C. L. Stacking Interactions between Nitrogen-Containing Six-Membered Heterocyclic Aromatic Rings and Substituted Benzene: Studies in Solution and in the Solid State. *J. Org. Chem.* **2008**, *73* (5), 1803–1808. <https://doi.org/10.1021/JO702354X>.
- (90) Gung, B. W.; Emenike, B. U.; Alvarez, C. N.; Rakovan, J.; Kirschbaum, K.; Jain, N. Relative Substituent Position on the Strength of  $\pi$ - $\pi$  Stacking Interactions. *Tetrahedron Lett.* **2010**, *51* (13), 1648–1650. <https://doi.org/10.1016/J.TETLET.2009.12.095>.
- (91) Kim, E. I.; Paliwal, S.; Wilcox, C. S. Measurements of Molecular Electrostatic Field Effects in Edge-to-Face Aromatic Interactions and CH- $\pi$  Interactions with Implications for Protein Folding and Molecular Recognition. *J. Am. Chem. Soc.* **1998**, *120* (43), 11192–11193. <https://doi.org/10.1021/JA982620U>.
- (92) Ren, T.; Jin, Y.; Kim, K. S.; Kim, D. H. Aromatic-Aromatic Ring Interaction Revisited with Model Compounds of Wilcox. *J. Biomol. Struct. Dyn.* **2012**, *15* (2), 401–405. <https://doi.org/10.1080/07391102.1997.10508202>.
- (93) Fischer, F. R.; Schweizer, W. B.; Diederich, F. Substituent Effects on the Aromatic Edge-to-Face Interaction. *Chem. Commun.* **2008**, No. 34, 4031–4033. <https://doi.org/10.1039/B809058K>.
- (94) Bhayana, B.; Wilcox, C. S. A Minimal Protein Folding Model To Measure Hydrophobic and CH- $\pi$  Effects on Interactions between Nonpolar Surfaces in Water. *Angew. Chem. Int. Ed.* **2007**, *46* (36), 6833–6836. <https://doi.org/10.1002/ANIE.200700932>.
- (95) Hof, F.; Scofield, D. M.; Schweizer, W. B.; Diederich, F. A Weak Attractive Interaction between Organic Fluorine and an Amide Group. *Angew. Chem. Int. Ed.* **2004**, *43* (38), 5056–5059. <https://doi.org/10.1002/ANIE.200460781>.
- (96) Fischer, F. R.; Schweizer, W. B.; Diederich, F. Molecular Torsion Balances: Evidence for Favorable Orthogonal Dipolar Interactions Between Organic Fluorine and Amide Groups. *Angew. Chem. Int. Ed.* **2007**, *46* (43), 8270–8273. <https://doi.org/10.1002/ANIE.200702497>.
- (97) Fischer, F. R.; Wood, P. A.; Allen, F. H.; Diederich, F. Orthogonal Dipolar Interactions between Amide Carbonyl Groups. *P. Natl. Acad. Sci. USA* **2008**, *105* (45), 17290–17294. <https://doi.org/10.1073/PNAS.0806129105>.
- (98) Cockroft, S. L.; Hunter, C. A. Desolvation Tips the Balance: Solvent Effects on Aromatic Interactions. *Chem. Commun.* **2006**, No. 36, 3806–3808. <https://doi.org/10.1039/B608165G>.

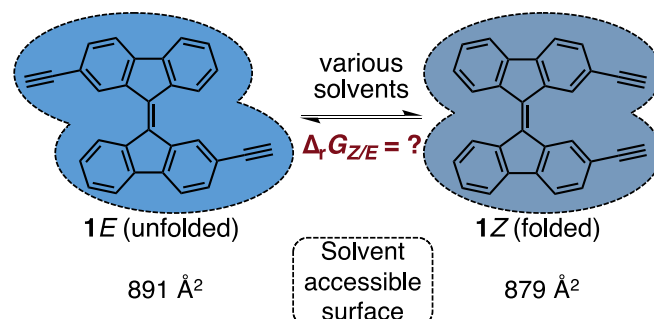
- (99) Cockroft, S. L.; Hunter, C. A. Desolvation and Substituent Effects in Edge-to-Face Aromatic Interactions. *Chem. Commun.* **2009**, No. 26, 3961–3963. <https://doi.org/10.1039/B902351H>.
- (100) Carroll, W. R.; Pellechia, P.; Shimizu, K. D. A Rigid Molecular Balance for Measuring Face-to-Face Arene-Arene Interactions. *Org. Lett.* **2008**, *10* (16), 3547–3550. <https://doi.org/10.1021/OL801286K>.
- (101) Hwang, J.; Dial, B. E.; Li, P.; Kozik, M. E.; Smith, M. D.; Shimizu, K. D. How Important Are Dispersion Interactions to the Strength of Aromatic Stacking Interactions in Solution? *Chem. Sci.* **2015**, *6* (7), 4358–4364. <https://doi.org/10.1039/C5SC01370D>.
- (102) Li, P.; Zhao, C.; Smith, M. D.; Shimizu, K. D. Comprehensive Experimental Study of N-Heterocyclic  $\pi$ -Stacking Interactions of Neutral and Cationic Pyridines. *J. Org. Chem.* **2013**, *78* (11), 5303–5313. <https://doi.org/10.1021/JO400370E>.
- (103) Hwang, J.; Li, P.; Carroll, W. R.; Smith, M. D.; Pellechia, P. J.; Shimizu, K. D. Additivity of Substituent Effects in Aromatic Stacking Interactions. *J. Am. Chem. Soc.* **2014**, *136* (40), 14060–14067. <https://doi.org/10.1021/JA504378P>.
- (104) Carroll, W. R.; Zhao, C.; Smith, M. D.; Pellechia, P. J.; Shimizu, K. D. A Molecular Balance for Measuring Aliphatic CH- $\pi$  Interactions. *Org. Lett.* **2011**, *13* (16), 4320–4323. <https://doi.org/10.1021/OL201657P>.
- (105) Zhao, C.; Parrish, R. M.; Smith, M. D.; Pellechia, P. J.; Sherrill, C. D.; Shimizu, K. D. Do Deuteriums Form Stronger CH- $\pi$  Interactions? *J. Am. Chem. Soc.* **2012**, *134* (35), 14306–14309. <https://doi.org/10.1021/JA305788P>.
- (106) Zhao, C.; Li, P.; Smith, M. D.; Pellechia, P. J.; Shimizu, K. D. Experimental Study of the Cooperativity of CH- $\pi$  Interactions. *Org. Lett.* **2014**, *16* (13), 3520–3523. <https://doi.org/10.1021/OL5014729>.
- (107) Li, P.; Parker, T. M.; Hwang, J.; Deng, F.; Smith, M. D.; Pellechia, P. J.; Sherrill, C. D.; Shimizu, K. D. The CH- $\pi$  Interactions of Methyl Ethers as a Model for Carbohydrate-N-Heteroarene Interactions. *Org. Lett.* **2014**, *16* (19), 5064–5067. <https://doi.org/10.1021/OL502418K>.
- (108) Li, P.; Maier, J. M.; Vik, E. C.; Yehl, C. J.; Dial, B. E.; Rickher, A. E.; Smith, M. D.; Pellechia, P. J.; Shimizu, K. D. Stabilizing Fluorine- $\pi$  Interactions. *Angew. Chem. Int. Ed.* **2017**, *56* (25), 7209–7212. <https://doi.org/10.1002/ANIE.201702950>.
- (109) Li, P.; Vik, E. C.; Maier, J. M.; Karki, I.; Strickland, S. M. S.; Umana, J. M.; Smith, M. D.; Pellechia, P. J.; Shimizu, K. D. Electrostatically Driven CO- $\pi$  Aromatic Interactions. *J. Am. Chem. Soc.* **2019**, *141* (32), 12513–12517. <https://doi.org/10.1021/JACS.9B06363>.
- (110) Hwang, J.; Li, P.; Smith, M. D.; Warden, C. E.; Sirianni, D. A.; Vik, E. C.; Maier, J. M.; Yehl, C. J.; Sherrill, C. D.; Shimizu, K. D. Tipping the Balance between S- $\pi$  and O- $\pi$  Interactions. *J. Am. Chem. Soc.* **2018**, *140* (41), 13301–13307. <https://doi.org/10.1021/JACS.8B07617>.

- (111) Maier, J. M.; Li, P.; Hwang, J.; Smith, M. D.; Shimizu, K. D. Measurement of Silver- $\pi$  Interactions in Solution Using Molecular Torsion Balances. *J. Am. Chem. Soc.* **2015**, *137* (25), 8014–8017. <https://doi.org/10.1021/JACS.5B04554>.
- (112) Maier, J. M.; Li, P.; Vik, E. C.; Yehl, C. J.; Strickland, S. M. S.; Shimizu, K. D. Measurement of Solvent OH- $\pi$  Interactions Using a Molecular Balance. *J. Am. Chem. Soc.* **2017**, *139* (19), 6550–6553. <https://doi.org/10.1021/JACS.7B02349>.
- (113) Hwang, J.; Li, P.; Smith, M. D.; Shimizu, K. D. Distance-Dependent Attractive and Repulsive Interactions of Bulky Alkyl Groups. *Angew. Chem. Int. Ed.* **2016**, *128* (28), 8218–8221. <https://doi.org/10.1002/ANGE.201602752>.
- (114) Van Craen, D.; Rath, W. H.; Huth, M.; Kemp, L.; Räuber, C.; Wollschläger, J. M.; Schalley, C. A.; Valkonen, A.; Rissanen, K.; Albrecht, M. Chasing Weak Forces: Hierarchically Assembled Helicates as a Probe for the Evaluation of the Energetics of Weak Interactions. *J. Am. Chem. Soc.* **2017**, *139* (46), 16959–16966. <https://doi.org/10.1021/JACS.7B10098>.
- (115) Rösel, S.; Balestrieri, C.; Schreiner, P. R. Sizing the Role of London Dispersion in the Dissociation of All-Meta Tert-Butyl Hexaphenylethane. *Chem. Sci.* **2016**, *8* (1), 405–410. <https://doi.org/10.1039/C6SC02727J>.
- (116) Rösel, S.; Becker, J.; Allen, W. D.; Schreiner, P. R. Probing the Delicate Balance between Pauli Repulsion and London Dispersion with Triphenylmethyl Derivatives. *J. Am. Chem. Soc.* **2018**, *140* (43), 14421–14432. <https://doi.org/10.1021/JACS.8B09145>.
- (117) Schweighauser, L.; Strauss, M. A.; Bellotto, S.; Wegner, H. A. Attraction or Repulsion? London Dispersion Forces Control Azobenzene Switches. *Angew. Chem. Int. Ed.* **2015**, *54* (45), 13436–13439. <https://doi.org/10.1002/ANIE.201506126>.
- (118) Strauss, M. A.; Wegner, H. A. Exploring London Dispersion and Solvent Interactions at Alkyl–Alkyl Interfaces Using Azobenzene Switches. *Angew. Chem. Int. Ed.* **2019**, *58* (51), 18552–18556. <https://doi.org/10.1002/ANIE.201910734>.
- (119) Strauss, M. A.; Wegner, H. A. London Dispersion in Alkane Solvents. *Angew. Chem. Int. Ed.* **2021**, *60* (2), 779–786. <https://doi.org/10.1002/ANIE.202012094>.
- (120) Minabe, M.; Oba, T.; Tanaka, M.; Kanno, K.; Tsubota, M. Z/E Selectivity on the Formation of 2,2'-Diacyl-9,9'-Bifluorenylidene Was Controlled by the Length of Acyl Side Chains. *Chem. Lett.* **2000**, *29* (5), 498–499. <https://doi.org/10.1246/cl.2000.498>.
- (121) Minabe, M.; Yamazaki, A.; Imai, T.; Takanezawa, T.; Karikomi, M. Formation of 2,2'-Diacyl-9,9'-Bifluorenylidene Isomers from 2-Acyl-9-Bromofluorene and Base-Catalyzed Isomerization of the Formed Alkenes. *B. Chem. Soc. Jpn.* **2006**, *79* (11), 1758–1765. <https://doi.org/10.1246/bcsj.79.1758>.
- (122) Wilming, F. M.; Marazzi, B.; Debes, P. P.; Becker, J.; Schreiner, P. R. Probing the Size Limit of Dispersion Energy Donors with a Bifluorenylidene Balance: Magic Cyclohexyl. *J. Org. Chem.* **2023**, *88* (2), 1024–1035. <https://doi.org/10.1021/ACS.JOC.2C02444>.



## 2. Publications

### 2.1 Quantifying Solvophobic Effects in Organic Solvents Using a Hydrocarbon Molecular Balance



#### *Abstract:*

We evaluate the use of the cohesive energy density (ced) as a quantitative descriptor for solvophobic effects in organic solvents by measuring  $\Delta G_{Z/E}$  of the rigid *Z*- and *E*-2,2'-diethynyl-9,9'-bifluorenylidene. In line with previously employed balances, solvent dependent changes in  $\Delta G_{Z/E}$  are predominantly induced by solvophobic effects, leading to a strong correlation with the solvent's ced. We re-emphasize the role of ceds as quantitative descriptors of solvophobic effects of organic solvents. Our experimental findings are well supported by B3LYP-D3/def2TZVP computations.

#### *Reference:*

Finn M. Wilming, Jonathan Becker, and Peter R. Schreiner *J. Org. Chem.* **2022**, *87* (3), 1874–1878. (DOI: 10.1021/ACS.JOC.1C01813)

#### *Declaration of own contribution:*

Literature research, synthesis planning, synthesis, analysis of spectroscopic data, sample preparation for equilibrium measurements, analysis of equilibrium measurements, computations, analysis of computational data, preparation of the manuscript, responses to reviewers.

#### *Reproduced with permission from:*

© 2022, American Chemical Society

1155 16<sup>th</sup> Street NW

Washington, DC, 20036

United States of America

## Quantifying Solvophobic Effects in Organic Solvents Using a Hydrocarbon Molecular Balance

 Finn M. Wilming, Jonathan Becker,<sup>||</sup> and Peter R. Schreiner\*


 Cite This: *J. Org. Chem.* 2022, 87, 1874–1878


 Read Online

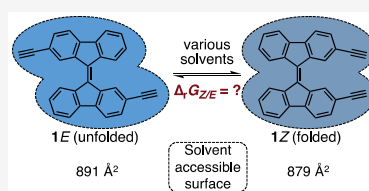
ACCESS |


 Metrics & More


 Article Recommendations


 Supporting Information

**ABSTRACT:** We evaluate the use of the cohesive energy density (ced) as a quantitative descriptor for solvophobic effects in organic solvents by measuring  $\Delta G_{Z/E}$  of the rigid *Z*- and *E*-2,2'-diethynyl-9,9'-bifluorenylidene. In line with previously employed balances, solvent-dependent changes in  $\Delta G_{Z/E}$  are predominantly induced by solvophobic effects, leading to a strong correlation with the solvent's ced. We re-emphasize the role of ceds as quantitative descriptors of solvophobic effects of organic solvents. Our experimental findings are well supported by B3LYP-D3/def2TZVP computations.



The immiscibility of water and oil is a result of the hydrophobic effect. In mixtures with nonpolar solutes, water strives to minimize the intermolecular contact areas with the solute due to enthalpically favorable competing interactions with itself.<sup>1</sup> The generalization of this phenomenon is called the solvophobic effect. It explains the biomimetic folding of complex organic oligomers,<sup>2</sup> solvent-dependent rate enhancement of reactions,<sup>3,4</sup> and the coiling of *n*-alkanes in perfluoroalkane solutions.<sup>5</sup> Solvophobicity also is able to attenuate noncovalent interactions in solution.<sup>6,7</sup> The degree of this attenuation has been studied with various molecular balances.<sup>8</sup> In addition to studying solvophobic effects, molecular balances<sup>9</sup> have previously been used to investigate  $\pi$ - $\pi$ ,<sup>10</sup>  $\sigma$ - $\pi$ ,<sup>11</sup> functional group- $\pi$ ,<sup>12,13</sup> and London Dispersion (LD) interactions<sup>14,15</sup> in solution. They rely on quantifiable intra- or intermolecular equilibria between two states generally called “folded” and “unfolded”. In the folded state, two moieties of the molecular balance are brought into close proximity and can therefore interact. In the unfolded state these intramolecular interactions are “switched off” due to a structural change of the molecular balance resulting in much larger distances between the interacting groups. Since studies with molecular balances are primarily carried out in solution, the observed folding behavior is influenced not only by both states differing in their intramolecular noncovalent interactions but also, to a certain degree, by their difference in solvation free energies. The strength of noncovalent interactions in the folded state of molecular balances measured in solution is therefore reduced compared to gas phase measurements. Cockroft et al. studied these effects using Wilcox type<sup>16</sup> molecular torsion balances substituted with alkyl, perfluoroalkyl, and phenyl substituents.<sup>17,18</sup> In these systems, noncovalent solute–solvent interactions in the unfolded state are the reason for a considerable compensation of intramolecular stabilization of the folded state via LD interactions. Subsequent

studies refined this view for more rigid functional groups with higher polarizabilities, where intramolecular LD is attenuated but not canceled in a series of very different organic solvents.<sup>6,15</sup> The deliberate use of LD to affect chemical reactions<sup>19</sup> has led to the consideration of LD to explain selectivities in catalysis<sup>20–22</sup> and the utilization of LD corrections in quantum chemical computations.<sup>23</sup> Consequently, solvophobic interactions have also received increasing attention due to their inextricable link to LD in solution. Various studies proposed the cohesive energy density (ced) of the solvent, which is the energy required to completely separate a certain volume of molecules from each other, as a quantitative descriptor for solvophobic effects in the molecular recognition of organic molecules.<sup>7,17,18,24,25</sup> Most molecular balances employed in these studies are organic compounds bearing multiple heteroatoms that in turn also affect solvent induced structural changes through dipolar interactions.<sup>26</sup> Strikingly, solvents or solvent mixtures with high ceds show a better correlation than solvents with small ceds. This prompted us to consider a reinvestigation of the role the ced plays as a universal descriptor of solvophobic effects in organic solvents.

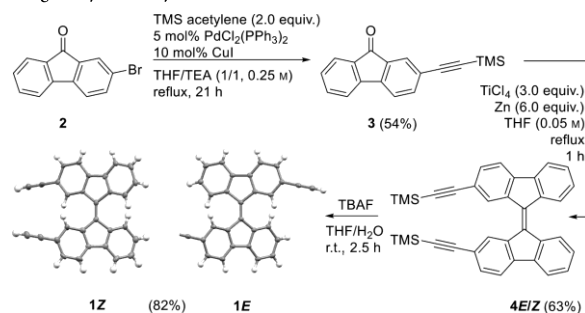
We chose to design a molecular balance for the measurements of solvophobic effects based on *E/Z*-2,2'-substituted-9,9'-bifluorenylidenes which were introduced as molecular balances by Minabe et al.<sup>27,28</sup> Because of the nonplanar structure of 9,9'-bifluorenylidenes, the *E/Z*-isomerization through a biradical transition state occurs even at ambient

Special Issue: Solvation Effects in Organic Chemistry

Received: July 30, 2021

Published: November 11, 2021



Scheme 1. Synthesis and Single Crystal X-ray Structures of the Molecular Balance 1E/Z<sup>a</sup>

<sup>a</sup>The bond distances and torsion angles of the central double bonds are 1.377 Å and 34.6° (1Z) as well as 1.375 Å and 31.5° (1E), respectively. Thermal ellipsoid plots of the X-ray single crystal structures were drawn at 50% probability level.

temperatures. Still, it is slow enough to allow the definitive assignment of NMR signals to the individual *E*- and *Z*-isomers.  $K_{Z/E}$  values can be determined directly from the NMR-integration.<sup>29</sup> We chose the 2,2'-diethynyl-substitution pattern to create a rigid hydrocarbon molecular balance that still possesses a small difference in the solvent accessible surfaces of 1E and 1Z (see single crystal X-ray diffraction data in the Supporting Information). This should lead to the minimization of solvent-dependent influences on the *E/Z* equilibrium, other than the solvophobic effect. We therefore measured the 1E/Z equilibrium in 15 organic solvents to determine the influence of solvophobic effects and clarify the role of the ced as a universally applicable descriptor of solvophobic effects.

We obtained 2,2'-diethynyl-9,9'-bifluorenylidene 1E/Z using a three-step synthesis starting from commercially available 2-bromofluorenone 2. In the first step, we performed a Sonogashira coupling reaction<sup>30</sup> with trimethylsilylacetylene to yield 2-((trimethylsilyl)ethynyl)-9H-fluoren-9-one 3, which was transformed to 2,2'-bis((trimethylsilyl)ethynyl)-9,9'-bifluorenylidene 4E/Z with a McMurry coupling reaction.<sup>31</sup> In the last step, the trimethylsilyl groups were cleaved using tetra-*n*-butylammonium fluoride (TBAF) to form 1E/Z (Scheme 1).

To ensure that all samples were fully equilibrated at the time of the NMR measurements, we studied the equilibration kinetics of 1E/Z by generating an isomerically enriched sample via column chromatography. This sample was then continuously equilibrated at 60 °C inside of an NMR spectrometer while obtaining the *E/Z* ratio every 30 min. We found that equilibration at 60 °C is completed after about 450 min (Figure 1).

After equilibration of 1E/Z in 15 deuterated organic solvents (acetic acid-*d*<sub>4</sub>, benzene-*d*<sub>6</sub>, bromobenzene-*d*<sub>5</sub>, chlorobenzene-*d*<sub>3</sub>, cyclohexane-*d*<sub>12</sub>, *n*-dodecane-*d*<sub>26</sub>, ethanol-*d*<sub>6</sub>, methanol-*d*<sub>4</sub>, nitrobenzene-*d*<sub>5</sub>, *n*-octane-*d*<sub>18</sub>, pyridine-*d*<sub>5</sub>, 1,1,2,2-tetrachloroethane-*d*<sub>2</sub>, THF-*d*<sub>8</sub>, toluene-*d*<sub>8</sub>, *p*-xylene-*d*<sub>10</sub>) at 60 °C,  $K_{Z/E}$  was determined via integration of the <sup>1</sup>H NMR signals in 1, 1', 8, and 8' positions of the bifluorenylidene backbone. We calculated the difference in free energy of both isomers via  $\Delta G_{Z/E} = -RT \ln(K_{Z/E})$ , and the obtained values for  $\Delta G_{Z/E}$  were plotted against various solvent parameters. As previous studies have suggested,<sup>18,24,25</sup> the best correlation of our experimental values was obtained with the ced of the solvent (Figure 2). With increasing ced, the *E/Z* equilibrium shifts

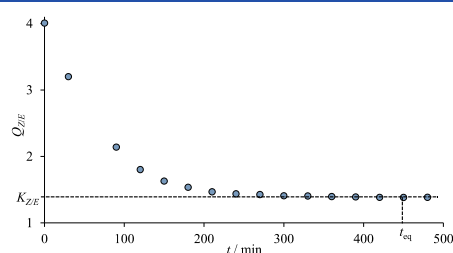


Figure 1. Time resolved equilibration of 1E/Z in toluene-*d*<sub>8</sub> at 60 °C.

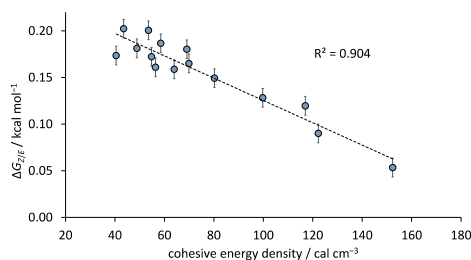


Figure 2. Experimentally obtained  $\Delta G_{Z/E}$  values of 1E/Z measured in 15 deuterated organic solvents at 60 °C show a high correlation with the solvent's ced.

toward the *Z*-isomer. This behavior could be explained with the difference in solvent accessible surface (sas) of the folded *Z*-isomer (879 Å<sup>2</sup> in benzene) compared to the unfolded *E*-isomer (891 Å<sup>2</sup> in benzene) evoking a solvophobic effect. The sas was computed at B3LYP-D3/def2SVP utilizing seven different solvents employing the SMD continuum solvation model<sup>32</sup> (Table S16). The differences in the sas of both isomers as a percentage of the overall molecular surface of 1E ranged from 1.1% for a small solvent probe like methanol ( $r_{\text{solv}} = 1.86$  Å) to 1.3% for larger solvents like toluene ( $r_{\text{solv}} = 2.82$  Å), underlining that the differences in  $r_{\text{solv}}$  only have a small effect on both isomer's difference in sas. These results suggest not only that, for each solvent,  $\Delta G_{Z/E}$  is slightly influenced by

differences in  $r_{\text{solV}}$  but also that these are not the decisive quantities for understanding the observed correlation.

To underline that the observed correlation is indeed to a large extent caused by the difference in  $s_{\text{as}}$ , we studied other potential solvent effects on  $\Delta G_{Z/E}$ . By equilibrating a series of differently concentrated solutions of **1E/Z**, we found no concentration dependence of  $K_{Z/E}$ . Also, the influence of the difference in dipole moment of **1E** (0.76 D in benzene) and **1Z** (1.67 D in benzene) on  $K_{Z/E}$  does not seem to be decisive. This is indicated by the solvent insensitivity of the equilibrium between *E*- and *Z*-3,3'-dibromo-9,9'-bifluorenylidene **S1E/Z**, which is a molecular balance that should mainly be influenced by the difference of the dipole moments of the *E/Z* isomers (Figure S1).

Throughout all solvents the experimental  $\Delta G_{Z/E}$  values of **1E/Z** are positive, indicating that the *E*-isomer is generally energetically favored. Gas phase computations at the B3LYP-D3/def2TZVP (Tables S14 and S15) level of theory also favor **1E** slightly by 0.13 kcal mol<sup>-1</sup>.<sup>33–37</sup> These results are supported by SAPT computations (Figure S15) performed with the acetylene dimer resulting from removing the 9,9'-bifluorenylidene moiety from the computed structure of **1Z**, predicting the overall interaction energy of the two acetylene moieties to be a mere 0.08 kcal mol<sup>-1</sup>. Still, due to the rigidity of **1E/Z** we expect these interactions to be essentially solvent independent and therefore only create a marginal offset of our experimental data.

To summarize, the experimentally obtained  $\Delta G_{Z/E}$  values correlate very well with the  $s_{\text{as}}$  of the solvents. This correlation is caused by the solvophobic effect which arises due to the difference in  $s_{\text{as}}$  of **1E** and **1Z**. With this, we were able to experimentally underline that the  $s_{\text{as}}$  of a particular solvent is a good quantitative descriptor for solvophobic effects in organic solvents.

## EXPERIMENTAL SECTION

**General Information.** Flash column chromatography was performed using a Büchi Reveleris X2 equipped with Büchi FlashPure EcoFlex columns of varying sizes. Thin layer chromatography was performed using Polygram SIL G/UV<sub>254</sub> plates. All dry solvents used were bought from Acros Organics in AcroSeal bottles stored over molecular sieve (4 Å). All NMR spectra were obtained using Bruker Avance II 400 MHz, Bruker Avance III HD 400 MHz, and Bruker Avance III HD 600 MHz spectrometers. All high resolution mass spectrometric data were obtained with a Bruker micrOTOF mass spectrometer. Equilibration of NMR samples was performed using an IKA ICC basic eco 8 temperature control device.

**Equilibration of NMR Samples.** At room temperature, **1E/Z** was dissolved in the respective dry deuterated solvent and transferred to a screw cap NMR tube that was placed in a thermostat heated to 60 °C. After 3 days of equilibration, the sample was quickly transferred into a Bruker Avance III HD 600 MHz NMR spectrometer preheated to 60 °C. The sample was then equilibrated for an additional 30 min inside the spectrometer to reduce the influence of small temperature changes that might occur during sample transfer.

**2-[(Trimethylsilyl)ethynyl]-9H-fluoren-9-one (3).** In a heat-dried 100 mL round-bottom Schlenk flask equipped with a reflux condenser, **2** (2.61 g, 10 mmol), PdCl<sub>2</sub>(PPh<sub>3</sub>)<sub>2</sub> (351 mg, 0.5 mmol), and CuI (197 mg, 1.0 mmol) were dissolved in dry THF (20 mL) at room temperature under a nitrogen atmosphere. Subsequently, ethynyltrimethylsilane (2.77 mL, 20 mmol) and triethylamine (20 mL) were added to the reaction mixture. The mixture was refluxed for 9 h using an oil bath. After cooling to rt, the mixture was quenched with saturated aqueous NH<sub>4</sub>Cl solution (20 mL) and extracted with dichloromethane three times (20 mL each). The combined organic layer was washed with saturated aqueous NH<sub>4</sub>Cl

solution and dried over Na<sub>2</sub>SO<sub>3</sub>. After filtration, the solvents were removed by evaporation. The crude product was purified by flash column chromatography (SiO<sub>2</sub>, *n*-hexane/dichloromethane, 5:1) to obtain **3** (1.48 g, 5.36 mmol, 54%) as a yellow solid.

<sup>1</sup>H NMR (400 MHz, CDCl<sub>3</sub>): δ 7.73 (d, *J* = 1.6 Hz, 1H), 7.65 (d, *J* = 7.3 Hz, 1H), 7.57 (dd, *J* = 7.7, 1.5 Hz, 1H), 7.53–7.41 (m, 3H), 7.30 (m, 1H), 0.26 (s, 9H).

<sup>13</sup>C{<sup>1</sup>H} NMR (100 MHz, CDCl<sub>3</sub>): δ 193.1, 144.04, 144.03, 138.1, 135.0, 134.5, 134.2, 129.5, 127.9, 124.6, 124.2, 120.8, 120.3, 104.2, 96.4, 0.0.

HRMS (ESI-TOF) *m/z*: [M + Na]<sup>+</sup> calcd for C<sub>18</sub>H<sub>16</sub>O<sub>2</sub>SiNa 299.0862; found 299.0862.

**2,2'-Bis[(trimethylsilyl)ethynyl]-9,9'-bifluorenylidene (4E/Z).** Zn powder (392 mg, 6.0 mmol) was placed in a 50 mL round-bottom Schlenk flask equipped with a reflux condenser and was heated under reduced pressure. Then, dry THF (10 mL) was added to the flask and the resulting suspension was cooled in an ice bath. To the reaction mixture, TiCl<sub>4</sub> (0.33 mL, 3.0 mmol) was added dropwise and the mixture was refluxed for 3 h using an oil bath. After cooling to rt, a solution of **3** (276 mg, 1.0 mmol) in dry THF (5 mL) was added to the reaction mixture which was then refluxed for 1 h, cooled to rt, and poured into a mixture of ice and saturated aqueous NH<sub>4</sub>Cl (1:1). The mixture was extracted with dichloromethane three times (40 mL each). The combined organic layer was dried over Na<sub>2</sub>SO<sub>3</sub>. After filtration, the solvents were removed by evaporation. The crude product was purified by flash column chromatography (SiO<sub>2</sub>, *n*-hexane) to obtain **4E/Z** (164 mg, 0.315 mmol, 63%) as a red solid.

<sup>1</sup>H NMR (400 MHz, CDCl<sub>3</sub>) for **4E**: δ 8.41 (s, 2H), 8.36 (d, *J* = 8.0 Hz, 2H), 7.70 (d, *J* = 6.6 Hz, 2H), 7.65 (s, 2H), 7.45 (dd, *J* = 4.9, 1.2 Hz, 2H), 7.40–7.17 (m, 4H), 0.24 (s, 18H).

<sup>1</sup>H NMR (400 MHz, CDCl<sub>3</sub>) for **4Z**: δ 8.44 (s, 2H), 8.34 (d, *J* = 8.0 Hz, 2H), 7.68 (d, *J* = 6.7 Hz, 2H), 7.63 (s, 2H), 7.47 (dd, *J* = 4.9, 1.2 Hz, 2H), 7.40–7.17 (m, 4H), 0.23 (s, 18H).

<sup>13</sup>C{<sup>1</sup>H} NMR (100 MHz, CDCl<sub>3</sub>) for **4E/Z**: δ 141.4, 141.3, 141.04, 141.00, 138.6, 138.11, 138.05, 133.22, 133.17, 130.2, 130.0, 129.676, 127.668, 127.4, 127.1, 126.9, 122.0, 121.7, 120.40, 120.37, 119.90, 119.86, 105.6, 105.5, 94.6, 94.5, 0.2, 0.1.

HRMS (APCI-TOF) *m/z*: [M + H]<sup>+</sup> calcd for C<sub>36</sub>H<sub>33</sub>Si<sub>2</sub> 521.2116; found 521.2118.

**2,2'-Diethynyl-9,9'-bifluorenylidene (1E/Z).** In a 50 mL round-bottom Schlenk flask, **4E/Z** was dissolved in THF (3 mL) and H<sub>2</sub>O (0.05 mL) at rt under air. A TBAF solution in THF (1 M, 0.69 mL, 0.69 mmol) was added to the reaction mixture. After stirring for 2.5 h, brine (40 mL) was added to the reaction mixture that was subsequently extracted with DCM (40 mL × 3). The combined organic layer was dried over Na<sub>2</sub>SO<sub>3</sub>. After filtration, the solvents were removed by evaporation. The crude product was purified by flash column chromatography (SiO<sub>2</sub>, *n*-hexane/DCM, 90:10) to obtain **1E/Z** (97 mg, 0.258 mmol, 82%) as a red solid.

<sup>1</sup>H NMR (400 MHz, CDCl<sub>3</sub>) for **1E**: δ 8.49 (s, 2H), 8.33 (d, *J* = 7.8, 0.9 Hz, 2H), 7.69 (d, *J* = 2.7, 0.9 Hz, 2H), 7.65 (s, 2H), 7.49 (dd, *J* = 2.3, 1.3 Hz, 2H), 7.41–7.32 (m, 2H), 7.32–7.19 (m, 2H), 3.07 (s, 2H).

<sup>1</sup>H NMR (400 MHz, CDCl<sub>3</sub>) for **1Z**: δ 8.44 (s, 2H), 8.37 (d, *J* = 7.9, 0.9 Hz, 2H), 7.71 (d, *J* = 2.7, 0.9 Hz, 2H), 7.67 (s, 2H), 7.47 (dd, *J* = 2.3, 1.4 Hz, 2H), 7.41–7.32 (m, 2H), 7.32–7.19 (m, 2H), 3.08 (s, 2H).

<sup>13</sup>C{<sup>1</sup>H} NMR (100 MHz, CDCl<sub>3</sub>) for **1E/Z**: δ 141.69, 141.67, 140.99, 140.98, 140.91, 140.89, 138.6, 138.5, 138.15, 138.07, 133.3, 133.2, 130.5, 130.2, 129.8, 127.8, 127.6, 127.0, 126.8, 120.8, 120.6, 120.51, 120.49, 120.0, 84.1, 84.0.

HRMS (APCI-TOF) *m/z*: [M + H]<sup>+</sup> calcd for C<sub>30</sub>H<sub>17</sub> 377.1325; found 377.1323.

## ASSOCIATED CONTENT

### Supporting Information

The Supporting Information is available free of charge at <https://pubs.acs.org/doi/10.1021/acs.joc.1c01813>.

<sup>1</sup>H NMR and <sup>13</sup>C{<sup>1</sup>H} NMR data for **1E/Z**, **3**, and **4E/Z**; error estimation for experimental  $\Delta G_{Z/E}$  values; single crystal X-ray diffraction data; HRMS data; computational details (PDF)

#### Accession Codes

CCDC 2098838–2098839 contain the supplementary crystallographic data for this paper. These data can be obtained free of charge via [www.ccdc.cam.ac.uk/data\\_request/cif](http://www.ccdc.cam.ac.uk/data_request/cif), or by emailing [data\\_request@ccdc.cam.ac.uk](mailto:data_request@ccdc.cam.ac.uk), or by contacting The Cambridge Crystallographic Data Centre, 12 Union Road, Cambridge CB2 1EZ, UK; fax: +44 1223 336033.

#### ■ AUTHOR INFORMATION

##### Corresponding Author

Peter R. Schreiner – *Institute of Organic Chemistry, Justus Liebig University, 35392 Giessen, Germany; Center for Materials Research (ZfM), Justus Liebig University, 35392 Giessen, Germany; [orcid.org/0000-0002-3608-5515](https://orcid.org/0000-0002-3608-5515); Email: [prs@uni-giessen.de](mailto:prs@uni-giessen.de)*

##### Authors

Finn M. Wilming – *Institute of Organic Chemistry, Justus Liebig University, 35392 Giessen, Germany; Center for Materials Research (ZfM), Justus Liebig University, 35392 Giessen, Germany*

Jonathan Becker – *Institute of Inorganic and Analytical Chemistry, Justus Liebig University, 35392 Giessen, Germany*

Complete contact information is available at:

<https://pubs.acs.org/10.1021/acs.joc.1c01813>

##### Author Contributions

<sup>1</sup>H X-ray crystal structure determination.

##### Notes

The authors declare no competing financial interest.

#### ■ ACKNOWLEDGMENTS

Financial support from the Deutsche Forschungsgemeinschaft (GRK 2204 and SPP 1807) is gratefully acknowledged. The authors thank Heike Hausmann for performing the NMR experiments. F.M.W. thanks Yu Ozawa for preliminary synthetic contributions and Sören Rösel, Jan M. Schümann, Lars Rummel, Bastian Bernhardt, and Henrik F. König for fruitful discussions and advice on the computations.

#### ■ REFERENCES

- (1) Chandler, D. Interfaces and the driving force of hydrophobic assembly. *Nature* **2005**, *437*, 640–647.
- (2) Nelson, J. C.; Saven, J. G.; Moore, J. S.; Wolyne, P. G. Solvophobically Driven Folding of Nonbiological Oligomers. *Science* **1997**, *277*, 1793–1796.
- (3) Keaveney, S. T.; Haines, R. S.; Harper, J. B. Investigating Solvent Effects of an Ionic Liquid on Pericyclic Reactions through Kinetic Analyses of Simple Rearrangements. *ChemPlusChem* **2017**, *82*, 449–457.
- (4) Marin-Luna, M.; Pöloth, B.; Zott, F.; Zipse, H. Size-dependent rate acceleration in the silylation of secondary alcohols: the bigger the faster. *Chem. Sci.* **2018**, *9*, 6509–6515.
- (5) Morgado, P.; García, A. R.; Martins, L. F. G.; Ilharco, L. M.; Filipe, E. J. M. Alkane Coiling in Perfluoroalkane Solutions: A New Primitive Solvophobic Effect. *Langmuir* **2017**, *33*, 11429–11435.
- (6) Pollice, R.; Bot, M.; Kobylanski, I. J.; Shenderovich, I.; Chen, P. Attenuation of London Dispersion in Dichloromethane Solutions. *J. Am. Chem. Soc.* **2017**, *139*, 13126–13140.

(7) Yang, L.; Adam, C.; Nichol, G. S.; Cockcroft, S. L. How much do van der Waals dispersion forces contribute to molecular recognition in solution? *Nat. Chem.* **2013**, *5*, 1006–1010.

(8) Elmi, A.; Cockcroft, S. L. Quantifying Interactions and Solvent Effects Using Molecular Balances and Model Complexes. *Acc. Chem. Res.* **2021**, *54*, 92–103.

(9) Mati, I. K.; Cockcroft, S. L. Molecular balances for quantifying non-covalent interactions. *Chem. Soc. Rev.* **2010**, *39*, 4195–4205.

(10) Chong, Y. S.; Carroll, W. R.; Burns, W. G.; Smith, M. D.; Shimizu, K. D. A High-Barrier Molecular Balance for Studying Face-to-Face Arene–Arene Interactions in the Solid State and in Solution. *Chem. - Eur. J.* **2009**, *15*, 9117–9126.

(11) Carroll, W. R.; Zhao, C.; Smith, M. D.; Pellechia, P. J.; Shimizu, K. D. A Molecular Balance for Measuring Aliphatic CH– $\pi$  Interactions. *Org. Lett.* **2011**, *13*, 4320–4323.

(12) Motherwell, W. B.; Moise, J.; Aliev, A. E.; Nič, M.; Coles, S. J.; Horton, P. N.; Hursthouse, M. B.; Chessari, G.; Hunter, C. A.; Vinter, J. G. Noncovalent Functional-Group–Arene Interactions. *Angew. Chem., Int. Ed.* **2007**, *46*, 7823–7826.

(13) Li, P.; Vik, E. C.; Shimizu, K. D. N-Arylimide Molecular Balances: A Comprehensive Platform for Studying Aromatic Interactions in Solution. *Acc. Chem. Res.* **2020**, *53*, 2705–2714.

(14) Strauss, M. A.; Wegner, H. A. Molecular Systems for the Quantification of London Dispersion Interactions. *Eur. J. Org. Chem.* **2019**, *2019*, 295–302.

(15) Schümann, J. M.; Wagner, J. P.; Eckhardt, A. K.; Quanz, H.; Schreiner, P. R. Intramolecular London Dispersion Interactions Do Not Cancel in Solution. *J. Am. Chem. Soc.* **2021**, *143*, 41–45.

(16) Paliwal, S.; Geib, S.; Wilcox, C. S. Molecular Torsion Balance for Weak Molecular Recognition Forces. Effects of “Tilted-T” Edge-to-Face Aromatic Interactions on Conformational Selection and Solid-State Structure. *J. Am. Chem. Soc.* **1994**, *116*, 4497–4498.

(17) Adam, C.; Yang, L.; Cockcroft, S. L. Partitioning Solvophobic and Dispersion Forces in Alkyl and Perfluoroalkyl Cohesion. *Angew. Chem., Int. Ed.* **2015**, *54*, 1164–1167.

(18) Yang, L.; Adam, C.; Cockcroft, S. L. Quantifying Solvophobic Effects in Nonpolar Cohesive Interactions. *J. Am. Chem. Soc.* **2015**, *137*, 10084–10087.

(19) Wagner, J. P.; Schreiner, P. R. London Dispersion in Molecular Chemistry—Reconsidering Steric Effects. *Angew. Chem., Int. Ed.* **2015**, *54*, 12274–12296.

(20) Eschmann, C.; Song, L.; Schreiner, P. R. London Dispersion Interactions Rather than Steric Hindrance Determine the Enantioselectivity of the Corey–Bakshi–Shibata Reduction. *Angew. Chem., Int. Ed.* **2021**, *60*, 4823–4832.

(21) Wende, R. C.; Seitz, A.; Niedeck, D.; Schuler, S. M. M.; Hofmann, C.; Becker, J.; Schreiner, P. R. The Enantioselective Dakin–West Reaction. *Angew. Chem., Int. Ed.* **2016**, *55*, 2719–2723.

(22) Neel, A. J.; Hilton, M. J.; Sigman, M. S.; Toste, F. D. Exploiting non-covalent  $\pi$  interactions for catalyst design. *Nature* **2017**, *543*, 637–646.

(23) Grimme, S. Density functional theory with London dispersion corrections. *Wiley Interdiscip. Rev.: Comput. Mol. Sci.* **2011**, *1*, 211–228.

(24) Maier, J. M.; Li, P.; Vik, E. C.; Yehl, C. J.; Strickland, S. M. S.; Shimizu, K. D. Measurement of Solvent OH– $\pi$  Interactions Using a Molecular Balance. *J. Am. Chem. Soc.* **2017**, *139*, 6550–6553.

(25) Otto, S. The role of solvent cohesion in nonpolar solvation. *Chem. Sci.* **2013**, *4*, 2953–2959.

(26) Rauche, M.; Ehrling, S.; Krause, S.; Senkovska, I.; Kaskel, S.; Brunner, E. New insights into solvent-induced structural changes of <sup>13</sup>C labelled metal–organic frameworks by solid state NMR. *Chem. Commun.* **2019**, *55*, 9140–9143.

(27) Minabe, M.; Yamazaki, A.; Imai, T.; Takanezawa, T.; Karikomi, M. Formation of 2,2'-Diacyl-9,9'-bifluorenylidene Isomers from 2-Acyl-9-bromofluorene and Base-Catalyzed Isomerization of the Formed Alkenes. *Bull. Chem. Soc. Jpn.* **2006**, *79*, 1758–1765.

(28) Minabe, M.; Oba, T.; Tanaka, M.; Kanno, K.; Tsubota, M. Z/E Selectivity on the Formation of 2,2'-Diacyl-9,9'-bifluorenylidene Was

Controlled by the Length of Acyl Side Chains. *Chem. Lett.* **2000**, *29*, 498–499.

(29) Biedermann, P. U.; Stezowski; John, J.; Agranat, I. Conformational Space and Dynamic Stereochemistry of Overcrowded Homomeric Bistricyclic Aromatic Enes – A Theoretical Study. *Eur. J. Org. Chem.* **2001**, *2001*, 15–34.

(30) Sonogashira, K.; Tohda, Y.; Hagihara, N. A convenient synthesis of acetylenes: catalytic substitutions of acetylenic hydrogen with bromoalkenes, iodoarenes and bromopyridines. *Tetrahedron Lett.* **1975**, *16*, 4467–4470.

(31) McMurry, J. E.; Fleming, M. P. New method for the reductive coupling of carbonyls to olefins. Synthesis of  $\beta$ -carotene. *J. Am. Chem. Soc.* **1974**, *96*, 4708–4709.

(32) Marenich, A. V.; Cramer, C. J.; Truhlar, D. G. Universal Solvation Model Based on Solute Electron Density and on a Continuum Model of the Solvent Defined by the Bulk Dielectric Constant and Atomic Surface Tensions. *J. Phys. Chem. B* **2009**, *113*, 6378–6396.

(33) Becke, A. D. Density-functional thermochemistry. III. The role of exact exchange. *J. Chem. Phys.* **1993**, *98*, 5648–5652.

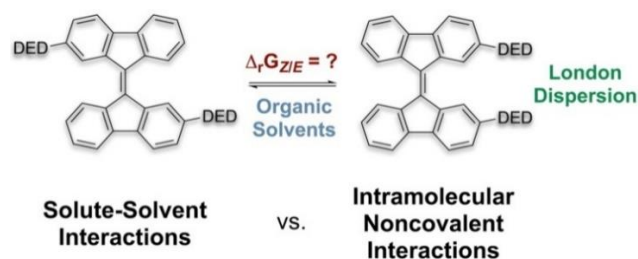
(34) Stephens, P. J.; Devlin, F. J.; Chabalowski, C. F.; Frisch, M. J. Ab Initio Calculation of Vibrational Absorption and Circular Dichroism Spectra Using Density Functional Force Fields. *J. Phys. Chem.* **1994**, *98*, 11623–11627.

(35) Grimme, S.; Ehrlich, S.; Goerigk, L. Effect of the damping function in dispersion corrected density functional theory. *J. Comput. Chem.* **2011**, *32*, 1456–1465.

(36) Weigend, F.; Ahlrichs, R. Balanced basis sets of split valence, triple zeta valence and quadruple zeta valence quality for H to Rn: Design and assessment of accuracy. *Phys. Chem. Chem. Phys.* **2005**, *7*, 3297–3305.

(37) Frisch, M. J.; Trucks, G. W.; Schlegel, H. B.; Scuseria, G. E.; Robb, M. A.; Cheeseman, J. R.; Scalmani, G.; Barone, V.; Petersson, G. A.; Nakatsuji, H.; Li, X.; Caricato, M.; Marenich, A. V.; Bloino, J.; Janesko, B. G.; Gomperts, R.; Mennucci, B.; Hratchian, H. P.; Ortiz, J. V.; Izmaylov, A. F.; Sonnenberg, J. L.; Williams, J.; Ding, F.; Lipparini, F.; Egidi, F.; Goings, J.; Peng, B.; Petrone, A.; Henderson, T.; Ranasinghe, D.; Zakrzewski, V. G.; Gao, J.; Rega, N.; Zheng, G.; Liang, W.; Hada, M.; Ehara, M.; Toyota, K.; Fukuda, R.; Hasegawa, J.; Ishida, M.; Nakajima, T.; Honda, Y.; Kitao, O.; Nakai, H.; Vreven, T.; Throssell, K.; Montgomery, J. A., Jr.; Peralta, J. E.; Ogliaro, F.; Bearpark, M. J.; Heyd, J. J.; Brothers, E. N.; Kudin, K. N.; Staroverov, V. N.; Keith, T. A.; Kobayashi, R.; Normand, J.; Raghavachari, K.; Rendell, A. P.; Burant, J. C.; Iyengar, S. S.; Tomasi, J.; Cossi, M.; Millam, J. M.; Klene, M.; Adamo, C.; Cammi, R.; Ochterski, J. W.; Martin, R. L.; Morokuma, K.; Farkas, O.; Foresman, J. B.; Fox, D. J. *Gaussian 16 Rev. A.03*; Gaussian Inc.: Wallingford, CT, 2016.

## 2.2 Probing the Size-Limit of Dispersion Energy Donors with a Bifluorenylidene Balance: Magic Cyclohexyl



### Abstract:

We report the synthesis of fourteen 2,2'-disubstituted 9,9'-bifluorenylidenes as molecular balances for the quantification of London dispersion interactions between various dispersion energy donors. For all balances, we measured  $\Delta G_{Z/E}$  at 333 K using  $^1\text{H-NMR}$  in seven organic solvents. For various alkyl and aryl substituents we generally observe a preference for the “folded” *Z*-isomer due to attractive London dispersion interactions. The cyclohexyl substituted system shows the largest *Z*-preference in this study with  $\Delta G_{Z/E} \sim -0.6 \pm 0.05 \text{ kcal mol}^{-1}$  in all solvents, owing to the rotational freedom of cyclohexyl groups paired with their large polarizability that maximizes London dispersion interactions. On the other hand, rigid and sterically more demanding substituents like *tert*-butyl unexpectedly favor the unfolded *E*-isomer. This is a result of the close relative position in which the functional groups are positioned in this molecular balance. This close proximity is the reason for the increase of Pauli repulsion in the *Z*-isomers with large rigid substituents (*tert*-butyl, adamantyl, diamantyl) which leads to an equilibrium shift towards the unfolded *E*-form. While we were able to reproduce most of our experimental trends qualitatively using contemporary computational chemistry methods, quantitative accuracy of the employed methods still needs further improvement.

### Reference:

Finn M. Wilming, Benito Marazzi, Paul P. Debes, Jonathan Becker, Peter R. Schreiner, *J. Org. Chem.* **2023**, 88 (2), 1024–1035. (DOI: 10.1021/ACS.JOC.2C02444.)

### Declaration of own contribution:

Literature research, synthesis planning, synthesis of all molecular balances except **1Dia** and **1PFP**, analysis of spectroscopic data, sample preparation for equilibrium measurements, analysis of equilibrium measurements, computations, analysis of computational data, preparation of the manuscript, responses to reviewers.

### Reproduced with permission from:

© 2023, American Chemical Society

1155 16<sup>th</sup> Street NW

Washington, DC, 20036

United States of America

## Probing the Size Limit of Dispersion Energy Donors with a Bifluorenylidene Balance: Magic Cyclohexyl

Finn M. Wilming, Benito Marazzi, Paul P. Debes, Jonathan Becker,<sup>||</sup> and Peter R. Schreiner<sup>\*§</sup>

Cite This: *J. Org. Chem.* 2023, 88, 1024–1035

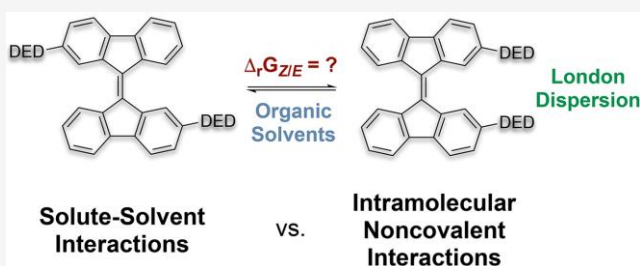
Read Online

ACCESS |

Metrics & More

Article Recommendations

Supporting Information



**ABSTRACT:** We report the synthesis of 14 2,2'-disubstituted 9,9'-bifluorenylidenes as molecular balances for the quantification of London dispersion interactions between various dispersion energy donors. For all balances, we measured  $\Delta G_{Z/E}$  at 333 K using  $^1\text{H}$  NMR in seven organic solvents. For various alkyl and aryl substituents, we generally observe a preference for the “folded” Z-isomer due to attractive London dispersion interactions. The cyclohexyl-substituted system shows the largest Z-preference in this study with  $\Delta G_{Z/E} = -0.6 \pm 0.05 \text{ kcal mol}^{-1}$  in all solvents, owing to the rotational freedom of cyclohexyl groups paired with their large polarizability that maximizes London dispersion interactions. On the other hand, rigid and sterically more demanding substituents like *tert*-butyl unexpectedly favor the unfolded *E*-isomer. This is a result of the close relative position in which the functional groups are positioned in this molecular balance. This close proximity is the reason for the increase of Pauli repulsion in the Z-isomers with large rigid substituents (*tert*-butyl, adamantyl, and diamantyl) which leads to an equilibrium shift toward the unfolded *E*-form. While we were able to reproduce most of our experimental trends qualitatively using contemporary computational chemistry methods, quantitative accuracy of the employed methods still needs further improvement.

### INTRODUCTION

London dispersion (LD), which constitutes the attractive part of the van der Waals (vdW) potential, is ubiquitously present in chemistry.<sup>1,2</sup> In recent years, the targeted use of LD to influence structures<sup>3–9</sup> and reactivities<sup>10–12</sup> brought the importance of LD to the fore.<sup>13–15</sup> Influence can be exerted by the introduction of preferably electron-rich and polarizable groups called dispersion energy donors (DEDs).<sup>14,16</sup> Because organic reactions are predominantly performed in solution, it is of great importance to understand how the presence of solvation affects the interactions of different DEDs.<sup>17,18</sup> Therefore, molecular balances were used to study LD in solution using various DEDs.<sup>19–22</sup>

Most molecular balances for the quantification of noncovalent interactions are generally based on the equilibrium between a “folded” state of a molecule, where two substituents of interest are brought in close proximity to each other, and an “unfolded” state where the substituents are not interacting due to a larger distance (Figure 1).<sup>23</sup> To acquire unbiased experimental results, it is important to use molecular balance

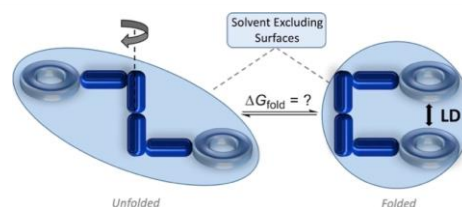


**Figure 1.** Schematic depiction of a molecular balance for the quantification of LD in solution.

Received: October 10, 2022

Published: December 28, 2022



systems that do not influence the folded/unfolded equilibrium via heteroatom-induced dipolar interactions.

In the gas phase, the folded/unfolded equilibrium of a molecular balance ideally is solely influenced by attractive or repulsive interactions between the DEDs in the folded state. Upon transfer of the system into solution, the difference in  $\Delta G_{\text{sol}}$  of the folded and unfolded states arising from differences in the solvent excluding surface area (SES) has to be taken into account as well, especially because, for linear alkyl-alkyl interactions, a "very large cancellation of dispersion forces due to competitive dispersion interactions with the solvent" was claimed in 2013.<sup>17</sup> In more recent studies, the importance of entropic contributions to the self-assembly of flexible alkyl chains in solution was emphasized, weakening the initial argument.<sup>24–26</sup> For a broad variety of different linear, branched, and cyclic hydrocarbon substituents it was found that there is an attenuation of LD-stabilization of about 70% in dichloromethane solutions compared to gas phase experiments due to competing LD interactions with the solvent.<sup>27</sup> Another study has shown that the LD-driven preference (expressed in  $\Delta G$ ) of folded 1,6-di-*tert*-butyl-cyclooctatetraene compared to its unfolded 1,4-valence bond isomer is essentially unaffected in a large variety of organic solvents, and it is clear that LD does not disappear in solution.<sup>21</sup> In the present work, we extend these studies toward the interactions of a variety of different DEDs in different organic solvents using a nonpolar, highly symmetric, and readily synthesized molecular balance<sup>28</sup> to understand how size, structure, and flexibility of different DED classes influence the folding behavior of a nonpolar molecular balance. With this, we aim at clarifying the influence of LD, Pauli repulsion, and solvophobic effects on the studied systems and give some general guidelines for experimental DED usage.

The bifluorenylidene backbone employed in this work was first utilized as a molecular balance to study the chain length dependence of the interaction of different acyl groups.<sup>29,30</sup> As a nonplanar and nonpolar olefin with an activation energy for double bond isomerization of roughly 26 kcal mol<sup>-1</sup>,<sup>31</sup> its *E/Z* isomerization takes place already at slightly elevated temperatures and allows quantification of its *E/Z* ratios via NMR spectroscopy without major conformational or dipole-induced biases. Its rigid backbone structure is also suitable for this study because it allows us to introduce substituents in the 2- and 2'-positions in very close proximity to each other (Figure 2).

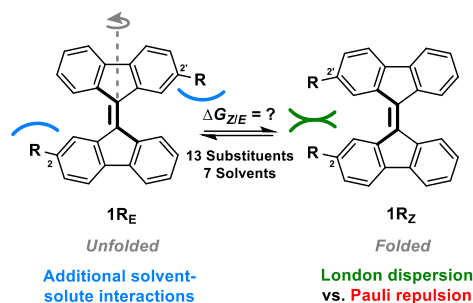


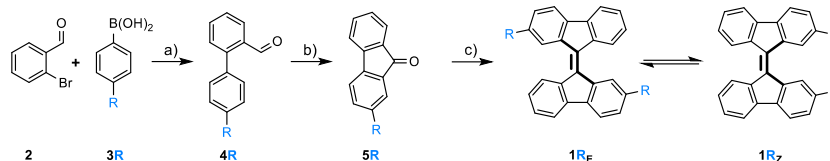
**Figure 2.** Equilibrium between the unfolded *E*-2,2'-disubstituted-9,9'-bifluorenylidene  $1R_E$  and its folded *Z*-isomer  $1R_Z$  can be used to study the interplay of intramolecular LD and solvophobic effects.

## RESULTS AND DISCUSSION

**General Information.** The experimental data presented in the following paragraph were generated via NMR-integration after *E/Z* equilibration of 13 differently 2,2'-disubstituted 9,9'-bifluorenylidenes dissolved in seven different deuterated organic solvents. Additionally, we synthesized the sterically overcrowded 2,2'-ditrityl-9,9'-bifluorenylidene of which we could spectroscopically only identify the *E*-isomer, suggesting that very large substituents influence the *E/Z* equilibrium toward the *E*-isomer. We chose the *Z*-isomer to be the product of our equilibration reaction, therefore negative values for  $\Delta G_{Z/E}$  indicate that the *Z*-isomer is favored. In previous work, we found that the *E/Z* equilibrium of 2,2'-disubstituted 9,9'-bifluorenylidenes is generally independent of concentration effects or moderate differences in the dipole moment of the two isomers (0.8 D for the *E*-vs 1.7 D for the *Z*-isomer).<sup>29</sup> If, for certain solvents, no  $\Delta G_{Z/E}$  is given, this indicates that there were (a) solubility issues or (b) overlapping NMR signals of both isomers not allowing us to determine exact *E/Z* ratios. The numbering convention in this work consists of a number symbolizing one of the structures depicted in Scheme 1 of the Experimental Section in combination with a two to three letter code that stands for the substituents in the R-position. For example, 1Cy is short for 2,2'-dicyclohexyl(Cy)-9,9'-bifluorenylidene(1). Use of the letter R, like in 1R, summarizes all differently substituted compounds of one class.

**Linear Alkyl Substituents.** Figure 3 shows the experimentally obtained  $\Delta G_{Z/E}$  values of six linear alkyl disubstituted 9,9'-bifluorenylidenes in seven organic solvents. For 1Me, we measured the *Z/E* ratio to be very close to 1:1 ( $\Delta G_{Z/E} \sim 0$  kcal mol<sup>-1</sup>). This indicates that small substituents in the 2- and 2'-positions of our molecular balance do not influence the *E/Z* equilibrium significantly due to a large distance between the groups (computed as  $d_{R-R} \sim 4.4$  Å at PBEh-3c). Hence, 1Me serves us as a reference point to estimate the random experimental errors of our measurements. With increasing chain length, we observe an increase in the *Z*-preference, which plateaus at a maximum of  $\Delta G_{Z/E}$  between  $-0.15$  to  $-0.20$  kcal mol<sup>-1</sup> for 1Pr and 1Bu and then slightly declines for 1Pe and 1No. These findings generally support our working hypothesis that the *Z*-isomer of 1R is stabilized due to LD interactions between the adjacent substituents. The reduction in the *Z*-preference for longer alkyl chains may be attributed to the entropic penalty generated by the increasing number of possible conformers and the competing interactions between the alkyl chains and the bifluorenylidene backbone. Other studies that used different molecular balance systems to study alkyl-alkyl interactions in solution observed similar experimental trends.<sup>24–26</sup> DLPNO-CCSD(T)/def2-TZVP single point energies of the lowest energy conformer of the *E*- and *Z*-isomers of our molecular balances fail to reproduce our experimental data because they neglect the conformational freedom of these systems. Therefore, we used a conformer-rotamer ensemble sampling tool<sup>32,33</sup> (CREST, see computational details) to generate conformer ensembles of all *E*- and *Z*-isomers of the ethyl-, *n*-propyl-, *n*-butyl-, *n*-pentyl-, and *n*-nonyl-substituted molecular balances to take all conformers into account. We used these ensembles to compute Boltzmann averaged free energies for each isomer in the gas phase and in benzene using the command line energetic sorting of conformer rotamer ensembles<sup>34</sup> (CENSO, see computational details). For every substituent, these computed free energies of

Scheme 1. Synthetic Route toward 2,2'-Disubstituted 9,9'-Bifluorenylidenes: (a) Pd(OAc)<sub>2</sub>, Na<sub>2</sub>CO<sub>3</sub>, DMF/H<sub>2</sub>O (2:1), rt, 16 h; (b) Fe(Cp)<sub>2</sub>, tBuOOH, MeCN, Reflux, 16 h; and (c) TiCl<sub>4</sub>, Zn, THF, Reflux, 3 h; then SR, Reflux 1 h



R = Methyl, Ethyl, *n*-Propyl, *n*-Butyl, *n*-Pentyl, *n*-Nonyl, 2-Propyl, Cyclohexyl, *t*-Butyl, Adamantyl, Diamantyl, Trityl, Phenyl, Pentafluorophenyl.

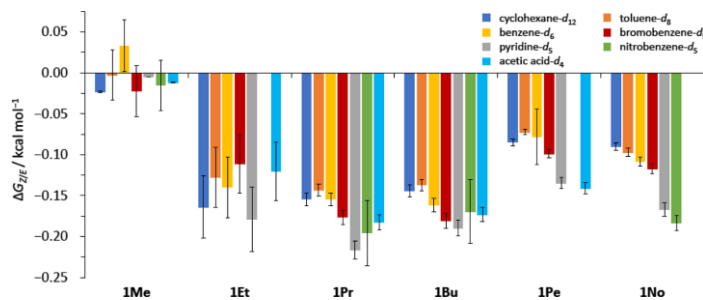


Figure 3.  $\Delta G_{Z/E}$  measured at 333 K for all linear alkyl-substituted molecular balances. 1Me = methyl, 1Et = ethyl, 1Pr = *n*-propyl, 1Bu = *n*-butyl, 1Pe = *n*-pentyl, and 1No = *n*-nonyl. The solvents' cohesive energy density is increasing from left to right in each group of measurements.

the *E*- and *Z*-isomers were offset against each other to give computed  $\Delta G_{Z/E}$ , which is compared to experimental data in Table 1.

Table 1. Computationally Obtained  $\Delta G_{Z/E}$  for Linear Alkyl-Substituted 1R at 333 K in the Gas Phase and Benzene [solvation model based on density (SMD)] Compared to Experimental Data in Benzene-*d*<sub>6</sub> in kcal mol<sup>-1</sup>

	$\Delta G_{Z/E}$ , CENSO		experiment
	gas phase	benzene	benzene- <i>d</i> <sub>6</sub>
1Et	-0.15	0.02	-0.14 ± 0.04
1Pr	-0.20	-0.06	-0.15 ± 0.01
1Bu	-0.34	-0.03	-0.16 ± 0.01
1Pe	-0.45	-0.21	-0.08 ± 0.03
1No	0.27	-0.31	-0.11 ± 0.01

While the gas phase computations do not reproduce our experimental data quantitatively, they support the experimental finding that at a certain chain length, further elongation of the alkyl chain leads to a decrease in the *Z*-preference. In contrast, the computed  $\Delta G_{Z/E}$  values in benzene do not fit our experimental data, neither quantitatively nor qualitatively. This suggests a significant deficiency of the employed solvation model based on density (SMD) in accurately reproducing the experimental results which was also previously observed in the literature.<sup>27,35</sup>

#### Branched, Cyclic, and Polycyclic Alkyl Substituents.

Figure 4 shows the experimentally obtained  $\Delta G_{Z/E}$  values of five branched, cyclic-, or polycyclic alkyl-substituted 9,9'-bifluorenylidene balances in seven different solvents. For the *iso*-propyl derivative 1iPr,  $\Delta G_{Z/E}$  was measured between -0.10

and -0.15 kcal mol<sup>-1</sup> favoring the *Z*-isomer in all solvents. The cyclohexyl-substituted derivative 1Cy shows the largest *Z*-preference presented in this study with  $\Delta G_{Z/E}$  ranging from -0.50 to -0.65 kcal mol<sup>-1</sup>. 1tBu is the only molecular balance that strongly favors the *E*-isomer with  $\Delta G_{Z/E}$  being 0.3 to 0.4 kcal mol<sup>-1</sup>. For the bulkier tertiary alkyl-substituted balance 1Ad, we measured  $\Delta G_{Z/E}$  to be between -0.10 and -0.25 kcal mol<sup>-1</sup> favoring the *Z*-isomer. The even bulkier 1Dia was measured to have  $\Delta G_{Z/E}$  essentially around 0 kcal mol<sup>-1</sup>. The comparison of  $\Delta G_{Z/E}$  obtained for 1iPr and 1Cy again supports our working hypothesis that, due to an increase in the substituent size and polarizability from iPr to Cy, the *E/Z* equilibrium shifts toward the "folded" *Z*-isomer due to stabilizing LD interactions between the substituents. When looking at the solvent dependence of  $\Delta G_{Z/E}$  for the various balances, we generally observe an increase in the *Z*-preference with an increase of the solvents' cohesive energy densities (ced), which is a measure for the amount of intermolecular interactions present in a defined volume of solvent. This can be rationalized by the fact that the *Z*-isomer generally has a smaller SES due to solvent exclusion between the two substituents. For example, SMD computations predict the *Z*-isomer of 1Cy to have a SES of 1681 Å<sup>2</sup>, whereas the *E*-isomers' SES is larger (1738 Å<sup>2</sup>). In contrast to previous studies,<sup>28</sup> in which we have used solvent accessible surface areas (SAS), which are strongly solvent dependent, we decided to use the rather solvent-independent SES in this work to emphasize the difference in SES of the differently substituted molecular balances (discussed in more detail later).

The nonlinear experimental results obtained for 1tBu, 1Ad, and 1Dia were rather unexpected because these substituents, compared to 1Cy, have similar or higher polarizabilities and

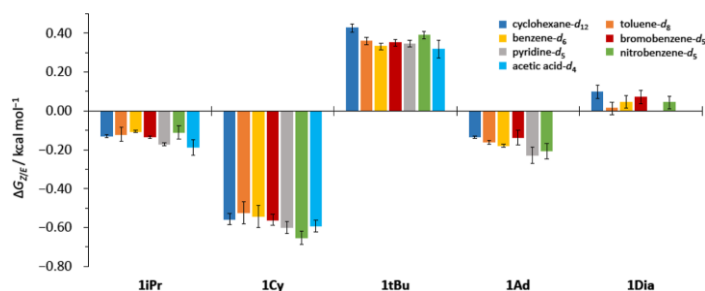


Figure 4.  $\Delta G_{Z/E}$  measured at 333 K for all branched, cyclic, and polycyclic alkyl-substituted molecular balances. **iPr** = *iso*-propyl, **1Cy** = cyclohexyl, **1tBu** = *tert*-butyl, **1Ad** = adamantyl, and **1Dia** = diamantyl. The solvents' cohesive energy density increases from left to right in this group of measurements.

are generally considered to be equally excellent DEDs.<sup>7,8</sup> To rationalize these findings, we performed a variety of computations. We obtained the lowest energy conformer of both *E*- and *Z*-isomers of all five molecular balances, as presented in Figure 4, using CREST. Optimization of these structures was performed with the PBEh-3c composite approach. Single points were computed at revDSD-PBEP86-D4/def2-QZVPP//PBEh-3c employing the SMD solvation model. Selected experimental and computational data are compared in Table 2.

Table 2. Comparison of Selected Experimentally and Computationally Obtained Values for  $\Delta G_{Z/E}$  in Different Organic Solvents in kcal mol<sup>-1</sup>

	$\Delta G_{Z/E}$ , experimental		$\Delta G_{Z/E}$ , computed	
	benzene	pyridine	benzene	pyridine
<b>iPr</b>	-0.11 ± 0.01	-0.17 ± 0.01	0.07	-0.01
<b>1Cy</b>	-0.54 ± 0.06	-0.60 ± 0.03	-0.08	-0.28
<b>1tBu</b>	0.33 ± 0.02	0.35 ± 0.02	0.21	0.02
<b>1Ad</b>	-0.18 ± 0.01	-0.23 ± 0.04	-0.03	-0.25
<b>1Dia</b>	0.05 ± 0.03	- <sup>a</sup>	0.44	0.13

<sup>a</sup>No experimental data available due to non-integrable NMR signals.

We observe that, although our experimental trends are computationally reproduced qualitatively, the quantitative errors are still considerable.

To elucidate how the  $\sim 1.0$  kcal mol<sup>-1</sup> difference in experimental  $\Delta G_{Z/E}$  between **1Cy** and **1tBu** can be explained, we performed sSAPT0/def2-TZVP computations on the five dimers generated by excluding the 9,9'-bifluorenylidene backbone from all PBEh-3c-optimized *Z*-isomers and saturating the resulting radicals with hydrogen atoms (Figure 5). Strikingly, the resulting LD versus Pauli repulsion ratios are the lowest (0.96) for the *iso*-butane dimer and highest (1.48) for the cyclohexane dimer. These results suggest that the interplay of LD and Pauli repulsion is decisive for explaining the experimental trends. To underline these findings, we measured the closest H...H contacts between the substituents in computed and experimental data (see Figure 6). We found that the minimal H-H distance  $r_{H-H}$  is computed to decrease from  $\sim 2.45$  Å for the secondary substituents **iPr** and **Cy** to 2.10 to 2.25 Å for the tertiary substituents **tBu**, **Ad**, and **Dia**. These distances are in very good agreement with literature data, where the change of position of a *tert*-butyl group from

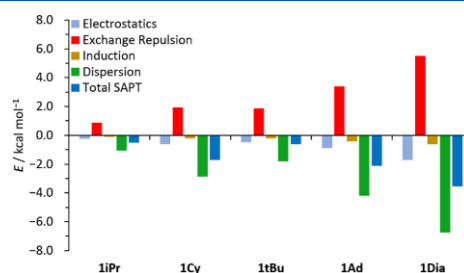


Figure 5. SAPT analysis at the sSAPT0/def2TZVP level of theory. **iPr** = *iso*-propyl, **1Cy** = cyclohexyl, **1tBu** = *tert*-butyl, **1Ad** = adamantyl, and **1Dia** = diamantyl.

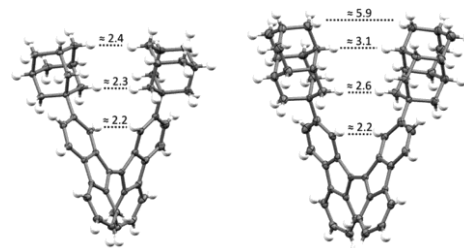


Figure 6. Comparison of the molecular structure of the *Z*-isomers of **1Ad** and **1Dia** obtained via X-ray crystal structure determination. Thermal ellipsoid plots are drawn at a 50% probability level.

*para*- ( $r_{H-H} \approx 2.5$  Å) to *meta*-position ( $r_{H-H} \approx 2.3$  Å) changed its effect from stabilizing to destabilizing.<sup>36</sup> The XRD data for the tertiary-substituted balances generally indicate slightly larger distances, which may be explained with the inaccuracy of XRD in determining the exact H-atom positions and the presence of packing effects. These findings suggest that in the cyclohexyl balance, due to conformational flexibility, the DEDs can orientate themselves in relative positions such that the LD versus Pauli repulsion ratio and therefore also the *Z*-preference is maximized. On the other hand, rigid and bulky groups are increasingly destabilizing the *Z*-isomer due to dominating repulsive interactions arising from very short distances between

Table 3. SES Areas and  $\Delta\Delta G_{\text{sol}}^{\text{v}}$  of all Branched, Cyclic-, and Polycyclic-Substituted Molecular Balances Computed at PBBeh-3c Employing the SMD Model

	SES (E)/Å <sup>2</sup>	SES (Z)/Å <sup>2</sup>	$\Delta\text{SES}$ (E/Z)/%	$\Delta\Delta G_{\text{sol}}^{\text{v}}$ E/Z/kcal mol <sup>-1</sup>
1Pr	1489.6	1474.4	1.0	0.12
1Cy	1737.6	1681.3	3.3	0.53
1tBu	1558.7	1523.6	2.3	0.18
1Ad	1915.7	1847.8	3.7	0.53
1Dia	2167.5	2073.1	4.6	0.86

the DEDs, which can, due to their rigidity, not be overcome by group rotation. Still, even for sterically very demanding substituents, these increasing repulsive interactions are mostly compensated (tBu) or even overwhelmed (Ad and Dia) by LD.

These findings still do not explain the experimentally obtained decline in the Z-preference from 1Ad to 1Dia. To understand this behavior, we studied the influence of solvophobic effects on our molecular balance system. In Table 3, we compare SES with the computed difference in solvation free energy ( $\Delta\Delta G_{\text{sol}}^{\text{v}}$ ) of the E- and Z-isomers.

Owing to vdW contacts between the substituents in the Z-isomer, the SES of all E-isomers is larger than that of their corresponding Z-isomers. Therefore, all E-isomers generally have a higher  $\Delta G_{\text{sol}}^{\text{v}}$  resulting in exclusively positive values for  $\Delta\Delta G_{\text{sol}}^{\text{v}}$ . Also, the isomers' percentage difference in SES ( $\Delta\text{SES}$ ) increases with increasing substituent size. This indicates that (a) solvophobic effects generally shift the equilibrium toward the unfolded E-isomer and (b) this shift is stronger with increasing substituent size due to a larger  $\Delta\text{SES}$ .

Figure 6 illustrates why the increase in  $\Delta\Delta G_{\text{sol}}^{\text{v}}$  from 1Ad to 1Dia can in this case not be compensated by increasing LD interactions. Due to the V-shaped structure of bifluorenylidene balances, the additional atoms present in 1Dia are in relative distances ( $r_{\text{R-R}} = 5.9 \text{ \AA}$ ) such that the resulting additional LD interactions are small compared to the resulting increase in  $\Delta\Delta G_{\text{sol}}^{\text{v}}$ .

The presented molecular balances, therefore, nicely show the interplay of LD, Pauli repulsion, and solvophobic effects in solution. 1Cy is the most Z-favored system due to its ability to rotate the cyclohexyl groups in a position where the ratio of LD versus Pauli repulsion is maximized. For the molecular balances with rigid tertiary substituents (1tBu, 1Ad, and 1Dia), the system has to cope with increasing influence of Pauli repulsion, which destabilizes the Z-isomer and, therefore, shifts the equilibrium toward the E-isomer. Still, LD has the overall strongest influence on  $\Delta G_{\text{Z/E}}$  for all presented balances.

**Aromatic Substituents.** Figure 7 shows experimentally obtained  $\Delta G_{\text{Z/E}}$  for 1Ph and 1PFPh in seven different solvents. Both balances favor the Z-isomer in any solvent chosen. For 1Ph,  $\Delta G_{\text{Z/E}}$  was measured between  $-0.25$  and  $-0.30$  kcal mol<sup>-1</sup> for all solvents besides cyclohexane-*d*<sub>12</sub>, where we obtained a Z-preference of  $-0.45$  kcal mol<sup>-1</sup>. For 1PFPh, we obtained  $\Delta G_{\text{Z/E}}$  between  $-0.10$  and  $-0.35$  kcal mol<sup>-1</sup> in 6 solvents. Cyclohexane-*d*<sub>12</sub> again is the outlier with a  $\Delta G_{\text{Z/E}}$  of  $-0.53$  kcal mol<sup>-1</sup>. Because 1PFPh is the only molecular balance in this study that is substituted with fluorine, its isomers' computed dipole moments in benzene ( $E = 2.4 \text{ D}$  and  $Z = 5.1 \text{ D}$ ) differ significantly from its hydrocarbon-analogue 1Ph ( $E = 0.05 \text{ D}$ ,  $Z = 0.11 \text{ D}$ ). This difference could be the reason for the increase in solvent dependency that we observe in our experimental data for 1PFPh. For a comparison, we have

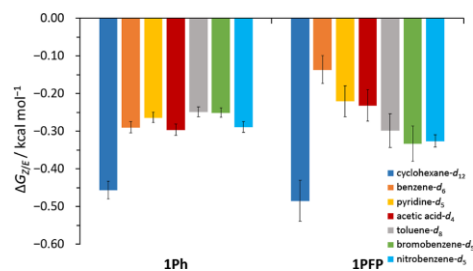


Figure 7.  $\Delta G_{\text{Z/E}}$  measured at 333 K for 1Ph and 1PFPh. 1Ph = phenyl and 1PFPh = pentafluorophenyl. The solvents' cohesive energy density is increasing from left to right in each group of measurements.

computed  $\Delta G_{\text{Z/E}}$  at revDSD-PBEP86-D4/def2-QZVPP//PBBeh-3c and DLPNO-CCSD(T)/def2-TZVP//PBBeh-3c employing the SMD solvation model (Table 4).

We observe that computations at DLPNO-CCSD(T)/def2-TZVP//PBBeh-3c better describe the experimental findings for 1Ph, whereas revDSD-PBEP86-D4/def2-QZVPP//PBBeh-3c gives more accurate results for 1PFPh. Both computational methods fail to identify cyclohexane as the experimental outlier. Although we are not able to provide a simple explanation for the special behavior of 1Ph and 1PFPh in cyclohexane-*d*<sub>12</sub>, we emphasize the structural difference of cyclohexane compared to the other solvents which are mostly aromatic. The bulky and flexible structure of cyclohexane could lead to larger SESs of 1Ph and 1PFPh as compared to the measurements in planar and rigid aromatic solvents. This would increase  $\Delta\text{SES}$  and therefore, the influence of solvophobic effects in cyclohexane, which would explain the shift toward the "folded" Z-isomer that we observe experimentally. Further insights toward this behavior could be obtained by employing explicit solvation methods.

## CONCLUSIONS

We experimentally and computationally determined  $\Delta G_{\text{Z/E}}$  for 13 different 2,2'-disubstituted 9,9'-bifluorenylidene in seven different organic solvents. The vast majority of DEDs in this work shift the E/Z equilibrium toward the apparently sterically more crowded Z-isomer. This behavior can be explained with attractive LD interactions between the two substituents that are brought into close proximity to each other in the Z-isomer. Almost all balances show an increase in the Z-preference with increasing ced of the solvent. This finding can be attributed to the influence of solvophobic effects, which push the equilibrium toward the Z-isomer because it displays a smaller SES.

For linear alkyl substituents, we obtained a peak in the Z-preference for nPr and nBu substitution. The decrease in the Z-

Table 4. Comparison of Experimental and Computational Results for  $\Delta G_{Z/E}$  of 1Ph and 1PPF<sup>a</sup>

solvents	1Ph			1PPF		
	exp.	1)	2)	exp.	1)	2)
cyclohexane	-0.4(6)	-0.04	-0.68	-0.4(8)	-0.36	-1.31
toluene	-0.2(9)	0.05	-0.58	-0.1(4)	-0.36	-1.32
benzene	-0.2(6)	0.05	-0.59	-0.2(2)	-0.35	-1.30
bromobenzene	-0.3(0)	0.31	-0.33	-0.2(3)	-0.40	-1.36
pyridine	-0.2(5)	0.33	-0.31	-0.3(0)	-0.60	-1.55
nitrobenzene	-0.2(5)	0.42	-0.22	-0.3(3)	-0.55	-1.51
acetic acid	-0.2(9)	0.04	-0.60	-0.3(3)	-0.88	-1.84

<sup>a</sup>1) Computed at revDSD-PBEP86-D4/def2-QZVPP//PBEh-3c and 2) Computed at DLPNO-CCSD(T)/def2-TZVP//PBEh-3c; all computations include SMD solvation; all energies in kcal mol<sup>-1</sup>; all experiments were performed in the corresponding deuterated solvent.

preference for longer alkyl chains can be attributed to an increasing entropic penalty required for association of both alkyl chains in the *Z*-isomer and to competing LD interactions between the alkyl chains and the backbone of the molecular balance, stabilizing the *E*- and *Z*-isomers equally. The strongest *Z*-preference in this work was obtained for 1Cy with  $\Delta G_{Z/E} \sim 0.60$  kcal mol<sup>-1</sup>. The cyclohexyl substituent combines high polarizability and moderate flexibility with the ability to rotate into a position to maximize LD interactions and minimize Pauli repulsion. For rigid and sterically very demanding substituents like *t*Bu, Ad, and Dia, we observe an increase in Pauli repulsion between the DEDs, destabilizing the *Z*-isomer. Still, we were able to show that for the larger and highly polarizable Ad and Dia, LD is able to compensate the repulsive interactions. The two aromatic substituents tested in this work (phenyl and perfluorophenyl) favor the *Z*-isomer in all solvents and gave comparable results to each other. We computed  $\Delta G_{Z/E}$  for all molecular balances in this study and found the computational results to reproduce most of our experimental trends qualitatively.

While the introduction of large, rigid, and highly polarizable DEDs has proven to be very successful in influencing chemical processes, this work underlines that there is no “one size fits all” DED, with the cyclohexyl moiety possibly being a notable exception.

## EXPERIMENTAL SECTION

**Synthesis.** Scheme 1 depicts the general synthetic approach for the synthesis of most of the 14 molecular balances 1R prepared in the context of the present study. We used commercially available 2-bromobenzaldehyde 2 and 4-substituted phenylboronic acids 3R in Suzuki–Miyaura coupling reactions to form 4'-substituted [1,1'-biphenyl]-2-carboxaldehydes 4R. 3Ad, 3Dia, and 3Tr are not commercially available and were synthesized from the corresponding 4-substituted bromobenzenes. In the next step, cross dehydrogenative coupling was employed to form the corresponding fluorenones 5R.<sup>37</sup> 5Ph and 5PPF were synthesized via Suzuki–Miyaura coupling reaction of 2-bromofluorenone with the required boronic acids. In the last step, we performed McMurry coupling to give a mixture of the *E*- and *Z*-isomers of 2,2'-disubstituted 9,9'-bifluorenylidene 1R. Detailed spectroscopic data and procedures for the preparation of precursors can be found in the Supporting Information.

**NMR Measurements.** After purification of 1R, the compounds were stored under inert conditions. Depending on solubility, 2–20 mg of 1R were dissolved in acetic acid-*d*<sub>6</sub>, benzene-*d*<sub>6</sub>, bromobenzene-*d*<sub>5</sub>, cyclohexane-*d*<sub>12</sub>, nitrobenzene-*d*<sub>5</sub>, pyridine-*d*<sub>5</sub>, or toluene-*d*<sub>6</sub>. We used NMR-grade solvents stored in glass ampoules of highest commercially available purity. The samples were transferred into a screw-cap NMR tube, flushed with dinitrogen, sealed with parafilm, heated for 16 h at 60 °C using a thermostat, and were then quickly transferred to a 600 MHz Bruker Avance III HD NMR spectrometer.

NMR measurements were performed using a 5 mm BBO probe with Z-gradient pre-tempered to 60 °C. After short re-equilibration inside the probe at 60 °C to minimize experimental errors produced by temperature changes during sample insertion, <sup>1</sup>H NMR spectra were measured with standard parameters and a relaxation delay of 1 s. The NMR-integration workflow was described in the Supporting Information and in previous works.<sup>28</sup> Structural assignments were made with additional information from gCOSY, gHSQC, and gHMBC experiments.

**General Experimental Procedures. General Synthesis of 4'-Substituted [1,1'-Biphenyl]-2-carboxaldehydes 4R.** In a round-bottomed flask, 1.0 equiv of 2-bromobenzaldehyde was dissolved in 15 mL/mmol of DMF/H<sub>2</sub>O (2:1). To the stirred solution, 1.1 equiv of the 4-substituted phenylboronic acid 3R, 1.0 equiv of Na<sub>2</sub>CO<sub>3</sub>, and 2.5 mol % of Pd(OAc)<sub>2</sub> were added in this order. The reaction mixture was stirred at r.t. for 18 h and extracted with dichloromethane (DCM). The combined organic layers were washed with 2 L of dist. H<sub>2</sub>O, dried over Na<sub>2</sub>SO<sub>4</sub>, concentrated under reduced pressure, and purified using flash column chromatography (silica; *n*-hexane/DCM 85:15).

**4'-Ethyl-[1,1'-biphenyl]-2-carboxaldehyde (4Et).** Colorless oil (502 mg, 89%). <sup>1</sup>H NMR (400 MHz, CDCl<sub>3</sub>):  $\delta$  10.00 (s, 1H), 8.02 (dd, *J* = 7.8, 1.2 Hz, 1H), 7.63 (td, *J* = 7.5, 1.4 Hz, 1H), 7.52–7.42 (m, 2H), 7.30 (s, 4H), 2.73 (q, *J* = 7.6 Hz, 2H), 1.30 (t, *J* = 7.6 Hz, 3H) ppm. The obtained spectroscopic data are in good agreement to the literature.<sup>38</sup>

**4'-*n*-Propyl-[1,1'-biphenyl]-2-carboxaldehyde (4Pr).** Colorless oil (481 mg, 87%). <sup>1</sup>H NMR (400 MHz, CDCl<sub>3</sub>):  $\delta$  10.00 (d, *J* = 0.7 Hz, 1H), 8.02 (dd, *J* = 7.8, 1.1 Hz, 1H), 7.63 (td, *J* = 7.5, 1.4 Hz, 1H), 7.52–7.41 (m, 2H), 7.29 (s, 4H), 2.66 (t, *J* = 7.4 Hz, 2H), 1.70 (h, *J* = 7.4 Hz, 2H), 0.99 (t, *J* = 7.3 Hz, 3H) ppm. The obtained spectroscopic data are in good agreement to the literature.<sup>38</sup>

**4'-*n*-Butyl-[1,1'-biphenyl]-2-carboxaldehyde (4Bu).** Colorless oil (1135 mg, 93%). <sup>1</sup>H NMR (400 MHz, CDCl<sub>3</sub>):  $\delta$  10.00 (d, *J* = 0.7 Hz, 1H), 8.02 (dd, *J* = 7.8, 1.1 Hz, 1H), 7.63 (td, *J* = 7.5, 1.4 Hz, 1H), 7.55–7.41 (m, 2H), 7.29 (s, 4H), 2.74–2.65 (m, 2H), 1.71–1.61 (m, 2H), 1.40 (h, *J* = 7.3 Hz, 2H), 0.96 (t, *J* = 7.3 Hz, 3H) ppm. <sup>13</sup>C{<sup>1</sup>H} NMR (101 MHz, CDCl<sub>3</sub>):  $\delta$  192.9, 146.2, 143.2, 135.1, 133.9, 133.7, 130.9, 130.2, 128.7, 127.7, 35.5, 33.7, 22.6, 14.1 ppm. HRMS (ESI-TOF) *m/z*: [M + Na]<sup>+</sup> calcd for C<sub>17</sub>H<sub>18</sub>ONa, 261.1250; found, 261.1248. IR (Film): 446 (w), 633 (w), 647 (w), 763 (s), 830 (m), 1005 (w), 1193 (m), 1254 (w), 1392 (w), 1449 (w), 1475 (w), 1597 (m), 1691 (s), 2857 (w), 2929 (w), 2956 (w) cm<sup>-1</sup>.

**4'-*n*-Pentyl-[1,1'-biphenyl]-2-carboxaldehyde (4Pe).** Colorless oil (251 mg, 85%). <sup>1</sup>H NMR (400 MHz, CDCl<sub>3</sub>):  $\delta$  10.00 (d, *J* = 0.7 Hz, 1H), 8.02 (dd, *J* = 7.7, 1.2 Hz, 1H), 7.63 (td, *J* = 7.5, 1.5 Hz, 1H), 7.52–7.42 (m, 2H), 7.29 (s, 4H), 2.73–2.62 (m, 2H), 1.73–1.61 (m, 2H), 1.46–1.29 (m, 4H), 0.98–0.86 (m, 3H) ppm. <sup>13</sup>C{<sup>1</sup>H} NMR (101 MHz, CDCl<sub>3</sub>):  $\delta$  192.7, 146.1, 143.1, 135.0, 133.8, 133.5, 130.8, 130.1, 128.5, 127.5, 35.6, 31.6, 31.1, 22.6, 14.0 ppm. HRMS (ESI-TOF) *m/z*: [M + Na]<sup>+</sup> calcd for C<sub>18</sub>H<sub>20</sub>ONa, 275.1406; found, 275.1409. IR (Film): 408 (s), 422 (s), 765 (m), 830 (w), 1194 (m), 1254 (m), 1392 (m), 1597 (m), 1693 (s), 2856 (m), 2929 (s), 2956 (m) cm<sup>-1</sup>.

**4'-n-Nonyl-[1,1'-biphenyl]-2-carboxaldehyde (4No).** Colorless oil (246 mg, 85%). <sup>1</sup>H NMR (400 MHz, CDCl<sub>3</sub>): δ 10.00 (d, J = 0.7 Hz, 1H), 8.01 (dd, J = 7.8, 1.1 Hz, 1H), 7.62 (td, J = 7.5, 1.4 Hz, 1H), 7.50–7.42 (m, 2H), 7.28 (s, 4H), 2.71–2.64 (m, 2H), 1.72–1.60 (m, 2H), 1.39–1.23 (m, 12H), 0.93–0.83 (m, 3H) ppm. <sup>13</sup>C{<sup>1</sup>H} NMR (101 MHz, CDCl<sub>3</sub>): δ 192.7, 146.1, 143.1, 135.0, 133.8, 133.5, 130.8, 130.0, 128.5, 127.5, 35.7, 31.9, 31.4, 29.6, 29.5, 29.4, 29.3, 22.7, 14.1 ppm. HRMS (ESI-TOF) *m/z*: [M + Na]<sup>+</sup> calcd for C<sub>23</sub>H<sub>28</sub>ONa, 331.2032; found, 331.2035. IR (Film): 445 (w), 633 (w), 647 (w), 763 (s), 828 (m), 1193 (m), 1254 (m), 1597 (m), 1692 (s), 2853 (s), 2923 (s) cm<sup>-1</sup>.

**4'-Isopropyl-[1,1'-biphenyl]-2-carboxaldehyde (4iPr).** Colorless oil (488 mg, 92%). <sup>1</sup>H NMR (400 MHz, CDCl<sub>3</sub>): δ 10.00 (d, 1H), 8.02 (dd, J = 7.8, 1.1 Hz, 1H), 7.63 (td, J = 7.5, 1.4 Hz, 1H), 7.51–7.42 (m, 2H), 7.37–7.28 (m, 4H), 3.05–2.92 (m, 1H), 1.31 (d, J = 6.9 Hz, 6H) ppm. <sup>13</sup>C{<sup>1</sup>H} NMR (101 MHz, CDCl<sub>3</sub>): δ 192.7, 149.0, 146.1, 135.1, 133.8, 133.5, 130.8, 130.1, 127.53, 127.50, 126.5, 33.9, 24.0 ppm. HRMS (ESI-TOF) *m/z*: [M + Na]<sup>+</sup> calcd for C<sub>18</sub>H<sub>18</sub>ONa, 247.1093; found, 247.1092. IR (ATR): 746 (m), 767 (s), 837 (s), 1194 (m), 1254 (m), 1597 (m), 1691 (s), 2869 (w), 2960 (m) cm<sup>-1</sup>.

**4'-Cyclohexyl-[1,1'-biphenyl]-2-carboxaldehyde (4Cy).** Colorless oil (233 mg, 86%). <sup>1</sup>H NMR (400 MHz, CDCl<sub>3</sub>): δ 10.00 (d, J = 0.7 Hz, 1H), 8.02 (dd, J = 7.8, 1.0 Hz, 1H), 7.63 (td, J = 7.5, 1.4 Hz, 1H), 7.55–7.40 (m, 2H), 7.31 (s, 4H), 2.68–2.44 (m, 1H), 2.01–1.82 (m, 4H), 1.83–1.73 (m, 1H), 1.54–1.36 (m, 4H), 1.36–1.19 (m, 1H) ppm. <sup>13</sup>C{<sup>1</sup>H} NMR (101 MHz, CDCl<sub>3</sub>): δ 192.8, 148.2, 146.1, 135.1, 133.8, 133.5, 130.8, 130.1, 127.50, 127.48, 126.92, 44.3, 34.4, 26.9, 26.1 ppm. HRMS (ESI-TOF) *m/z*: [M + Na]<sup>+</sup> calcd for C<sub>19</sub>H<sub>20</sub>ONa, 287.1406; found, 287.1409. IR (Film): 408 (s), 420 (s), 766 (m), 833 (m), 1194 (w), 1255 (m), 1448 (w), 1598 (m), 1694 (s), 2851 (m), 2925 (s) cm<sup>-1</sup>.

**4'-tert-Butyl-[1,1'-biphenyl]-2-carboxaldehyde (4Cy).** Colorless oil (863 mg, 94%). <sup>1</sup>H NMR (400 MHz, CDCl<sub>3</sub>): δ 10.01 (d, J = 0.7 Hz, 1H), 8.02 (dd, J = 7.8, 1.0 Hz, 1H), 7.63 (td, J = 7.5, 1.5 Hz, 1H), 7.51–7.43 (m, 4H), 7.36–7.28 (m, 2H), 1.38 (s, 9H) ppm. <sup>13</sup>C{<sup>1</sup>H} NMR (101 MHz, CDCl<sub>3</sub>): δ 192.7, 151.3, 146.0, 134.8, 133.8, 133.5, 130.8, 129.9, 127.53, 127.49, 125.4, 34.7, 31.4 ppm. HRMS (ESI-TOF) *m/z*: [M + Na]<sup>+</sup> calcd for C<sub>17</sub>H<sub>18</sub>ONa, 261.1250; found, 261.1247.

**General Synthesis of 4'-substituted phenylboronic acids 3R** with subsequent Suzuki coupling to 4'-substituted [1,1'-biphenyl]-2-carboxaldehydes **4R**. In a dried, N<sub>2</sub> flushed one-neck Schlenk flask equipped with a septum, 1.0 equiv of the 4-substituted phenyl halide was dissolved in 5 mL/mmol dry THF. The solution was cooled to –78 °C with an acetone/N<sub>2</sub> bath and 1.2 equiv of *n*-BuLi was added over 20 min at constant temperature using a syringe pump. After stirring for 15 min at –78 °C, 1.5 equiv of B(OMe)<sub>3</sub> was added over 1 h at constant temperature using a syringe pump. After addition, the cooling bath was removed and the reaction mixture was allowed to slowly warm to r.t. After 30 min at r.t., the reaction mixture was acidified using 1.8 equiv of 1 M HCl aqueous solution, extracted with DCM and the combined organic layers were dried over Na<sub>2</sub>SO<sub>4</sub> and concentrated under reduced pressure. The crude product was used in a Suzuki coupling reaction as described before.

**4'-Adamantyl-[1,1'-biphenyl]-2-carboxaldehyde (4Ad).** Colorless solid (755 mg, 52%). <sup>1</sup>H NMR (400 MHz, CDCl<sub>3</sub>): δ 10.00 (s, 1H), 8.02 (d, J = 8.0 Hz, 1H), 7.62 (td, J = 7.5, 1.4 Hz, 1H), 7.51–7.42 (m, 4H), 7.36–7.30 (m, 2H), 2.17–2.09 (m, 3H), 1.97 (d, J = 2.7 Hz, 6H), 1.87–1.73 (m, 6H) ppm. <sup>13</sup>C{<sup>1</sup>H} NMR (101 MHz, CDCl<sub>3</sub>): δ 192.8, 151.5, 146.1, 134.8, 133.8, 133.5, 130.8, 129.9, 127.49, 127.47, 125.0, 43.2, 36.8, 36.2, 28.9 ppm. HRMS (ESI-TOF) *m/z*: [M + Na]<sup>+</sup> calcd for C<sub>23</sub>H<sub>24</sub>ONa, 339.1719; found, 339.1721. IR (ATR): 445 (w), 579 (m), 644 (w), 779 (s), 1193 (m), 1254 (m), 1393 (m), 1448 (m), 1594 (m), 1690 (s), 2845 (m), 2899 (m) cm<sup>-1</sup>.

**4'-Diamantyl-[1,1'-biphenyl]-2-carboxaldehyde (4Dia).** Colorless solid (1960 mg, 66%). <sup>1</sup>H NMR (400 MHz, CDCl<sub>3</sub>): δ 10.01 (s, 1H), 8.09–7.96 (m, 1H), 7.63 (td, J = 7.5, 1.4 Hz, 1H), 7.54–7.42 (m, 4H), 7.38–7.30 (m, 2H), 1.98–1.92 (m, 9H), 1.88–1.83 (m, 1H), 1.83–1.76 (m, 9H) ppm. <sup>13</sup>C{<sup>1</sup>H} NMR (101 MHz, CDCl<sub>3</sub>): δ 192.8, 150.9, 146.1, 134.8, 133.8, 133.5, 130.8, 129.9, 127.49, 127.5,

125.3, 44.0, 38.3, 37.8, 36.8, 34.4, 25.8 ppm. HRMS (APCI-TOF) *m/z*: [M + H]<sup>+</sup> calcd for C<sub>25</sub>H<sub>29</sub>O 369.2213; found, 369.2182. IR (ATR): 437 (w), 493 (w), 538 (w), 572 (m), 655 (m), 742 (s), 763 (s), 833 (s), 1193 (m), 1254 (m), 1595 (m), 1688 (s), 2844 (s), 2870 (s), 2907 (m) cm<sup>-1</sup>.

**4'-Trityl-[1,1'-biphenyl]-2-carboxaldehyde (4Tr).** Colorless solid (1340 mg, 47%). <sup>1</sup>H NMR (400 MHz, CDCl<sub>3</sub>): δ 10.03 (s, 1H), 8.02 (d, J = 7.9 Hz, 1H), 7.63 (td, J = 7.5, 1.4 Hz, 1H), 7.53–7.43 (m, 2H), 7.38–7.17 (m, 19H) ppm. <sup>13</sup>C{<sup>1</sup>H} NMR (101 MHz, CDCl<sub>3</sub>): δ 192.6, 147.0, 146.5, 145.7, 135.2, 133.7, 133.6, 131.2, 131.1, 130.7, 129.3, 127.7, 127.6, 127.5, 126.1, 64.9 ppm. HRMS (ESI-TOF) *m/z*: [M + Na]<sup>+</sup> calcd for C<sub>23</sub>H<sub>24</sub>ONa, 447.1719; found, 447.1716. IR (ATR): 636 (s), 700 (s), 748 (s), 837 (m), 1198 (w), 1255 (w), 1442 (w), 1490 (w), 1597 (w), 1693 (s), 3030 (vw) cm<sup>-1</sup>.

**General Synthesis of 2-Substituted 9-Fluorenone 5R.** In a dried, N<sub>2</sub> flushed 50 mL one-neck Schlenk flask equipped with a reflux condenser, 1.0 equiv of 4'-substituted [1,1'-biphenyl]-2-carboxaldehyde was dissolved in 5 mL/mmol dry MeCN. To the stirred solution, 1.1 equiv of tBuOOH solution in *n*-decane (5–6 mol L<sup>-1</sup>) and 0.1 mol % FeCp<sub>2</sub> in MeCN (5 mmol L<sup>-1</sup>) were added, and the mixture was refluxed for 6 h using an oil bath. After cooling to r.t., additional 1.1 equiv of tBuOOH solution in *n*-decane (5–6 mol L<sup>-1</sup>) was added and the mixture was refluxed for 18 h. After cooling to r.t., the reaction mixture was extracted with 50 mL of DCM. The combined organic layers were washed with water, dried over Na<sub>2</sub>SO<sub>4</sub>, concentrated under reduced pressure, and purified using flash column chromatography (silica; *n*-hexane/ethyl acetate 99:1).

**2-Ethyl-9-fluorenone (5Et).** Yellow oil (140 mg, 57%). <sup>1</sup>H NMR (400 MHz, CDCl<sub>3</sub>): δ 7.63 (d, J = 7.3 Hz, 1H), 7.53–7.38 (m, 4H), 7.32–7.22 (m, 2H), 2.67 (q, J = 7.6 Hz, 2H), 1.26 (t, J = 7.6 Hz, 3H) ppm. <sup>13</sup>C{<sup>1</sup>H} NMR (101 MHz, CDCl<sub>3</sub>): δ 194.4, 145.9, 144.8, 142.2, 134.8, 134.7, 134.5, 134.3, 128.7, 124.4, 124.0, 120.2, 28.9, 15.5 ppm. HRMS (ESI-TOF) *m/z*: [M + Na]<sup>+</sup> calcd for C<sub>15</sub>H<sub>12</sub>ONa, 231.0780; found, 231.0782. IR (ATR): 416 (s), 737 (m), 1107 (w), 1177 (w), 1292 (w), 1458 (m), 1604 (m), 1716 (s), 2966 (w) cm<sup>-1</sup>.

**2-n-Propyl-9-fluorenone (5Pr).** Yellow oil (167 mg, 56%). <sup>1</sup>H NMR (400 MHz, CDCl<sub>3</sub>): δ 7.61 (d, J = 7.3 Hz, 1H), 7.49–7.36 (m, 4H), 7.29–7.20 (m, 2H), 2.59 (t, J = 7.3 Hz, 2H), 1.65 (h, J = 7.4 Hz, 2H), 0.94 (t, J = 7.3 Hz, 3H) ppm. <sup>13</sup>C{<sup>1</sup>H} NMR (101 MHz, CDCl<sub>3</sub>): δ 194.4, 144.8, 144.3, 142.2, 134.8, 134.7, 134.5, 128.7, 124.5, 124.3, 120.1, 37.9, 24.4, 13.8 ppm. HRMS (ESI-TOF) *m/z*: [M + Na]<sup>+</sup> calcd for C<sub>16</sub>H<sub>14</sub>ONa, 245.0937; found, 245.0939. IR (ATR): 416 (s), 743 (m), 767 (w), 1458 (w), 1601 (m), 1708 (s), 2867 (vw), 2925 (vw), 2955 (w) cm<sup>-1</sup>.

**2-n-Butyl-9-fluorenone (5Bu).** Yellow oil (165 mg, 83%). <sup>1</sup>H NMR (400 MHz, CDCl<sub>3</sub>): δ 7.63 (dt, J = 7.3, 0.9 Hz, 1H), 7.51–7.38 (m, 4H), 7.31–7.22 (m, 2H), 2.63 (t, J = 7.3 Hz, 2H), 1.67–1.55 (m, 2H), 1.36 (h, J = 7.3 Hz, 2H), 0.93 (t, J = 7.3 Hz, 3H) ppm. <sup>13</sup>C{<sup>1</sup>H} NMR (101 MHz, CDCl<sub>3</sub>): δ 194.4, 144.8, 144.6, 142.2, 134.80, 134.77, 134.6, 134.5, 128.7, 124.5, 124.4, 120.3, 120.1, 35.6, 33.5, 22.4, 14.1 ppm. HRMS (ESI-TOF) *m/z*: [M + Na]<sup>+</sup> calcd for C<sub>17</sub>H<sub>16</sub>ONa, 259.1093; found, 259.1092. IR (ATR): 490 (w), 650 (m), 737 (s), 765 (s), 835 (m), 962 (w), 1108 (m), 1177 (m), 1292 (m), 1457 (s), 1603 (s), 1713 (s), 2857 (w), 2928 (w), 2952 (w) cm<sup>-1</sup>.

**2-n-Pentyl-9-fluorenone (5Pe).** Yellow oil (68 mg, 53%). <sup>1</sup>H NMR (400 MHz, CDCl<sub>3</sub>): δ 7.63 (dt, J = 7.3, 1.0 Hz, 1H), 7.51–7.38 (m, 4H), 7.31–7.22 (m, 2H), 2.62 (t, J = 7.5 Hz, 2H), 1.63 (p, J = 7.5 Hz, 2H), 1.41–1.26 (m, 4H), 0.89 (t, J = 6.9 Hz, 3H) ppm. <sup>13</sup>C{<sup>1</sup>H} NMR (101 MHz, CDCl<sub>3</sub>): δ 194.5, 144.8, 144.6, 142.2, 134.81, 134.78, 134.6, 134.5, 128.7, 124.5, 124.4, 120.3, 120.1, 35.9, 31.5, 31.0, 22.7, 14.2 ppm. HRMS (ESI-TOF) *m/z*: [M + Na]<sup>+</sup> calcd for C<sub>18</sub>H<sub>18</sub>ONa, 273.1250; found, 273.1248. IR (ATR): 738 (s), 765 (m), 845 (w), 956 (w), 1108 (m), 1177 (m), 1292 (m), 1458 (s), 1604 (s), 1715 (s), 2857 (w), 2928 (m), 2955 (w) cm<sup>-1</sup>.

**2-n-Nonyl-9-fluorenone (5No).** Yellow oil (166 mg, 61%). <sup>1</sup>H NMR (400 MHz, CDCl<sub>3</sub>): δ 7.63 (d, J = 7.3 Hz, 1H), 7.51–7.38 (m, 4H), 7.30–7.26 (m, 1H), 7.26–7.21 (m, 1H), 2.66–2.58 (m, 2H), 1.66–1.58 (m, 2H), 1.35–1.23 (m, 12H), 0.90–0.85 (m, 3H) ppm.

$^{13}\text{C}\{^1\text{H}\}$  NMR (101 MHz,  $\text{CDCl}_3$ ):  $\delta$  194.6, 144.9, 144.7, 142.2, 134.81, 134.78, 134.7, 128.7, 124.5, 124.4, 120.3, 120.1, 35.9, 32.0, 31.3, 29.7, 29.6, 29.5, 29.3, 22.8, 14.3 ppm. HRMS (ESI-TOF)  $m/z$ :  $[\text{M} + \text{Na}]^+$  calcd for  $\text{C}_{23}\text{H}_{26}\text{ONa}$ , 329.1876; found, 329.1873. IR (ATR): 650 (w), 737 (s), 766 (m), 834 (w), 963 (w), 1107 (m), 1177 (m), 1292 (m), 1458 (s), 1603 (s), 1715 (s), 2853 (s), 2923 (s)  $\text{cm}^{-1}$ .

**2-Isopropyl-9-fluorenone (5iPr).** Yellow oil (414 mg, 71%).  $^1\text{H}$  NMR (400 MHz,  $\text{CDCl}_3$ ):  $\delta$  7.63 (d,  $J = 7.3$  Hz, 1H), 7.55 (d,  $J = 1.6$  Hz, 1H), 7.50–7.40 (m, 3H), 7.37–7.31 (m, 1H), 7.28–7.22 (m, 1H), 2.94 (hept,  $J = 6.9$  Hz, 1H), 1.27 (d,  $J = 6.9$  Hz, 6H) ppm.  $^{13}\text{C}\{^1\text{H}\}$  NMR (101 MHz,  $\text{CDCl}_3$ ):  $\delta$  194.3, 150.5, 144.7, 142.2, 134.7, 134.5, 134.4, 132.9, 128.6, 124.3, 122.4, 120.2, 120.0, 34.1, 23.8 ppm. HRMS (ESI-TOF)  $m/z$ :  $[\text{M} + \text{Na}]^+$  calcd for  $\text{C}_{16}\text{H}_{14}\text{ONa}$ , 245.0937; found, 245.0936. IR (ATR): 517 (m), 737 (m), 1109 (m), 1256 (m), 1385 (m), 1458 (w), 1605 (w), 1718 (s), 2960 (w)  $\text{cm}^{-1}$ .

**2-Cyclohexyl-9-fluorenone (5Cy).** Yellow oil (142 mg, 57%).  $^1\text{H}$  NMR (600 MHz,  $\text{CDCl}_3$ ):  $\delta$  7.62 (d,  $J = 7.3$  Hz, 1H), 7.53 (d,  $J = 1.5$  Hz, 1H), 7.48–7.39 (m, 3H), 7.31 (dd,  $J = 7.6, 1.6$  Hz, 1H), 7.26–7.22 (m, 1H), 2.56–2.48 (m, 1H), 1.92–1.82 (m, 4H), 1.80–1.71 (m, 1H), 1.48–1.34 (m, 4H), 1.31–1.20 (m, 1H) ppm.  $^{13}\text{C}\{^1\text{H}\}$  NMR (151 MHz,  $\text{CDCl}_3$ ):  $\delta$  194.5, 149.8, 144.8, 142.3, 134.8, 134.58, 134.55, 133.5, 128.7, 124.4, 122.9, 120.4, 120.1, 44.6, 34.3, 26.9, 26.1 ppm. HRMS (ESI-TOF)  $m/z$ :  $[\text{M} + \text{Na}]^+$  calcd for  $\text{C}_{19}\text{H}_{18}\text{ONa}$ , 285.1250; found, 285.1252. IR (ATR): 492 (m), 735 (s), 767 (m), 834 (m), 960 (w), 1103 (m), 1177 (m), 1291 (m), 1457 (s), 1603 (s), 1712 (s), 2850 (m), 2922 (s)  $\text{cm}^{-1}$ .

**2-tert-Butyl-9-fluorenone (5tBu).** Yellow oil (755 mg, 61%).  $^1\text{H}$  NMR (600 MHz,  $\text{CDCl}_3$ ):  $\delta$  7.71 (d,  $J = 1.7$  Hz, 1H), 7.63 (d,  $J = 7.3$  Hz, 1H), 7.52–7.41 (m, 4H), 7.26–7.22 (m, 1H), 1.34 (s, 9H) ppm.  $^{13}\text{C}\{^1\text{H}\}$  NMR (151 MHz,  $\text{CDCl}_3$ ):  $\delta$  194.4, 152.8, 144.5, 141.8, 134.6, 134.5, 134.2, 131.5, 128.6, 124.2, 121.6, 120.1, 120.0, 35.1, 31.2 ppm. HRMS (ESI-TOF)  $m/z$ :  $[\text{M} + \text{Na}]^+$  calcd for  $\text{C}_{17}\text{H}_{16}\text{ONa}$ , 259.1093; found, 259.1096.

**2-Adamantyl-9-fluorenone (5Ad).** Yellow solid (87 mg, 53%).  $^1\text{H}$  NMR (400 MHz,  $\text{CDCl}_3$ ):  $\delta$  7.71 (dd,  $J = 1.8, 0.7$  Hz, 1H), 7.63 (dt,  $J = 7.3, 1.0$  Hz, 1H), 7.51–7.41 (m, 4H), 7.29–7.21 (m, 1H), 2.17–2.08 (m, 3H), 1.96–1.90 (m, 6H), 1.85–1.71 (m, 6H) ppm.  $^{13}\text{C}\{^1\text{H}\}$  NMR (101 MHz,  $\text{CDCl}_3$ ):  $\delta$  194.6, 153.3, 144.8, 142.0, 134.8, 134.4, 131.4, 128.7, 124.4, 121.5, 120.2, 43.2, 36.79, 36.76, 29.0 ppm. HRMS (ESI-TOF)  $m/z$ :  $[\text{M} + \text{Na}]^+$  calcd for  $\text{C}_{23}\text{H}_{22}\text{ONa}$ , 337.1563; found, 337.1560. IR (ATR): 491 (m), 587 (m), 725 (s), 762 (m), 811 (m), 835 (m), 1106 (m), 1181 (m), 1291 (m), 1461 (m), 1603 (m), 1713 (s), 2847 (m), 2880 (s), 2910 (m)  $\text{cm}^{-1}$ .

**2-Diamantyl-9-fluorenone (5Dia).** Yellow solid (290 mg, 45%).  $^1\text{H}$  NMR (400 MHz,  $\text{CDCl}_3$ ):  $\delta$  7.72 (d,  $J = 1.5$  Hz, 1H), 7.63 (d,  $J = 7.3$  Hz, 1H), 7.53–7.42 (m, 4H), 7.28–7.22 (m, 1H), 1.98–1.91 (m, 3H), 1.91–1.87 (m, 6H), 1.86–1.82 (m, 1H), 1.81–1.75 (m, 9H) ppm.  $^{13}\text{C}\{^1\text{H}\}$  NMR (101 MHz,  $\text{CDCl}_3$ ):  $\delta$  194.5, 152.6, 144.7, 141.8, 134.62, 134.59, 134.3, 131.5, 128.6, 124.2, 121.6, 120.1, 120.0, 43.8, 38.1, 37.7, 36.6, 34.8, 25.7 ppm. HRMS (APCI-TOF)  $m/z$ :  $[\text{M} + \text{H}]^+$  calcd for  $\text{C}_{27}\text{H}_{27}\text{O}$ , 367.2066; found, 367.2056. IR (ATR): 496 (m), 585 (m), 738 (s), 767 (m), 840 (m), 1457 (m), 1603 (m), 1702 (s), 2843 (m), 2897 (s)  $\text{cm}^{-1}$ .

**2-Trityl-9-fluorenone (5Tr).** Yellow solid (45 mg, 53%).  $^1\text{H}$  NMR (400 MHz,  $\text{CDCl}_3$ ):  $\delta$  7.62 (d,  $J = 7.3$  Hz, 1H), 7.58 (t,  $J = 1.2$  Hz, 1H), 7.49–7.41 (m, 2H), 7.39 (d,  $J = 1.2$  Hz, 2H), 7.30–7.16 (m, 16H) ppm.  $^{13}\text{C}\{^1\text{H}\}$  NMR (101 MHz,  $\text{CDCl}_3$ ):  $\delta$  194.0, 148.8, 146.3, 144.3, 142.3, 137.4, 134.83, 134.79, 133.8, 131.1, 129.0, 127.9, 127.1, 126.3, 124.4, 120.4, 119.7, 65.2 ppm. HRMS (ESI-TOF)  $m/z$ :  $[\text{M} + \text{Na}]^+$  calcd for  $\text{C}_{32}\text{H}_{22}\text{ONa}$ , 445.1563; found, 445.1566. IR (ATR): 476 (w), 635 (m), 651 (m), 700 (s), 737 (s), 907 (m), 1103 (m), 1455 (m), 1490 (m), 1601 (m), 1708 (s), 3056 (vw)  $\text{cm}^{-1}$ .

**Synthesis of 2-Methyl-9-fluorenone 5Me.** In a nitrogen flushed, dried 50 mL Schlenk flask, equipped with a magnetic stir bar and septum, 1 equiv 2-bromo-9-fluorenone (1.00 g, 3.86 mmol), 5 mol % Sphos (97 mg, 0.24 mmol), and 2.5 mol %  $\text{Pd}(\text{Oac})_2$  (27 mg, 0.12 mmol) were added. After the mixture was dissolved in 10 mL dry THF, 8.9 mL of a 0.53 M  $\text{MeZnCl}$  solution in THF was added

dropwise over a period of 45 min. After stirring for 1 h, the reaction was quenched with excess aqueous  $\text{NH}_4\text{Cl}$  solution, extracted with ethyl acetate ( $3 \times 20$  mL), and the combined organic layers were concentrated under reduced pressure. After column chromatography (silica; *n*-hexane/ $\text{Et}_2\text{O}$  50:1), 2-methyl-9-fluorenone (403 mg, 2.05 mmol) was obtained as yellow oil in 53% yield.  $^1\text{H}$  NMR (400 MHz,  $\text{CDCl}_3$ ):  $\delta$  7.60 (dt,  $J = 7.3, 0.9$  Hz, 1H), 7.47–7.40 (m, 3H), 7.39–7.33 (m, 1H), 7.28–7.19 (m, 2H), 2.35 (s, 3H) ppm.  $^{13}\text{C}\{^1\text{H}\}$  NMR (101 MHz,  $\text{CDCl}_3$ ):  $\delta$  193.1, 143.6, 140.8, 138.2, 134.1, 133.6, 133.4, 133.3, 127.5, 124.0, 123.2, 119.1, 118.9, 20.3 ppm. Obtained spectroscopic data are in good agreement to the literature.<sup>58</sup>

**Synthesis of 2-Phenyl-9-fluorenone 5Ph.** 2-Bromofluorenone, phenylboronic acid (1.3 equiv), and  $\text{Pd}(\text{PPh}_3)_4$  (0.02 equiv) were dissolved in 54 mL  $\text{mmol}^{-1}$  tetrahydrofuran (THF).  $\text{K}_2\text{CO}_3$  aqueous solution (3 equiv, 25%) was added, the reaction mixture was refluxed overnight using an oil bath, cooled to room temperature, filtered, dried over  $\text{MgSO}_4$ , and concentrated under reduced pressure. The crude product was purified via silica gel column chromatography (*n*-hexane/DCM 95:5). 2-Phenyl-9-fluorenone (360 mg, 76%) was obtained as a yellow solid.  $^1\text{H}$  NMR (400 MHz,  $\text{CDCl}_3$ ):  $\delta$  7.91 (d,  $J = 1.7$  Hz, 1H), 7.72 (dd,  $J = 7.7, 1.8$  Hz, 1H), 7.68 (d,  $J = 7.3$  Hz, 1H), 7.66–7.43 (m, 7H), 7.42–7.35 (m, 1H), 7.34–7.27 (m, 1H) ppm.  $^{13}\text{C}\{^1\text{H}\}$  NMR (101 MHz,  $\text{CDCl}_3$ ):  $\delta$  194.0, 144.5, 143.4, 142.5, 140.0, 135.1, 135.0, 134.7, 133.4, 129.2, 129.1, 128.1, 127.0, 124.6, 123.1, 120.8, 120.5 ppm. HRMS (ESI-TOF)  $m/z$ :  $[\text{M} + \text{Na}]^+$  calcd for  $\text{C}_{19}\text{H}_{12}\text{ONa}$ , 279.0780; found, 279.0778. IR (ATR): 476 (w), 697 (s), 735 (s), 755 (s), 846 (w), 1455 (w), 1600 (w), 1709 (s), 3055 (vw)  $\text{cm}^{-1}$ .

**Synthesis of 2-Pentafluorophenyl-9-fluorenone 5PF2P.** 2-Bromofluorenone (0.1039 g, 0.401 mmol, 1 equiv) was dissolved in 4 mL DMF under Schlenk conditions. (Pentafluorophenyl)boronic acid (0.1106 g, 0.522 mmol, 1.3 eq),  $\text{Pd}_2(\text{dba})_3$  (0.0197 g, 0.0215 mmol, 0.05 equiv), CsF (0.1224 g, 0.806 mmol, 2 equiv),  $\text{Ag}_2\text{O}$  (0.1112 g, 0.480 mmol, 1.2 equiv), and  $\text{P}(t\text{-Bu})_3$  (0.015 mL, 0.0618 mmol, 0.15 equiv) were added and the reaction mixture was stirred under a nitrogen atmosphere overnight in a 100 °C oil bath. After cooling to room temperature, the reaction mixture was filtered over a Celite plug, which was washed with 50 mL  $\text{EtOAc}$ . The organic phase was washed two times with brine, dried over  $\text{MgSO}_4$ , and the solvent was removed under reduced pressure. The crude product was purified by silica gel column chromatography (DCM/*n*-hexane 2:1). 2-(pentafluorophenyl)-9-fluorenone (71 mg, 51%) was obtained as a yellow solid.  $^1\text{H}$  NMR (400 MHz,  $\text{CDCl}_3$ ):  $\delta$  7.74–7.69 (m, 2H), 7.66 (dd,  $J = 7.8, 0.7$  Hz, 1H), 7.60 (dt,  $J = 7.4, 1.0$  Hz, 1H), 7.57–7.52 (m, 2H), 7.36 (td,  $J = 7.4, 1.1$  Hz, 1H) ppm.  $^{13}\text{C}\{^1\text{H}, ^{19}\text{F}\}$  NMR (101 MHz,  $\text{CDCl}_3$ ):  $\delta$  193.0, 145.3, 144.4, 143.8, 140.9, 138.1, 136.5, 135.2, 134.8, 134.4, 129.9, 127.3, 126.2, 124.8, 120.9, 120.8, 115.0 ppm. HRMS (ESI-TOF)  $m/z$ :  $[\text{M} + \text{Na}]^+$  calcd for  $\text{C}_{19}\text{H}_7\text{F}_5\text{ONa}$ , 369.0309; found, 369.0310. IR (ATR): 479 (m), 570 (w), 653 (w), 739 (s), 761 (s), 844 (s), 929 (m), 954 (m), 985 (s), 1053 (m), 1206 (m), 1457 (m), 1484 (s), 1496 (s), 1602 (m), 1651 (w), 1709 (s)  $\text{cm}^{-1}$ .

**General Synthesis of 2,2'-Substituted 9,9'-Bifluorenylidenes 1R.** To a  $\text{N}_2$  flushed 50 mL one-neck Schlenk flask, 6.0 equiv of zinc powder were added. After heat-drying and adding 20 mL/mmol of dry THF, the stirred suspension was cooled to 0 °C and 3.0 equiv of  $\text{TiCl}_4$  were added dropwise using a syringe. After refluxing for 3 h using an oil bath, 1.0 equiv of 2-substituted 9-fluorenone was added and the mixture was refluxed for 1 h. After cooling to r.t., the reaction mixture was poured onto a mixture of ice and  $\text{NH}_4\text{Cl}$  and extracted with DCM. The combined organic layers were dried over  $\text{Na}_2\text{SO}_4$  and concentrated under reduced pressure. After flash column chromatography (silica; *n*-hexane/DCM 95:5), a mixture of *E* and *Z*-isomer of the desired product was obtained.

**2,2'-Dimethyl-9,9'-bifluorenylidene (1Me).** Red solid (35 mg, 68%).  $^1\text{H}$  NMR (600 MHz,  $\text{CDCl}_3$ ):  $\delta$  8.37 (d,  $J = 7.9$  Hz, 2H), 8.34 (d,  $J = 7.9$  Hz, 2H), 8.24 (s, 2H), 8.19 (s, 2H), 7.67–7.62 (m, 4H), 7.60–7.54 (m, 4H), 7.32–7.27 (m, 4H), 7.19–7.11 (m, 8H), 2.50–2.17 (m, 12H) ppm.  $^{13}\text{C}\{^1\text{H}\}$  NMR (151 MHz,  $\text{CDCl}_3$ ):  $\delta$  141.43, 141.37, 141.02, 141.00, 138.9, 138.8, 138.57, 138.55, 138.4, 138.3,

- 136.6, 136.5, 130.03, 130.00, 129.0, 127.21, 127.19, 126.7, 126.6, 126.4, 126.3, 119.61, 119.60, 119.55, 119.55, 21.8, 21.7 ppm. HRMS (APCI-TOF)  $m/z$ :  $[M + H]^+$  calcd for  $C_{28}H_{23}$ , 357.1638; found, 357.1641. IR (ATR): 425 (s), 649 (w), 726 (s), 768 (m), 817 (m), 1344 (w), 1416 (w), 1446 (m), 2913 (vw), 3040 (vw)  $cm^{-1}$ .
- 2,2'-Diethyl-9,9'-bifluorenylidene (1Et)**. Red solid (46 mg, 50%).  $^1H$  NMR (400 MHz,  $CDCl_3$ ):  $\delta$  8.41–8.33 (m, 4H), 8.30–8.21 (m, 4H), 7.69–7.63 (m, 4H), 7.63–7.57 (m, 4H), 7.34–7.27 (m, 4H), 7.20–7.13 (m, 8H), 2.70–2.57 (m, 8H), 1.27–1.21 (m, 12H) ppm.  $^{13}C\{^1H\}$  NMR (101 MHz,  $CDCl_3$ ):  $\delta$  143.30, 143.26, 141.61, 141.56, 141.1, 139.3, 139.2, 138.8, 138.7, 138.6, 138.5, 129.23, 129.20, 129.19, 126.8, 126.7, 126.6, 126.5, 126.4, 126.3, 119.84, 119.82, 119.76, 119.7, 29.33, 29.28, 16.0, 15.9 ppm. HRMS (ESI-TOF)  $m/z$ :  $[M + H]^+$  calcd for  $C_{30}H_{25}$ , 385.1951; found, 385.1948. IR (ATR): 649 (w), 728 (s), 825 (s), 1028 (m), 1260 (m), 1347 (m), 1421 (s), 1449 (s), 2927 (m), 2960 (s)  $cm^{-1}$ .
- 2,2'-Dipropyl-9,9'-bifluorenylidene (1Pr)**. Red solid (63 mg, 68%).  $^1H$  NMR (400 MHz,  $CDCl_3$ ):  $\delta$  8.41–8.33 (m, 4H), 8.24 (s, 2H), 8.20 (s, 2H), 7.69–7.63 (m, 4H), 7.63–7.58 (m, 4H), 7.34–7.27 (m, 4H), 7.19–7.12 (m, 8H), 2.63–2.53 (m, 8H), 1.72–1.58 (m, 8H), 1.00–0.92 (m, 12H) ppm.  $^{13}C\{^1H\}$  NMR (101 MHz,  $CDCl_3$ ):  $\delta$  141.68, 141.66, 141.59, 141.56, 141.14, 141.12, 139.30, 139.25, 138.7, 138.60, 138.58, 138.5, 129.81, 129.78, 129.2, 127.0, 126.90, 126.85, 126.7, 126.6, 126.4, 119.7, 38.5, 38.4, 25.0, 24.8, 14.0, 13.8 ppm. HRMS (APCI-TOF)  $m/z$ :  $[M + H]^+$  calcd for  $C_{32}H_{29}$ , 413.2264; found, 413.2264. IR (ATR): 649 (w), 727 (s), 770 (m), 824 (m), 1345 (m), 1421 (s), 1447 (s), 2867 (w), 2925 (m), 2955 (m)  $cm^{-1}$ .
- 2,2'-Dibutyl-9,9'-bifluorenylidene (1Bu)**. Red solid (95 mg, 69%).  $^1H$  NMR (600 MHz,  $CDCl_3$ ):  $\delta$  8.33–8.22 (m, 4H), 8.19–8.08 (m, 4H), 7.59–7.54 (m, 4H), 7.54–7.48 (m, 4H), 7.21 (m, 4H), 7.11–7.02 (m, 8H), 2.56–2.47 (m, 8H), 1.57–1.47 (m, 8H), 1.34–1.24 (m, 8H), 0.88–0.80 (m, 12H) ppm.  $^{13}C\{^1H\}$  NMR (151 MHz,  $CDCl_3$ ):  $\delta$  141.91, 141.85, 141.6, 141.5, 141.13, 141.10, 139.24, 139.19, 138.7, 138.59, 138.57, 138.52, 129.74, 129.71, 129.18, 129.16, 127.0, 126.8, 126.7, 126.5, 126.4, 119.74, 119.72, 119.70, 36.2, 35.9, 34.1, 33.8, 22.6, 22.3, 14.2, 14.1 ppm. HRMS (APCI-TOF)  $m/z$ :  $[M + H]^+$  calcd for  $C_{34}H_{33}$ , 441.2577; found, 441.2580. IR (ATR): 650 (w), 736 (s), 765 (m), 833 (m), 961 (w), 1107 (m), 1176 (w), 1291 (m), 1457 (s), 1603 (s), 1714 (s), 2856 (w), 2926 (m), 2955 (m)  $cm^{-1}$ .
- 2,2'-Dipentyl-9,9'-bifluorenylidene (1Pe)**. Red solid (42 mg, 66%).  $^1H$  NMR (400 MHz,  $CDCl_3$ ):  $\delta$  8.37 (m, 4H), 8.24 (s, 2H), 8.20 (s, 2H), 7.66 (m, 4H), 7.60 (dd,  $J = 7.7, 2.9$  Hz, 4H), 7.34–7.27 (m, 4H), 7.20–7.12 (m, 8H), 2.65–2.54 (m, 8H), 1.69–1.56 (m, 8H), 1.41–1.27 (m, 16H), 0.95–0.82 (m, 12H) ppm.  $^{13}C\{^1H\}$  NMR (101 MHz,  $CDCl_3$ ):  $\delta$  142.0, 141.9, 141.60, 141.56, 141.2, 141.1, 139.3, 139.2, 138.71, 138.61, 138.59, 138.5, 129.74, 129.69, 129.19, 129.17, 127.0, 126.9, 126.8, 126.7, 126.5, 126.4, 119.74, 119.71, 36.5, 36.3, 31.72, 31.68, 31.5, 31.4, 22.8, 14.20, 14.18 ppm. HRMS (APCI-TOF)  $m/z$ :  $[M + H]^+$  calcd for  $C_{36}H_{37}$ , 469.2890; found, 469.2892. IR (ATR): 729 (s), 824 (m), 1029 (m), 1261 (w), 1347 (w), 1422 (m), 1451 (s), 2854 (m), 2925 (s), 2955 (m)  $cm^{-1}$ .
- 2,2'-Dinonyl-9,9'-bifluorenylidene (1No)**. Red solid (55 mg, 45%).  $^1H$  NMR (400 MHz,  $CDCl_3$ ):  $\delta$  8.40–8.32 (m, 4H), 8.26–8.17 (m, 4H), 7.69–7.57 (m, 8H), 7.33–7.27 (m, 4H), 7.20–7.11 (m, 8H), 2.65–2.54 (m, 8H), 1.67–1.56 (m, 8H), 1.39–1.19 (m, 48H), 0.93–0.81 (m, 12H) ppm.  $^{13}C\{^1H\}$  NMR (101 MHz,  $CDCl_3$ ):  $\delta$  141.98, 141.95, 141.61, 141.56, 141.14, 141.12, 139.24, 139.19, 138.7, 138.61, 138.59, 138.5, 129.74, 129.69, 129.2, 127.0, 126.9, 126.7, 126.5, 126.4, 119.73, 119.70, 36.5, 36.3, 32.1, 32.0, 31.7, 29.78, 29.76, 29.73, 29.71, 29.6, 29.51, 29.49, 29.3, 22.8, 14.3 ppm. HRMS (APCI-TOF)  $m/z$ :  $[M + H]^+$  calcd for  $C_{44}H_{53}$ , 581.4142; found, 581.4142.
- 2,2'-Di-iso-propyl-9,9'-bifluorenylidene (1iPr)**. Red solid (339 mg, 58%).  $^1H$  NMR (400 MHz,  $CDCl_3$ ):  $\delta$  8.41–8.31 (m, 4H), 8.31–8.23 (m, 4H), 7.70–7.57 (m, 8H), 7.33–7.26 (m, 4H), 7.23–7.12 (m, 8H), 3.00–2.79 (m, 4H), 1.31–1.19 (m, 24H) ppm.  $^{13}C\{^1H\}$  NMR (101 MHz,  $CDCl_3$ ):  $\delta$  147.82, 147.75, 141.43, 141.39, 141.0, 140.9, 139.3, 139.2, 138.6, 138.50, 138.48, 138.4, 129.1, 129.0, 127.8, 127.7, 126.7, 126.5, 126.4, 126.3, 124.9, 124.8, 119.8, 119.63, 119.57, 34.5, 34.3, 24.1, 23.9 ppm. HRMS (APCI-TOF)  $m/z$ :  $[M + H]^+$  calcd for  $C_{30}H_{25}$ , 413.2264; found, 413.2264. IR (ATR): 460 (w), 571 (w), 649 (w), 728 (s), 826 (m), 1421 (m), 1447 (m), 2956 (m)  $cm^{-1}$ .
- 2,2'-Dicyclohexyl-9,9'-bifluorenylidene (1Cy)**. Red solid (22 mg, 56%).  $^1H$  NMR (400 MHz,  $CDCl_3$ ):  $\delta$  8.40–8.32 (m, 4H), 8.31–8.21 (m, 4H), 7.69–7.57 (m, 8H), 7.33–7.26 (m, 4H), 7.22–7.12 (m, 8H), 2.55–2.41 (m, 4H), 1.96–1.67 (m, 20H), 1.52–1.13 (m, 20H) ppm.  $^{13}C\{^1H\}$  NMR (101 MHz,  $CDCl_3$ ):  $\delta$  147.00, 146.97, 141.5, 141.4, 141.0, 140.9, 139.3, 139.2, 138.6, 138.5, 138.44, 138.38, 129.04, 129.00, 128.22, 128.19, 126.7, 126.5, 126.4, 126.3, 125.4, 125.2, 119.7, 119.60, 119.56, 45.2, 44.7, 34.6, 34.4, 26.9, 26.1, 26.0 ppm. HRMS (APCI-TOF)  $m/z$ :  $[M + H]^+$  calcd for  $C_{38}H_{37}$ , 493.2890; found, 493.2887. IR (ATR): 727 (s), 823 (m), 1260 (w), 1345 (m), 1423 (m), 1447 (s), 2848 (m), 2920 (s)  $cm^{-1}$ .
- 2,2'-Di-tert-butyl-9,9'-bifluorenylidene (1Tb)**. Red solid (47 mg, 44%).  $^1H$  NMR (400 MHz,  $CDCl_3$ ):  $\delta$  8.50–8.28 (m, 8H), 7.71–7.57 (m, 8H), 7.44–7.34 (m, 4H), 7.33–7.26 (m, 4H), 7.19–7.11 (m, 4H), 1.32 (s, 36H) ppm.  $^{13}C\{^1H\}$  NMR (151 MHz,  $CDCl_3$ ):  $\delta$  150.2, 149.9, 141.33, 141.31, 141.2, 140.9, 138.9, 138.84, 138.79, 138.62, 138.56, 138.1, 129.1, 128.9, 127.1, 126.7, 126.5, 126.4, 126.24, 126.23, 124.4, 123.0, 119.7, 119.6, 119.4, 35.04, 35.01, 31.5, 31.3 ppm. HRMS (APCI-TOF)  $m/z$ :  $[M + H]^+$  calcd for  $C_{34}H_{33}$ , 441.2577; found, 441.2576.
- 2,2'-Diadamantyl-9,9'-bifluorenylidene (1Ad)**. Red solid (5 mg, 66%).  $^1H$  NMR (400 MHz,  $CDCl_3$ ):  $\delta$  8.46–8.29 (m, 8H), 7.70–7.61 (m, 8H), 7.43–7.26 (m, 8H), 7.21–7.12 (m, 4H), 2.14–2.01 (m, 12H), 1.99–1.86 (m, 24H), 1.83–1.65 (m, 24H) ppm.  $^{13}C\{^1H\}$  NMR (101 MHz,  $CDCl_3$ ):  $\delta$  150.6, 150.2, 141.39, 141.38, 141.2, 140.9, 139.0, 138.9, 138.9, 138.71, 138.70, 138.2, 129.1, 128.9, 126.7, 126.6, 126.5, 126.3, 126.2, 126.0, 124.1, 123.0, 119.7, 119.6, 119.4, 43.3, 43.1, 36.8, 36.7, 36.58, 36.55, 29.0, 28.9 ppm. HRMS (APCI-TOF)  $m/z$ :  $[M + H]^+$  calcd for  $C_{46}H_{43}$ , 597.3516; found, 597.3515. IR (ATR): 728 (s), 772 (m), 825 (m), 1047 (w), 1260 (w), 1342 (m), 1414 (m), 1454 (s), 2846 (s), 2867 (s), 2901 (s)  $cm^{-1}$ .
- 2,2'-Didiamantyl-9,9'-bifluorenylidene (1Dia)**. Red solid (194 mg, 41%).  $^1H$  NMR (600 MHz,  $CDCl_3$ ):  $\delta$  8.44 (d,  $J = 1.4$  Hz, 2H), 8.39 (d,  $J = 7.9$  Hz, 2H), 8.36 (d,  $J = 1.4$  Hz, 2H), 8.31 (d,  $J = 7.8$  Hz, 2H), 7.69–7.61 (m, 8H), 7.41 (dd,  $J = 8.1, 1.7$  Hz, 2H), 7.36 (dd,  $J = 8.0, 1.7$  Hz, 2H), 7.32–7.27 (m, 4H), 7.18–7.12 (m, 4H), 1.93–1.84 (m, 36H), 1.84–1.78 (m, 4H), 1.78–1.70 (m, 36H) ppm.  $^{13}C\{^1H\}$  NMR (151 MHz,  $CDCl_3$ ):  $\delta$  150.1, 149.8, 141.52, 141.50, 141.34, 141.28, 141.25, 141.2, 141.0, 139.14, 139.05, 139.0, 138.84, 138.81, 138.3, 129.2, 129.0, 126.9, 126.6, 126.5, 126.4, 126.3, 124.5, 123.3, 119.8, 119.72, 119.71, 119.5, 44.3, 44.1, 38.4, 37.9, 36.8, 34.9, 34.8, 25.89, 25.87 ppm. HRMS (APCI-TOF)  $m/z$ :  $[M + H]^+$  calcd for  $C_{54}H_{53}$ , 701.4142; found, 701.4080.
- 2,2'-Diphenyl-9,9'-bifluorenylidene (1Ph)**. Red solid (60 mg, 64%).  $^1H$  NMR (400 MHz,  $CDCl_3$ ):  $\delta$  8.76 (d,  $J = 1.2$  Hz, 2H), 8.66 (d,  $J = 1.2$  Hz, 2H), 8.49 (d,  $J = 7.8$  Hz, 2H), 8.44 (d,  $J = 7.9$  Hz, 2H), 7.80–7.69 (m, 8H), 7.64–7.50 (m, 8H), 7.47–7.39 (m, 8H), 7.38–7.32 (m, 4H), 7.29–7.20 (m, 12H) ppm.  $^{13}C\{^1H\}$  NMR (101 MHz,  $CDCl_3$ ):  $\delta$  141.33, 141.30, 141.27, 141.25, 141.2, 140.6, 140.5, 140.3, 140.0, 139.0, 138.8, 138.5, 129.5, 129.0, 128.9, 128.43, 128.40, 127.4, 127.3, 127.1, 127.0, 126.9, 126.8, 126.3, 125.6, 120.4, 120.3, 120.23, 120.17 ppm. HRMS (APCI-TOF)  $m/z$ :  $[M + H]^+$  calcd for  $C_{38}H_{35}$ , 481.1951; found, 481.1953. IR (ATR): 439 (m), 650 (m), 694 (s), 715 (s), 753 (s), 1020 (w), 1344 (m), 1413 (m), 1445 (m), 1598 (w), 2923 (vw), 3028 (vw)  $cm^{-1}$ .
- 2,2'-Di-pentafluorophenyl-9,9'-bifluorenylidene (1PFP)**. Red solid (248 mg, 32%).  $^1H$  NMR (400 MHz,  $CDCl_3$ ):  $\delta$  8.48–8.33 (m, 4H), 7.82 (dd,  $J = 7.9, 3.6$  Hz, 2H), 7.77 (d,  $J = 7.1$  Hz, 2H), 7.44–7.35 (m, 4H), 7.33–7.27 (m, 2H) ppm.  $^{13}C\{^1H, ^{19}F\}$  NMR (101 MHz,  $CDCl_3$ ):  $\delta$  144.5, 144.3, 142.2, 141.0, 140.8, 140.7, 140.5, 140.5, 138.5, 138.4, 138.4, 138.1, 138.0, 131.3, 131.1, 129.9, 129.9, 128.8, 128.6, 127.9, 127.9, 127.1, 126.9, 124.8, 124.8, 120.6, 120.6, 120.3, 120.3, 116.1, 116.0 ppm. HRMS (APCI-TOF)  $m/z$ :  $[M + H]^+$  calcd for  $C_{38}H_{15}F_{10}$ , 661.1009; found, 661.1010. IR (ATR):

726 (s), 768 (m), 835 (m), 936 (m), 986 (s), 1062 (s), 1411 (m), 1453 (s), 1491 (s), 1521 (s), 2851 (vw), 2921 (w)  $\text{cm}^{-1}$ .

2,2'-Ditriptyl-9,9'-bifluorenylidene (1Tr). Red solid (22 mg, 76%).  $^1\text{H}$  NMR (400 MHz,  $\text{CDCl}_3$ )  $\delta$  8.23–8.15 (m, 4H), 7.68 (m, 4H), 7.56–7.49 (m, 8H), 7.25–7.09 (m, 68H), 6.77 (t,  $J = 7.6$  Hz, 4H).  $^{13}\text{C}$  NMR (101 MHz,  $\text{CDCl}_3$ ):  $\delta$  146.6, 145.7, 140.9, 140.5, 139.2, 138.4, 137.7, 132.5, 131.2, 129.5, 128.5, 127.6, 127.1, 126.1, 126.0, 119.5, 118.6, 65.1 ppm. HRMS (APCI-TOF)  $m/z$ :  $[\text{M} + \text{H}]^+$  calcd for  $\text{C}_{64}\text{H}_{48}$ , 813.3516; found, 813.3516.

#### COMPUTATIONAL DETAILS

Conformational prescreening was performed using CREST (version 2.11.1).<sup>32,33</sup> All optimizations and single points were computed using ORCA (version 5.0.3).<sup>39–41</sup> For optimizations, we employed the PBEh-3c composite approach<sup>42</sup> with geometrical counterpoise correction<sup>43</sup> and dispersion corrections including Becke-Johnson damping (D3BJ).<sup>44,45</sup> Energy single points were computed using revDSD-PBEP86-D4/def2-QZVPP<sup>46–48</sup> and DLPNO-CCSD(T)/def2-TZVP.<sup>49,50</sup> Solvation free energies were computed at PBEh-3c using the SMD model<sup>51</sup> with SES areas generated by GEPOL.<sup>52,53</sup> Conformer ensembles were computed using CENSO (version 1.2.0)<sup>34</sup> employing the  $r^2\text{SCAN-3c}$  method<sup>54</sup> with SMD solvation. SAPT analysis was performed with PSI4 (version 1.5)<sup>55</sup> at sSAPT0/def2TZVP. Noncovalent interactions were visualized using NCIPLOT.<sup>56,57</sup>

#### ASSOCIATED CONTENT

##### Data Availability Statement

Data availability: The data underlying this study are available in the published article and in its online Supporting Information.

##### Supporting Information

The Supporting Information is available free of charge at <https://pubs.acs.org/doi/10.1021/acs.joc.2c02444>.

Experimental data; procedures;  $^1\text{H}$ ,  $^{13}\text{C}$  and NOESY NMR spectra; HRMS data; single-crystal X-ray diffraction data; and computational data (PDF)

##### Accession Codes

CCDC 2173987–2173992 contain the supplementary crystallographic data for this paper. These data can be obtained free of charge via [www.ccdc.cam.ac.uk/data\\_request/cif](http://www.ccdc.cam.ac.uk/data_request/cif), or by emailing [data\\_request@ccdc.cam.ac.uk](mailto:data_request@ccdc.cam.ac.uk), or by contacting The Cambridge Crystallographic Data Centre, 12 Union Road, Cambridge CB2 1EZ, UK; fax: +44 1223 336033.

#### AUTHOR INFORMATION

##### Corresponding Author

Peter R. Schreiner – *Institute of Organic Chemistry, Justus Liebig University, 35392 Giessen, Germany; Center for Materials Research (ZfM), Justus Liebig University, 35392 Giessen, Germany; [orcid.org/0000-0002-3608-5515](https://orcid.org/0000-0002-3608-5515); Email: [prs@uni-giessen.de](mailto:prs@uni-giessen.de)*

##### Authors

Finn M. Wilming – *Institute of Organic Chemistry, Justus Liebig University, 35392 Giessen, Germany; Center for Materials Research (ZfM), Justus Liebig University, 35392 Giessen, Germany; [orcid.org/0000-0002-5619-9931](https://orcid.org/0000-0002-5619-9931)*

Benito Marazzi – *Institute of Organic Chemistry, Justus Liebig University, 35392 Giessen, Germany; Center for Materials Research (ZfM), Justus Liebig University, 35392 Giessen, Germany; [orcid.org/0000-0001-7077-1394](https://orcid.org/0000-0001-7077-1394)*

Paul P. Debes – *Institute of Organic Chemistry, Justus Liebig University, 35392 Giessen, Germany; Center for Materials Research (ZfM), Justus Liebig University, 35392 Giessen, Germany; [orcid.org/0000-0002-1506-3296](https://orcid.org/0000-0002-1506-3296)*

Jonathan Becker – *Institute of Inorganic and Analytical Chemistry, Justus Liebig University, 35392 Giessen, Germany*

Complete contact information is available at:

<https://pubs.acs.org/doi/10.1021/acs.joc.2c02444>

##### Author Contributions

<sup>†</sup>J.B. did the X-ray crystal structure determination.

##### Funding

This research was supported by the GRK2204 and the priority program SPP1807 funded by the Deutsche Forschungsgemeinschaft (DFG).

##### Notes

The authors declare no competing financial interest.

#### ACKNOWLEDGMENTS

The authors thank Heike Hausmann for performing the NMR experiments as well as Yu Ozawa and Maya Ziegler for preliminary synthetic contributions. F.M.W. thanks Sören Rösel, Jan M. Schümmer, Lars Rummel, Bastian Bernhardt, Henrik F. König, and Dennis Gerbig for fruitful discussions.

#### REFERENCES

- (1) London, F. Zur Theorie und Systematik der Molekularkräfte. *Z. Phys.* **1930**, *63*, 245–279.
- (2) Eisenschitz, R.; London, F. Über das Verhältnis der van der Waalschen Kräfte zu den homöopolaren Bindungskräften. *Z. Phys.* **1930**, *60*, 491–527.
- (3) Schreiner, P. R.; Chernish, L. V.; Gunchenko, P. A.; Tikhonchuk, E. Y.; Hausmann, H.; Serafin, M.; Schlecht, S.; Dahl, J. E. P.; Carlson, R. M. K.; Fokin, A. A. Overcoming lability of extremely long alkane carbon-carbon bonds through dispersion forces. *Nature* **2011**, *477*, 308–311.
- (4) Grimme, S.; Djukic, J.-P. Cation–Cation “Attraction”: When London Dispersion Attraction Wins over Coulomb Repulsion. *Inorg. Chem.* **2011**, *50*, 2619–2628.
- (5) Kolář, M.; Kubař, T.; Hobza, P. On the Role of London Dispersion Forces in Biomolecular Structure Determination. *J. Phys. Chem. B* **2011**, *115*, 8038–8046.
- (6) Lüttschwager, N. O. B.; Wassermann, T. N.; Mata, R. A.; Suhm, M. A. The Last Globally Stable Extended Alkane. *Angew. Chem., Int. Ed.* **2013**, *52*, 463–466.
- (7) Rösel, S.; Balestrieri, C.; Schreiner, P. R. Sizing the role of London dispersion in the dissociation of all-*meta tert*-butyl hexaphenylethane. *Chem. Sci.* **2017**, *8*, 405–410.
- (8) Rösel, S.; Becker, J.; Allen, W. D.; Schreiner, P. R. Probing the Delicate Balance between Pauli Repulsion and London Dispersion with Triphenylmethyl Derivatives. *J. Am. Chem. Soc.* **2018**, *140*, 14421–14432.
- (9) Rösel, S.; Quanz, H.; Logemann, C.; Becker, J.; Mossou, E.; Cañadillas-Delgado, L.; Caldeweyher, E.; Grimme, S.; Schreiner, P. R. London Dispersion Enables the Shortest Intermolecular Hydrocarbon H...H Contact. *J. Am. Chem. Soc.* **2017**, *139*, 7428–7431.
- (10) Krenske, E. H.; Houk, K. N.; Harmata, M. Origin of Stereoselectivity in the (4 + 3) Cycloadditions of Chiral Alkoxy Siloxyallyl Cations with Furan. *Org. Lett.* **2010**, *12*, 444–447.
- (11) Eschmann, C.; Song, L.; Schreiner, P. R. London Dispersion Interactions Rather than Steric Hindrance Determine the Enantioselectivity of the Corey-Bakshi-Shibata Reduction. *Angew. Chem., Int. Ed.* **2021**, *60*, 4823–4832.

- (12) Rummel, L.; Hanke, K.; Becker, J.; Schreiner, P. R. London Dispersion Stabilizes Chloro-Substituted cis-Double Bonds. *Synlett* **2022**, DOI: 10.1055/a-1928-2473, (EFirst).
- (13) Liprot, D. J.; Power, P. P. London dispersion forces in sterically crowded inorganic and organometallic molecules. *Nat. Rev. Chem.* **2017**, *1*, 0004.
- (14) Wagner, J. P.; Schreiner, P. R. London Dispersion in Molecular Chemistry—Reconsidering Steric Effects. *Angew. Chem., Int. Ed.* **2015**, *54*, 12274–12296.
- (15) Mears, K. L.; Power, P. P. Beyond Steric Crowding: Dispersion Energy Donor Effects in Large Hydrocarbon Ligands. *Acc. Chem. Res.* **2022**, *55*, 1337–1348.
- (16) Grimme, S.; Huenerbein, R.; Ehrlich, S. On the Importance of the Dispersion Energy for the Thermodynamic Stability of Molecules. *ChemPhysChem* **2011**, *12*, 1258–1261.
- (17) Yang, L.; Adam, C.; Nichol, G. S.; Cockroft, S. L. How much do van der Waals dispersion forces contribute to molecular recognition in solution? *Nat. Chem.* **2013**, *5*, 1006–1010.
- (18) Schneider, H.-J. Dispersive Interactions in Solution Complexes. *Acc. Chem. Res.* **2015**, *48*, 1815–1822.
- (19) Strauss, M. A.; Wegner, H. A. Molecular Systems for the Quantification of London Dispersion Interactions. *Eur. J. Org. Chem.* **2019**, *2019*, 295–302.
- (20) Elmi, A.; Cockroft, S. L. Quantifying Interactions and Solvent Effects Using Molecular Balances and Model Complexes. *Acc. Chem. Res.* **2021**, *54*, 92–103.
- (21) Schümann, J. M.; Wagner, J. P.; Eckhardt, A. K.; Quanz, H.; Schreiner, P. R. Intramolecular London Dispersion Interactions Do Not Cancel in Solution. *J. Am. Chem. Soc.* **2021**, *143*, 41–45.
- (22) König, H. F.; Rummel, L.; Hausmann, H.; Becker, J.; Schümann, J. M.; Schreiner, P. R. Gauging the Steric Effects of Silyl Groups with a Molecular Balance. *J. Org. Chem.* **2022**, *87*, 4670–4679.
- (23) Paliwal, S.; Geib, S.; Wilcox, C. S. Molecular Torsion Balance for Weak Molecular Recognition Forces. Effects of “Tilted-T” Edge-to-Face Aromatic Interactions on Conformational Selection and Solid-State Structure. *J. Am. Chem. Soc.* **1994**, *116*, 4497–4498.
- (24) Van Craen, D.; Rath, W. H.; Huth, M.; Kemp, L.; Räuber, C.; Wollschläger, J. M.; Schalley, C. A.; Valkonen, A.; Rissanen, K.; Albrecht, M. Chasing Weak Forces: Hierarchically Assembled Helicates as a Probe for the Evaluation of the Energetics of Weak Interactions. *J. Am. Chem. Soc.* **2017**, *139*, 16959–16966.
- (25) Strauss, M. A.; Wegner, H. A. Exploring London Dispersion and Solvent Interactions at Alkyl-Alkyl Interfaces Using Azobenzene Switches. *Angew. Chem., Int. Ed.* **2019**, *58*, 18552–18556.
- (26) Strauss, M. A.; Wegner, H. A. London Dispersion in Alkane Solvents. *Angew. Chem., Int. Ed.* **2021**, *60*, 779–786.
- (27) Pollice, R.; Bot, M.; Kobylanski, I. J.; Shenderovich, I.; Chen, P. Attenuation of London Dispersion in Dichloromethane Solutions. *J. Am. Chem. Soc.* **2017**, *139*, 13126–13140.
- (28) Wilming, F. M.; Becker, J.; Schreiner, P. R. Quantifying Solvophobic Effects in Organic Solvents Using a Hydrocarbon Molecular Balance. *J. Org. Chem.* **2022**, *87*, 1874–1878.
- (29) Minabe, M.; Oba, T.; Tanaka, M.; Kanno, K.; Tsubota, M. Z/E Selectivity on the Formation of 2,2'-Diacyl-9,9'-bifluorenylidene Was Controlled by the Length of Acyl Side Chains. *Chem. Lett.* **2000**, *29*, 498–499.
- (30) Masahiro, M.; Ayumi, Y.; Toshinobu, I.; Takumi, T.; Michinori, K. Formation of 2,2'-Diacyl-9,9'-bifluorenylidene Isomers from 2-Acyl-9-bromofluorene and Base-Catalyzed Isomerization of the Formed Alkenes. *Bull. Chem. Soc. Jpn.* **2006**, *79*, 1758–1765.
- (31) Jee, A.-Y.; Lee, M. Elasticity-controlled molecular dynamics of 9,9'-bifluorenylidene as a function of temperature and force. *New J. Chem.* **2012**, *36*, 1308–1311.
- (32) Pracht, P.; Bohle, F.; Grimme, S. Automated exploration of the low-energy chemical space with fast quantum chemical methods. *Phys. Chem. Chem. Phys.* **2020**, *22*, 7169–7192.
- (33) Grimme, S. Exploration of Chemical Compound, Conformer, and Reaction Space with Meta-Dynamics Simulations Based on Tight-Binding Quantum Chemical Calculations. *J. Chem. Theory Comput.* **2019**, *15*, 2847–2862.
- (34) Grimme, S.; Bohle, F.; Hansen, A.; Pracht, P.; Spicher, S.; Stahn, M. Efficient Quantum Chemical Calculation of Structure Ensembles and Free Energies for Nonrigid Molecules. *J. Phys. Chem. A* **2021**, *125*, 4039–4054.
- (35) Zhang, J.; Zhang, H.; Wu, T.; Wang, Q.; van der Spoel, D. Comparison of Implicit and Explicit Solvent Models for the Calculation of Solvation Free Energy in Organic Solvents. *J. Chem. Theory Comput.* **2017**, *13*, 1034–1043.
- (36) Hwang, J.; Li, P.; Smith, M. D.; Shimizu, K. D. Distance-Dependent Attractive and Repulsive Interactions of Bulky Alkyl Groups. *Angew. Chem., Int. Ed.* **2016**, *55*, 8086–8089.
- (37) Wertz, S.; Leifert, D.; Studer, A. Cross Dehydrogenative Coupling via Base-Promoted Homolytic Aromatic Substitution (BHAS): Synthesis of Fluorenones and Xanthenes. *Org. Lett.* **2013**, *15*, 928–931.
- (38) Sarkar, S.; Tadigoppula, N.  $\text{PhI}(\text{OAc})\cdot\text{BF}_3\cdot\text{OEt}_2$  mediated domino imine activation, intramolecular C-C bond formation and  $\beta$ -elimination: new approach for the synthesis of fluorenones, xanthenes and phenanthridines. *RSC Adv.* **2014**, *4*, 40964–40968.
- (39) Neese, F. The ORCA program system. *WIREs Comput. Mol. Sci.* **2012**, *2*, 73–78.
- (40) Neese, F. Software update: the ORCA program system, version 4.0. *WIREs Comput. Mol. Sci.* **2018**, *8*, No. e1327.
- (41) Neese, F. Software update: The ORCA program system—Version 5.0. *WIREs Comput. Mol. Sci.* **2022**, *12*, No. e1606.
- (42) Grimme, S.; Brandenburg, J. G.; Bannwarth, C.; Hansen, A. Consistent structures and interactions by density functional theory with small atomic orbital basis sets. *J. Chem. Phys.* **2015**, *143*, 054107.
- (43) Kruse, H.; Grimme, S. A geometrical correction for the inter- and intra-molecular basis set superposition error in Hartree-Fock and density functional theory calculations for large systems. *J. Chem. Phys.* **2012**, *136*, 154101.
- (44) Grimme, S.; Ehrlich, S.; Goerigk, L. Effect of the damping function in dispersion corrected density functional theory. *J. Comput. Chem.* **2011**, *32*, 1456–1465.
- (45) Grimme, S.; Antony, J.; Ehrlich, S.; Krieg, H. A consistent and accurate ab initio parametrization of density functional dispersion correction (DFT-D) for the 94 elements H-Pu. *J. Chem. Phys.* **2010**, *132*, 154104.
- (46) Santra, G.; Sylvetsky, N.; Martin, J. M. L. Minimally Empirical Double-Hybrid Functionals Trained against the GMTKN55 Database: revDSD-PBEP86-D4, revDOD-PBE-D4, and DOD-SCAN-D4. *J. Phys. Chem. A* **2019**, *123*, S129–S143.
- (47) Martin, J. M. L.; Santra, G. Empirical Double-Hybrid Density Functional Theory: A ‘Third Way’ in Between WFT and DFT. *Isr. J. Chem.* **2020**, *60*, 787–804.
- (48) Caldeweyher, E.; Ehlert, S.; Hansen, A.; Neugebauer, H.; Spicher, S.; Bannwarth, C.; Grimme, S. A generally applicable atomic-charge dependent London dispersion correction. *J. Chem. Phys.* **2019**, *150*, 154122.
- (49) Riplinger, C.; Neese, F. An efficient and near linear scaling pair natural orbital based local coupled cluster method. *J. Chem. Phys.* **2013**, *138*, 034106.
- (50) Liakos, D. G.; Sparta, M.; Kesharwani, M. K.; Martin, J. M. L.; Neese, F. Exploring the Accuracy Limits of Local Pair Natural Orbital Coupled-Cluster Theory. *J. Chem. Theory Comput.* **2015**, *11*, 1525–1539.
- (51) Marenich, A. V.; Cramer, C. J.; Truhlar, D. G. Universal Solvation Model Based on Solute Electron Density and on a Continuum Model of the Solvent Defined by the Bulk Dielectric Constant and Atomic Surface Tensions. *J. Phys. Chem. B* **2009**, *113*, 6378–6396.
- (52) Pascual-Ahuir, J. L.; Silla, E. GEPOLE: An improved description of molecular surfaces. I. Building the spherical surface set. *J. Comput. Chem.* **1990**, *11*, 1047–1060.

(53) Silla, E.; Tuñón, I.; Pascual-Ahuir, J. L. GEPOL: An improved description of molecular surfaces II. Computing the molecular area and volume. *J. Comput. Chem.* 1991, *12*, 1077–1088.

(54) Grimme, S.; Hansen, A.; Ehlert, S.; Mewes, J.-M. r2SCAN-3c: A "Swiss army knife" composite electronic-structure method. *J. Chem. Phys.* 2021, *154*, 064103.

(55) Smith, D. G. A.; Burns, L. A.; Simmonett, A. C.; Parrish, R. M.; Schieber, M. C.; Galvelis, R.; Kraus, P.; Kruse, H.; Di Remigio, R. D.; Alenaizan, A.; James, A. M.; Lehtola, S.; Misiewicz, J. P.; Scheurer, M.; Shaw, R. A.; Schriber, J. B.; Xie, Y.; Glick, Z. L.; Sirianni, D. A.; O'Brien, J. S.; Waldrop, J. M.; Kumar, A.; Hohenstein, E. G.; Pritchard, B. P.; Brooks, B. R.; Schaefer, H. F.; Sokolov, A. Y.; Patkowski, K.; DePrince, A. E.; Bozkaya, U.; King, R. A.; Evangelista, F. A.; Turney, J. M.; Crawford, T. D.; Sherrill, C. D. Psi4.4: Open-source software for high-throughput quantum chemistry. *J. Chem. Phys.* 2020, *152*, 184108.

(56) Johnson, E. R.; Keinan, S.; Mori-Sánchez, P.; Contreras-García, J.; Cohen, A. J.; Yang, W. Revealing Noncovalent Interactions. *J. Am. Chem. Soc.* 2010, *132*, 6498–6506.

(57) Laplaza, R.; Peccati, F.; Boto, A. R.; Quan, C.; Carbone, A.; Piquemal, J.-P.; Maday, Y.; Contreras-García, J. NCIPLLOT and the analysis of noncovalent interactions using the reduced density gradient. *Wiley Interdiscip. Rev.: Comput. Mol. Sci.* 2021, *11*, No. e1497.

### 3. Acknowledgement – Danksagung

Abschließend möchte ich mich herzlich bei einer Reihe von Menschen bedanken, ohne deren Mithilfe diese Arbeit nicht zustande gekommen wäre. Vielen Dank an:

**Prof. Dr. Peter R. Schreiner, PhD** für die Aufnahme in seine Arbeitsgruppe, hilfreiche Ratschläge und das kontinuierliche Fördern meiner Fähigkeiten über insgesamt 7 Jahre.

**Prof. Dr. Derck Schlettwein** für die Übernahme des Zweitgutachtens dieser Arbeit.

**Dr. Sören Rösel** für die Betreuung meiner Bachelor- und Master-Thesis, die Möglichkeit von seinem Wissen zu profitieren und den stets freundschaftlichen Umgang.

Alle Mitglieder des **GRK 2204** für die gute interdisziplinäre Zusammenarbeit.

**Paul P. Debes, Silke Müsse, Benito Marazzi, Yu Ozawa, PhD** und **Emily Brown** für die sehr gute Zusammenarbeit im Labor im Rahmen ihrer Abschlussarbeiten oder Auslandsaufenthalte.

**Dr. Jonathan Becker** für die Analyse einer großen Zahl an Einkristallen.

**Dr. Heike Hausmann** und das gesamte **Team der OC-Analytik** für die zahlreichen für mich durchgeführten Messungen.

**Dr. Bastian Bernhardt, Dr. Lars Rummel** und **Henrik F. König** für die gemeinsame Zeit in B201, das immer freundschaftliche Verhältnis und den vielen Spaß den wir gemeinsam hatten.

**Dr. Dennis Gerbig, Dr. Raffael Wende, Jan M. Schümann, Lukas Ochmann** und **Jama Ariai** für wertvolle Diskussionen und Hilfestellungen im Labor und im Bereich der Computerchemie.

Die gesamte **PRS Group** für die angenehme Arbeitsatmosphäre.

Die anderen Arbeitsgruppen des **Instituts für organische Chemie** für die hilfreichen Diskussionen und die ausgeliehenen Geräte und Chemikalien.

**Michaela Richter** und **Dr. Jörg Neudert** für die Unterstützung bei administrativen Angelegenheiten.

**Dr. Martin Güngerich** für die administrative Betreuung des GRK 2204.

Meinen Kommilitonen und insbesondere **David S. Kröck, Dr. Bastian Bernhardt, Jaqueline Beppler, Tabea Köhler** und **Ruben Maile** für die vielen gemeinsamen Stunden in der Bibliothek, dem Labor oder vor der neusten Übung.

**Jennifer Redson Wiebers, Clara-Lisa Wiebers** und **Jama Ariai** für das Korrekturlesen dieser Arbeit.

**Silke Wagner** für die Begeisterung für organische Chemie die Sie in mir geweckt hat.

Der **Deutschen Forschungsgemeinschaft** für die finanzielle Unterstützung im Rahmen des GRK 2204.

**Meinen Freunden** und **meiner Familie** für die dauerhafte Unterstützung und das Leben abseits der Universität.